Beyond homogeneous dispersion: oriented conductive fillers for high κ nanocomposites

Seunggun Yu,*[a] Xi Shen[b], and Jang-Kyo Kim*[c]

[a]*Insulation Materials Research Center, Korea Electrotechnology Research Institute (KERI), Changwon 51543, Korea*

[b]*Department of Aeronautical and Aviation Engineering, The Hong Kong Polytechnic University, Hung Hom, Kowloon, Hong Kong*

[b]*Department of Mechanical and Aerospace Engineering, The Hong Kong University of Science and Technology, Clear Water Bay, Kowloon, Hong Kong*

Abstract

Rational design of structures for regulating the thermal conductivities (κ) of materials is critical to many components and products employed in electrical, electronics, energy, construction, and aerospace, as well as medical applications. As such, considerable efforts have been devoted to developing polymer composites with tailored conducting filler architectures and thermal conduits for highly improved κ. This paper is dedicated to overviewing recent advances in this area to offer perspectives for the next level of future development. The limitations of conventional particulate-filled composites and the issue of percolation are discussed. In view of different directions of heat dissipation in polymer composites for differing end applications, various approaches for designing the micro- and macroscopic structures of thermal conduction networks in the polymer matrix are highlighted. Methodological approaches devised to significantly ameliorate the thermal conduction are categorized with respect to the pathways of

heat dissipation. Future prospects for the development of thermally conductive polymer composites with modulated thermal conduction pathways are highlighted.

1. Introduction

Decades of progress in various technologies have contributed to the development of cheaper, faster, and high-performance electronic devices as well as equipment composed of such devices.[1-9] Next-generation electronic devices require miniaturization of their components to further enhance their performance satisfying various human requirements.[10-16] According to Moore's law, the number of transistors in a chip is expected to double every 18 months.[17] Circuits with micro- to nano-scale features may experience a rapid increase in heat accumulation arising from the high-density integration for faster information processing.[18] For instance, the complementary metal-oxide-semiconductor (CMOS) process for microelectronics promotes a rapid heat flux of approximately 100 W cm^{-2}, and the value may increase by several thousand orders of magnitude upon further integration and miniaturization.[19,20] These electronic components and the devices containing such high-density ICs often suffer from the accumulation of resistive heats, referred to as Joule heats, resulting in not only deterioration of the devices but also safety risks to human being.[21-25] For typical devices, the waste heat gradually dissipates through their package platforms to ensure a steady-state operation according to the second law of thermodynamics.[26] However, the main parts of these devices, including the substrate and IC package, are usually made of polymers which are difficult to dissipate the waste heat owing to their intrinsically low thermal conductivities of ~ 0.2 W m^{-1} K^{-1}.[27-29] Another example is light-emitting diodes (LEDs) that operate on the basis of

recombination of electrons and holes under an electrical field, giving rise to luminescence. They consist of many components fabricated using polymer-based materials, *e.g.*, encapsulant, molding materials, die attaches and lens. The electric-to-light energy conversion causes accumulation of heat by means of various resistances, leading to a device temperature rise beyond 80 °C and reducing the device lifetime by almost 1,000 h K^{-1}.[30, 31] As such, efficient thermal management is essential to mitigating the deterioration of device performance arising from the saturated heat energy. Exploring a variety of functional materials possessing a combination of useful characteristics, such as high κ and high electrical conductivity (σ) as well as good mechanical properties and processability, may facilitate the design of next-generation integrated electronic devices with controlled heat conduction.

While various metals and inorganic crystals are widely known as excellent thermal conductors by electron and phonon transport, amorphous polymers with poor crystallinity function as thermal insulators owing to their lower κ values.[32-37] When the heat first reaches the surface atom of the polymer, it propagates to the adjacent atoms. In contrast to crystalline materials capable of collective vibration, the heat transport accompanies various molecular motions, such as vibrational, rotational, and translational motions due to the amorphous and disordered structural characteristics.[38] Such defective structures easily cause internal phonon scattering between molecular chains, resulting in much slower diffusion of heat than in crystalline structures. Meanwhile, several types of polymers like thermoplastics possess ordered and semi-crystalline structures similar to those of inorganic crystals. The bulk form of such semi-crystalline polymers often carries a higher κ than amorphous polymers by means of long polymer chains with repeating units, *e.g.*, high-density polyethylene (HDPE) with κ ~0.5 W m^{-1} K^{-1}, or strong interactions between molecules, *e.g.*, liquid crystalline epoxy with κ ~1.0 W m^{-1}

^{1} K^{-1}.[39,40] Although recent advances in the thermal conduction properties of polymers by enhancing interchain interactions have led to an exceptionally high κ greater than 1.5 W m^{-1} K^{-1}, there remains a much room for improvement as the current κ values of polymers are significantly lower than those of metallic and inorganic materials.[41]

Most electronic packaging materials are prepared using polymeric materials that possess the advantages of light weights, facile processability, high mechanical properties, and low costs. Therefore, the development of polymer-based composite materials by introducing a variety of conducting fillers with high κ values is required to overcome the low κ of polymers.[42,43] Considerable efforts have been devoted to designing high-performance thermally conductive polymer composites with efficient heat dissipation by minimizing the heat accumulation while maintaining the current levels of cost, processability, and weight of the devices.

This review is dedicated to reviewing the ongoing efforts made to the development of polymer composites towards improved κ by means of structural modulation of fillers. The overall approaches and the detailed strategies used for designing filler architectures is schematically summarized in Fig. 1. Common fillers with high κ are introduced and recent progress is discussed in developing thermally conductive polymer composites containing conducting fillers chemically compatible with the polymer matrix. The drawbacks arising from conventional particulate fillers that fail to offer high κ of polymer composites are highlighted. Strategies devised for enhanced κ of polymer composites through controlled percolation are discussed. Finally, future perspectives and outlooks are proposed on the development of next-generation thermally conductive composites.

2. Polymer composites with high κ

2.1. Thermally conductive fillers

Thermally conductive fillers with inherently high κ values are essential to improving the κ of polymer composites for practical thermal management applications. The physical properties including the κ values of representative thermally conductive materials are summarized in Table 1. It is well known that metals have inherently high κ values because of high concentrations of free valence electrons, especially for monolithic atoms. Similar to metals, several carbon materials are conductors for both electricity and heat, but the anisotropy of their crystallographic structures causes high anisotropy of these properties. While most ceramic materials are known as insulators because of the absence of free electrons, some ceramic materials, *e.g.*, BN and diamond, allow only conduction of heat by phonon transport whereas the electron transport is blocked. In this section, we introduce a variety of metallic, carbonaceous, and ceramic materials with high κ values that can be used as filler for thermally conductive polymer composites, as well as their thermal conduction behaviors and structural characteristics.

2.1.1. Electrically conductive fillers

Metals with high κ have been widely used as heat dissipation materials in a variety of electronics applications, such as high-frequency packages that are used in data communications and microwave applications.[44-46] In spite of excellent heat dissipation performance, however, the use of the bulk metals is often discouraged because of their high densities while intrinsically high κ.[47] Recently, nanostructured metals – mostly nanowires (NWs) – are of much interest due to their unique optical, electrical, and thermal properties for various optoelectronics and energy

applications.[48,49] In view of their advantageous morphological features with high aspect ratios in particular, the thermal conduction properties of different metal NWs have been studied. The κ values of Al, Cu, and Ag NWs are lower than their bulk counterparts, but ranked still higher than other bulk metals.[50-52] Moreover, the mass density of such metallic NWs is obviously lower than that of bulk metals.[53] The κ values of metallic NWs are known to depend on their diameters because of the scattering of electrons and phonons on their large surface areas. Thus, when metallic NWs are introduced as filler for polymer composite, the formation of a network structure taking advantage of their high aspect ratios can provide conduction pathways through many junctions, leading to an efficient increase in κ even with a smaller amount of NWs.

Carbon nanomaterials have been widely employed as filler for functional composites exploiting their excellent electrical and thermal conduction properties and low densities as well as earth-abundant reserves of these materials.[54,55] Traditionally, carbon fibers (CFs) are one of the most important reinforcing fillers for structural composites especially for aerospace industries thanks to their excellent tensile strengths and moduli, and chemical resistance.[56] Pitch-derived CFs have a highly-aligned graphitic structure with a high packing density, giving rise to a κ value as high as 958 W m^{-1} K^{-1} along the fiber direction which is dozens of times higher than those of poly(acrylonitrile) (PAN)-based CFs or even exceeds that of silver.[57] Thus, CFs with high κ have been employed in a variety of forms, including chopped fibers as short fillers as well as organized bundles like yarns and roving for CF-reinforced plastic (CFRP) composites.

Graphene, one atomic layer of graphite, is known to possess an astonishing theoretical κ of 5,300 W m^{-1} K^{-1}, ever-known best thermal conductor.[58] However, the fabrication of single-layered graphene in large quantities is challenging. Those prepared by chemical vapor deposition (CVD) growth on a metal substrate suffer from the difficulty in scalable fabrication

and poor processability. Alternatively, few-layer graphene oxide (GO) can be obtained by intercalation and exfoliation of bulk graphite using high concentration acids through a facile solution process.[59] Arising from the destruction of inherent crystalline structure of graphite during oxidation, however, the electrical and thermal conduction properties are significantly impaired. Therefore, it is a great challenge to recover their intrinsic crystalline structure after oxidation for use as efficient thermally conductive fillers for polymer composites.

Meanwhile, a carbon nanotube (CNT) that is a form of single (or multi-layer) graphene sheet(s) rolled up into a long, flexible cylindrical shape exhibit extremely high theoretical κ up to approximately 6,600 W m^{-1} K^{-1} due to their long phonon mean free paths.[60,61] The actual κ values of CNTs vary depending on their structures, presence of defects, diameters, and lengths. Although the individual CNTs have high κ values, their uniform dispersion within a polymer matrix is hardly achieved due to the entangled nature of as-produced CNT bundles, resulting in poor κ of CNT/polymer composites. In addition, CNTs with large specific surface areas and ultralong lengths cause strong phonon scattering at the weak interfaces with the polymer matrix.[27] Therefore, it is essential to obtain good dispersion by loosening the individual CNTs while to design the interface for improved compatibility with the polymer matrix by introducing functional groups.

2.1.2. Electrically insulative fillers

Thermally conductive materials with electrically insulating properties have been extensively investigated for thermal management of electronic devices.[62,63] Beyond the high-performance materials that are conductive for both current and heat, several ceramic materials have recently received attention as new types of thermally conductive fillers due to their high κ and low σ.[64]

Diamond, a well-known allotrope of carbon, is better isotropic thermal conductor than metals. The κ of chemical vapor deposition (CVD)-grown diamond can be made as high as 2,100 W m^{-1} K^{-1} by controlling the lattice structure and impurity levels.[65] In spite of the advantageous κ, synthetic diamond suffers from poor processability and high cost, making it difficult to choose as filler for thermally conductive polymer composites. Hexagonal boron nitride (hBN), a structural analogue with a lattice constant similar to graphene, is among the best thermal conductors with a high electrical resistivity.[66] hBN is composed of alternating boron and nitrogen atoms and is the chemically most stable and mechanically soft among BN polymorphs. The bulk hBN has a layered structure similar to graphite and within each layer, boron and nitrogen atoms are bound by strong covalent bonds, whereas the layers are held together by weak van der Waals forces. Therefore, it possesses anisotropic κ values of about 390 and 2 W m^{-1} K^{-1} in the plane and transverse directions, respectively.[67] As such, κ of exfoliated BN nanosheets (BNNSs) is dependent on the number of hBN layers, in which one-atom-thin hBN has a remarkable κ of 751 W m^{-1} K^{-1} along the plane direction at room temperature.[66] Thus, the BNNSs have been widely used as thermally conductive fillers thanks to their high κ and low densities. As a polymorph of BN, BN nanotubes (BNNTs) also exist in the form of a tubular structure. Structurally they are similar to carbon nanotubes except that carbon atoms are alternately substituted by nitrogen and boron atoms.[68] In view of high κ of single BN sheets, much effort has been directed towards employing BNNTs as thermally conductive fillers, but in reality the κ values of BNNT/polymer composites remained far below the expectations because of the lack of dispersion of entangled bundles similar to CNTs.[69,70] In light of a recent report proposing potential application of cubic boron arsenide (BAs) among III-V compounds as thermal conductor, the κ value of BAs was estimated to be over 2,000 W m^{-1} K^{-1} according

to the first principle calculations.[71-73] The experimental κ of ~1,000 W m^{-1} K^{-1} – twice that of Cu – was also realized for high-purity BAs synthesized via chemical vapor growth, signifying the possibility of employing new materials for thermal management applications requiring better heat dissipation.

2.2. Interface Engineering for high κ composites

The distribution and surface properties of thermally conductive fillers in a composite have to be rationally designed to achieve high κ of composites. The preparation of polymer composites via conventional mixing of conducting fillers with molten or dissolved polymers often results in poor dispersion of the fillers.[74-76] Therefore, the surface of inorganic fillers is modified or functionalized using organic materials to enhance their dispersibility in the polymer matrix while mitigating the interfacial thermal resistance (ITR) between the fillers and matrix.[77-82] From the microscopic viewpoint, the resistance to thermal conduction commonly occurs at the interface of different materials or phases, which in turn reduces κ owing to strong phonon scattering. It also exists at the interface between the identical materials, referring to as Kapitza resistance.[83,84] Therefore, the design or engineering of the interface between the inorganic fillers and polymer matrix is essential to reducing phonon scattering by enhancing their chemical and/or physical interactions. To chemically modify the inorganic filler surface, a variety of approaches have been proposed on the basis of two major strategies: covalent and non-covalent functionalization.[85,86]

2.2.1. Covalent functionalization

Establishing a strong bond between the fillers and polymer matrix typically requires the formation of a variety of functional groups, including hydroxyl (-OH), carboxylic acid (-

COOH), carbonyl (-C=O), and oxide (-O) groups, on the surface of inorganic fillers. For covalent functionalization, oxidizers are often used to break the crystal bonds to create active sites for the initiation of organic reactions.[87-90] A variety of silane moieties have also been introduced as representative surface modification agents of inorganic fillers because the -SiOR group of the silane coupling agent favors the formation of covalent bonds with hydroxyl groups of the inorganic filler surface by a silylation reaction, while the other side of the silane molecule can be carefully designed by introducing a variety of functional groups to form a compatible interface with the polymeric matrix.[91-93] For instance, the κ value of epoxy nanocomposites was significantly increased by incorporating polyhedral oligosilsesquioxane (POSS)-modified BNNTs.[94] The BNNTs were oxidized using a strong HNO_3 acid for facile silylation, followed by connecting the POSS molecules through the silane group to form a strong interface between the BNNTs and the epoxy matrix allowing the incorporation of high filler loading with uniform dispersion. A variety of organic molecules or macromolecules that are compatible with given polymeric matrices have also been introduced from multiple defect sites of inorganic fillers to improve κ as well as their dispersibility via simple addition or growth.[95]

2.2.2. Non-covalent functionalization

Aforementioned covalent functionalization approaches of inorganic fillers inevitably create defects in their crystalline structures so as to impair the oscillation of phonon modes, giving rise to a significant loss of the intrinsic κ.[96,97] Therefore, non-covalent functionalization has also been explored to provide a functional surface while preserving the intrinsically high κ of fillers. In non-covalent functionalization, organic molecules with desired functional groups are introduced to bridge the gap between the fillers and the polymer matrix by a variety of secondary interactions, such as van der Waals forces and π–π stacking without creating defects

on fillers.[98-101] For instance, the use of 1-pyrenebutyric acid (PBA) allowed non-covalent functionalization of graphite flakes via the π–π interaction between the graphitic carbon and the pyrene molecules of PBA, augmenting both the dispersion of fillers and κ of the epoxy nanocomposites.[102] It is also shown that epicatechin gallate molecules served as a non-covalent coupling agent for dual functionalization with both the poly(vinyl alcohol) (PVA) matrix via hydrogen bonds and the BNNTs via π–π interactions, leading to increased κ of the composites.[103]

In summary, both the covalent or non-covalent functionalization of inorganic fillers have been extensively employed to improve their compatibility with the polymer matrix, resulting in not only uniform dispersion of fillers in the matrix but also augmented κ values. The covalent functionalization is advantageous for establishing a strong interfacial bond, while the non-covalent functionalization facilitates preservation of the intrinsic thermal conduction properties of inorganic fillers. Nevertheless, these approaches still have a large room for improvement in terms of achieving high κ values of composites because of the disadvantages arising from the discrete nature of inorganic fillers and the difficulties in dispersing them in the matrix in a desired manner. Therefore, discussed in the following is the limited increase in κ of particulate-filled composites from the viewpoint of filler geometry.

2.3. Challenges in achieving high κ

The properties of composites containing continuous fibers embedded in a matrix, such as modulus, strength, and electrical and thermal conductivities, can be predicted using the well-known rule of mixtures (ROM) equations.[104-107] The linearly proportional ROM equation sets the upper bound that linearly changes their properties depending on the volume fraction of

fibers, and the properties of the composites thus reach the maximum values, as shown in Fig. 2. Meanwhile, the inverse ROM equation sets the lower bound owing to the discontinuity of reinforcing fibers that are aligned in the transverse direction. Similarly, the particulate-filled polymer composites containing fillers dispersed in continuous polymer matrix exhibit properties including κ close to the lower bound because the geometric feature of discrete fillers is similar to that of the composite with uniaxial, continuous fibers aligned in the transverse direction. Moreover, it is common that the κ of composites is far below the expected value even though a high fraction of fillers with high κ is incorporated. For instance, the epoxy composite containing BN contents of 60 vol% showed a κ value of approximately 11 W m^{-1} K^{-1}, way below that of BN with in-plane κ of ~ 600 W m^{-1} K^{-1}.[108] In addition, the high loading of fillers creates many problems, such as the inhomogeneity of accumulated heat distribution by inadequate dispersion of fillers and poor processability arising from the increased viscosity making mixing difficult.[109] Moreover, it is practically difficult to implement such high loading of fillers to form composites owing to the large difference in surface energy between the filler and polymer matrix. Although the surface functionalization of fillers as introduced in Section 1 can mitigate the surface energy differences, the κ of composites may follow the lower bound as the inverse ROM owing to the existence of originally discrete fillers. Consequently, the particulate-filled composites always have lower κ values than those predicted by the ROM in the entire range of filler content because the fillers are spatially isolated by the surrounding polymer matrix, making the formation of continuous conduction pathways difficult even beyond the percolation.

Therefore, it is necessary to develop new approaches to realize high thermal conduction in polymer composites with low contents of thermally conductive fillers by rational design of

filler architecture and modulation of composite fabrication processes. Therefore, we introduce recent efforts devoted to the development of new approaches for achieving high κ of polymer composites by tuning the dispersion of conductive fillers so as to efficiently reduce the percolation threshold of fillers.

3. Rational design of conductive filler distribution for high κ composites

The preceding section indicates that new design approaches are needed to overcome the limited κ of conventional polymer composites with restricted geometries of fillers. Therefore, many studies have recently been directed towards tuning the geometric orientation and dispersion of thermally conductive fillers that serve as conductive networks in the polymeric matrix. The new approaches devised to achieve desired geometric configuration(s) include preferred orientation of fillers in a certain direction(s), in-plane alignment of 2D fillers and filler segregation. There have been many attempts based on these approaches to control the important properties of polymer composites for particular end applications, such as tensile and compressive strengths, electrical conductivity, electromagnetic interference shielding and barrier performance.[110-113] This section is devoted to reviewing recent efforts to achieving high κ of polymer composites by tuning the filler distribution in the polymer matrix for establishing intended thermally conductive networks.

3.1. Rational design of filler distribution for high in-plane κ

Among various fillers with high κ, we focus mainly on low-dimensional carbon materials and BN allotropes owing to their excellent thermal conduction along the preferred axis in their crystalline structures.[66] These materials offer opportunities to develop highly aligned

architectures along the x and y axes, facilitating high in-plane κ upon successful control of their orientation. Thanks to the high aspect ratios, *i.e.* large lateral size to thickness ratios, 2D materials can be easily transformed to films or sheets with strong anisotropic properties. For example, films made of large-sized graphene-derived materials have been utilized as high-performance thermal conductor with high in-plane κ exceeding that of metals. To fabricate graphene thin films, GO was used as precursor due to its excellent dispersibility in water, enabling homogeneous dispersion for uniformity of films.[114,115] Large-sized GO films were fabricated through filtration through a membrane or electrospray deposition integrated with a roll-to-roll process of GO suspension for stacking the GO sheets. These GO films were converted to highly-oriented graphene films after thermal reduction, resulting in superior κ values above several hundred W m^{-1} K^{-1} with a maximum 1,940 W m^{-1} K^{-1}.[116-120] Based on these findings on graphene thin films having remarkable in-plane κ values, various approaches have been explored to induce morphological orientation of fillers in the in-plane direction of polymer composites, such as prepregging of CFs, electrospinning, laminating, vacuum-assisted assembly, and compression molding. They are discussed in detail in the following and Table 2 summarizes the thermal conductivities of the polymer composites with different filler orientations taken from in the literature.

3.1.1. Fiber pre-impregnation (prepregging)

Traditionally, one-dimensional (1D) CFs have been widely used in various applications, such as aerospace, automotive, and energy industries, mainly in the form of textiles or CF-reinforced composites.[121-124] CFs are available in both PAN-based high strength CFs and highly-crystalline, high modulus graphite fibers. In particular, graphitic CFs have extraordinary κ along the fiber axis, exceeding that of conventional metals.[125,126] When uniaxially oriented

bundles of vapor-grown CFs (VGCFs) were impregnated in an epoxy resin, the VGCF/epoxy composite with 56 vol% of fibers exhibited an exceptionally high κ value of 695 W m^{-1} K-^{1} along the fiber direction, while the value reached 36 W m^{-1} K^{-1} in the transverse direction because of the anisotropic thermal conductivity of oriented VGCFs with κ of ~1,260 W m^{-1} K-^{1} in the fiber direction, as shown in Fig. 3a.[127] Furthermore, CNTs dispersed between CFs served as thermal paths, creating synergistic thermal conduction.[128]

Meanwhile, the amorphous form of CFs or partly crystalline, PAN-based CFs have been widely used owing to their mechanical durability under high deformations and their facile fabrication procedure, but they have an intrinsically poor κ of ~5 W m^{-1} K^{-1}. A simple strategy was developed for improving κ of amorphous CFs by electroplating or electroless plating of Cu with a higher κ value of approximately 400 W m^{-1} K^{-1} on the surface, forming continuous Cu thermal conduction along the fiber axis.[129] Fig. 3b and 3c present the SEM images of pristine and Cu-plated CFs respectively. After impregnation in an epoxy resin, the κ values of the Cu-plated CF/epoxy composites varied depending on Cu thickness which was determined by the plating condition. Further, the in-plane κ of the composite was enhanced by tuning the crystallinity of the electroplated Cu layer via a rapid thermal annealing (RTA) process, in which the κ linearly increased following the Hatta and Taya equation based on ROM.[130]

3.1.2. Electrospinning and laminating

Various low-dimensional nanomaterials, such as nanosheets and nanotubes, have attracted much attention as thermally conductive fillers for polymer composites. In contrast to prepregging which involves a continuous fiber medium, the orientation of these nanofillers can be achieved using the electrospinning method. Electrospinning has been widely used to

produce nanofiber (NF) webs by spraying and spinning the polymer solution under a high electric field.[131,132] When anisotropic nanofillers are mixed in the polymer precursor, they are collectively oriented along the fiber axis when escaping from a narrow nozzle, forming interconnected networks for thermal conduction, as shown in Fig. 4a.[133] One of the most important factors dictating κ is the alignment of NFs, which can be achieved using a rotating drum collector with a suitable rotating speed. On one hand, a relatively low rotating speed of 60 rpm led to random orientation of BNNS/PU NFs with interpenetrated BN networks (Fig. 4a-b).[134] On the other hand, highly aligned BNNS/ poly(vinylidene fluoride) (PVDF) NFs were achieved at a high rotating speed of 1600 rpm (Fig. 4c-d). The high rotating speed matching the ejection rate induced the alignment of fibers in the circumferential direction of the drum collector. The BNNS/PVDF NF sheets were cross-stacked (Fig. 4e-f), leading to an excellent in-plane κ of 16.3 W m^{-1} K^{-1} at 33 wt% BNNS.[135]

A myriad of thermally conductive nanofillers, including 1D nanotubes such as BNNTs and CNTs and 2D nanosheets such as thermally conductive reduced graphene oxide (rGO) and BNNSs, were employed to introduce highly anisotropic sheet structures with a variety of polymer matrices using electrospinning.[134-144] A comparison of the in-plane κ of these composites is given in Fig. 4g. Compared to rGO (pentagon symbols), relatively high loadings of BNNSs (square symbols) of over 10 vol% could be incorporated in the composites, translating into higher κ values. This was possible due to the lower aspect ratios of BNNSs than rGO, allowing a large amount BNNSs to be added in the polymer solution without causing high-viscosity issues. In addition, the composites made from aligned BNNS/polymer NFs (solid squares) showed higher κ than their randomly oriented counterparts (hollow squares) at similar filler loadings, indicating the benefit of fiber alignments in achieving continuous,

thermally conductive networks in the alignment direction. Electrospinning is a scalable process to produce not only thermally conductive films but also fabrics, enabling emerging applications in personal thermal management.[134,145]

3.1.3. Vacuum-assisted assembly vs. doctor blade method

The vacuum-assisted assembly methods have been widely used to prepare bucky papers of low-dimensional materials, *e.g.* CNTs, graphene and hBN.[146-149] The dispersion containing dissolved polymer and nanofillers in the solvent is infiltrated through a membrane under vacuum, filtering out the liquid solvent medium while the nanofillers form a thin film on the membrane by gravimetric sedimentation. 2D nanofillers such as graphene and BNNSs with high aspect ratios tend to form highly-aligned, layered structures in the plane direction aided by the excluded volume between the large nanosheets even in the absence of external forces.[149,150]

Thermally conductive graphene, BN, and MXene are ideal for achieving structures with in-plane orientation via vacuum-assisted filtration owing to their 2D nature, thus many studies have appeared in the literatures, as shown in Fig. 5a.[151,152] A few important parameters need to be controlled to yield high in-plane κ of composites, including functionalization, lateral size, and hybrid fillers. First, proper functionalization of 2D nanofillers is essential to improve the interfacial compatibility between the nanofillers with improved phonon transport, similar to the filler-matrix interfaces as discussed in Section 2.2. Noncovalent functionalization of polydopamine (PDA) on BNNSs was carried out to prepare PDA-coated BNNSs/polyvinyl alcohol (PVA) composite films via vacuum-assisted filtration (Fig. 5b).[153] The PDA on BNNSs enabled spontaneous self-assembly between PDA and the PVA matrix to form a nacre-like

stacked structure. The mitigated interfacial phonon scattering between BNNS and PVA by PDA functionalization contributed to a high κ of ~24.6 W m^{-1} K^{-1} by increasing the packing fraction of fillers up to 70 wt%, 23% higher than that without PDA coating (Fig. 5c). Furthermore, covalent functionalization of BNNS with amino groups (-NH_2) brought negative charges on their surfaces, allowing self-assembly of BNNSs with positively-charged poly(diallyl dimethyl ammonium chloride) (PDDA) after vacuum-assisted filtration. The κ of composites could reach ~200 W m^{-1} K^{-1} in the in-plane direction because of the highly oriented structure of negatively-charged BNNSs bonded by extremely thin layers of positively-charged PDDA through strong electrostatic interactions with a remarkable packing fraction 90 wt%.[154] Therefore, it can be said that increasing the interfacial compatibility between the 2D fillers by functionalization is the key to improving κ by modulating the orientation. Second, large lateral sizes and high aspect ratios of 2D nanofillers are crucial to inducing well aligned structures, as shown in Fig. 5d-e.[155] The increasing volume fraction of graphene sheets in the solution during the infiltration process forced the large graphene sheets to align in the horizontal plane for minimized excluded volumes, eventually forming an anisotropic film containing well aligned graphene sheets. In contrast, the small sheets naturally held small excluded volumes by forming a quasi-isotropic network of randomly-distributed graphene sheets. The alignment of graphene sheets led to a high in-plane κ of 12.7 W m^{-1} K^{-1} in the composite made from large sheets, 27% higher than that made from small ones with a random structure. Third, the hybrid fillers of 0D nanoparticles (NPs) or 1D nanotubes/wires are conducive to reduced interfacial phonon scattering by bridging the rigid 2D nanoplatelets. For example, composites of hybrid fillers of 2D BNNSs and 1D SiCNWs with bonded AgNPs exhibited a synergistic effect for improving not only κ but also the mechanical and electrical insulation properties, as shown in Fig. 5f-g.[156] The

hybrid-filler composite showed a κ of 21.7 W m^{-1} K^{-1}, more than twofold higher than its counterpart containing a single filler of BNNS because of enhanced interactions between the hybrid-fillers (Fig. 5h).

In contrast to the aforementioned spinning methods that can accommodate a relatively low content of fillers (< 50 vol%) in the matrix, the vacuum-assisted assembly allows composites with high filler contents of more than 80 vol% where the polymer mainly serves as binder to bridge the fillers, offering highly percolated geometries for achieving high κ.[157-162] Nevertheless, the vacuum-assisted assembly only applies to soluble polymers of low molecular weights to maintain a low viscosity of the solution for an efficient filtration process.

Meanwhile, inducing a shear force by utilizing a doctor blade has also been widely applied to fabricate composite films with a highly aligned microstructure of 2D fillers.[163,164] The doctor blade approach involves the application of a shear force to the polymer solution containing nanofillers along the blading direction, so that they are oriented horizontally along the flow (Fig. 6a-c).[165,166] Typically, BNNSs and graphene layers are most suited for this process.[167,168] This technique is particularly useful for polymer composite solutions with high viscosities because the viscous medium plays an important role in generating a collective flow to orient the fillers.[166] Therefore, horizontal orientation of BN microplatelets at a low concentration was achieved in a PVA matrix, resulting in increased κ.[169] Polymer solutions with high filler concentrations have also been prepared by ball milling followed by centrifugation to achieve higher κ values.[166,170,171] When the highly concentrated graphite nanoplates (GNP)/N-Methyl-2-pyrrolidone (NMP) ink mixed with thermoplastic urethane (TPU) was coated using a doctor blade, the resulting composite exhibited a high in-plane κ of 71.18 W m^{-1} K^{-1} at a filler loading of 80 wt%.[171] In addition, the introduction of a second filler, *e.g.*, nanodiamond particles, was

advantageous to increasing the in-plane κ by facilitating the connection of main 2D BNNSs.[172]

Although the microstructures of the resulting composites are quite similar, the vacuum-assisted assembly and doctor blade approach adopt different principles on how the forces are applied to achieve orientation of low-dimensional fillers. Consequently, these two approaches have their own advantages in terms of processing methods: the vacuum-assisted assembly is suitable for fabricating composite thin-films suitable for thin devices, whereas the doctor blade approach is easy to fabricate large-area sheets depending on the blade size and is also suitable to use high viscosity inks. This means that it is necessary to select an appropriate approach according to the application of final products.

3.1.4. Compression molding

Similar to injection molding, compression molding has been an important technique for the processing of ceramic powders to manufacture final products in bulk form with given shapes and sizes.[173-175] By introducing the heating zone, this approach also allows the processing of viscous polymers with specific transitions of glass transition temperature (T_g) and melting temperature (T_m). Polymer composites with 2D NSs having a high aspect ratio are fabricated using this technique under controllable pressure and temperature. As expected, 2D NSs are collectively oriented in the in-plane direction by uniaxial compression applied normal to the surface of the product, as shown in Fig. 6d. Thus, compression molding favors introducing alignment of 2D NSs in thermoplastic polymers that are melt-processible, unlike the electrospinning or vacuum filtration approaches based on a solution process. 2D NSs with high κ, such as graphite and BNNSs, have been studied to achieve oriented structures in a variety of polymers for enhanced κ in the in-plane direction.[176-179] For example, styrene–ethylene–

butylene–styrene (SEBS) films with highly-aligned hBN platelets were prepared by ball milling followed by hot pressing (Fig. 6e,f).[180] SEBS molecules adjacent to the hBN surface during precipitation served as a binder, while the hBN platelets were perfectly packed and connected along the longitudinal axis. The hBN/SEBS composite film exhibited an in-plane κ of ~45 W m^{-1} K^{-1} when 95 wt% hBN was added. A nacre-like layer-structured composite based on 2D Al_2O_3 platelets was also fabricated by compression molding of epoxy mixture.[181] By incorporating AgNPs onto each platelet, the resulting Al_2O_3-AgNPs/epoxy composites exhibited significantly improved κ compared to the Al_2O_3/epoxy composites without AgNPs. In addition, designing segregated structures was proposed to fabricate polymer composites with oriented fillers through compression molding. Hot-pressing of BNNS-assembled PS microspheres at a temperature above the T_g of PS allowed preferential in-plane orientation of BNNSs in the PS matrix, giving rise to a significantly enhanced in-plane κ of 8.0 W m^{-1} K^{-1} at a filler loading of 13.4 vol%.[182] Interestingly, the utilization of composite particles of PA6/GNPs with a hBN coating on their surface facilitated synergistic enhancement of κ up to 8.96 W^{-1} K^{-1} at a filler loading of 4.12 and 16.85 vol% of GNPs and hBN, respectively.[183]

The in-plane κ values of composites made from different 2D fillers by the foregoing three techniques are compared in Fig. 6g. Amongst different fillers, the amounts of graphene or rGO sheets (triangles) that can be added into the composites were limited to 10 vol%, much lower than other fillers such as MXene (squares), BNNS (circles), h-BN (diamonds), and graphite (hexagons).[184-187] This finding arose from the much higher aspect ratio of graphene/rGO than the other fillers, making the solution or molten polymers highly viscous at high loadings and thus difficult to process. Nevertheless, the excellent κ of graphene/rGO and their high aspect ratios led to high κ of over 10 W m^{-1} K^{-1} for composites with filler loadings lower than 7 vol%

using vacuum-assisted filtration (red triangles). A similarly high κ was only achieved at filler loadings higher than 10 vol% for composites containing other fillers. For different processing techniques, the vacuum-assisted filtration (red symbols) and the doctor blade method (blue symbol) seem to yield higher κ values of composites than the other two. This can be attributed to the better alignment of 2D fillers achieved by these two techniques than hot pressing or electrospinning. However, vacuum filtration is more difficult to scale up for mass production than the other two where the specimen size is limited by the size of the filtration setup and the time required to filtering out solvents especially when a thick film is desired. Meanwhile, the doctor blade method requires suitable processing conditions and high-purity dispersions because the blade may be worn by impurities or the film may be damaged during the casting process, degrading the quality of as-fabricated composite films. The electrospinning and hot pressing are scalable processes which require rather high filler loadings to achieve a κ of higher than 10 W m^{-1} K^{-1}. Compared to electrospinning, hot pressing seems to be more promising for incorporating extremely high loadings (> 50 vol%) of bulk fillers, such as hBN and graphite, resulting in ultrahigh in-plane κ of over 40 W m^{-1} K^{-1}.

3.2. Rational design of filler distribution for high through-plane κ

While the development of polymer composites with high in-plane κ is important, many heat dissipation components in electronic devices, such as the thermal interface materials (TIM), packaging materials, and flip-chip bonding materials, also require high through-plane κ values.[188-190] Therefore, much efforts have been devoted to developing processing strategies leading to vertical orientation of the fillers against the device plane for efficient heat dissipation. To this end, sensible geometrical arrangement of the fillers that form quasi-continuous pathways for thermal conduction in the polymer matrix is required. Here, we introduce

representative approaches that allow vertical arrangement of the fillers with a variety of dimensions through not only crystallographic growth in the vertical direction and the use of electrical and magnetic fields during the process, but also templating by ice and special phase separation of binary composite mixtures. Table 3 summarizes the thermal conductivities of the polymer composites made therefrom and the detail are discussed in the following.

3.2.1. Vertically grown anisotropic fillers

Two common approaches, including chemical vapor deposition (CVD) growth and template-assisted electrodeposition, have been used to vertically grow anisotropic fillers, as shown in Fig. 7. Designing a vertical array of fibrous materials can provide a specific geometry oriented along the z axis. The architecture can form perfectly continuous thermal conduction pathways without contact resistance between the fillers, which commonly occurs in conventional polymer composites.[191] An ideal geometry can be achieved by unidirectional growth along the z axis over a wide area with uniformity. Several studies have recently reported CNT arrays vertically grown by chemical vapor deposition (CVD) capable of large-scale synthesis of long CNTs, which delivered κ as high as 6,600 W m^{-1} K^{-1}.[192,193] The vertically grown CNT array was further densified by biaxial compression, followed by infiltration of a molten thermoset epoxy to form an aligned CNT/epoxy nanocomposites with a high CNT loading, as shown in Fig. 7a.[193] The composite with a high packing density of 17 vol% CNTs exhibited a through-plane κ of ~4.8 W m^{-1} K^{-1} (Fig. 7b). The κ value was quite low owing to the high ITR arising from the large surface area of CNTs. By introducing a proper surface treatment agent, such as pyrenylpropyl phosphonic acid (PPA), the ITR of the CNT array/copper interface was significantly reduced by 75–85% (Fig. 7c-e).[194] Beyond the direct growth of uniaxial tubes and fibers, the template-assisted growth using porous templates is another approach for fabricating

1D arrays of thermally conductive materials through controlled and confined growth. By combining electrodeposition techniques within common polymeric membranes with controlled pores, metal nanowire arrays of Ag or Cu were obtained (Fig. 7f).[195-197] The polymer composites with aligned metal nanowire arrays demonstrated κ as high as several hundred W m^{-1} K^{-1} owing to the intrinsically high κ of the materials, and the value was shown directly proportional to the nanowire volume fraction (Fig. 7g).

The bottom-up growth of 1D fillers is most useful for TIMs by directly constructing vertical thermal dissipation pathways on metal substrates with a small thickness. The highly packed, continuous NT or NW arrays aligned in the thickness direction provide excellent through-plane κ. Nevertheless, both CVD and electrodeposition are rather expensive processes relying very much on carefully controlled growth parameters.

3.2.2. External-field induced orientation of fillers

Controlling the perpendicular orientation of anisotropic fillers with a large aspect ratio allows the formation of quasi-arrays, effectively reducing the percolation threshold for thermal conduction. Among various efforts for controlling the directionality of anisotropic fillers, applying electric and magnetic fields is a useful route based on the intrinsic electrophoretic mobility of materials.[198,199] BNNSs can be polarized by electric fields and thus in-situ aligned in the polymer matrix depending on the type of field, their size, and loading (Fig. 8a).[200-202] The orientation of BNNSs was established in thermoset polymers using switching direct current (DC) and alternating current (AC) electric fields, as shown in Fig. 8b and c, respectively.[201-204] Under an AC field, BNNSs were oriented in the field direction forming thin bundles to connect the two electrodes. Relatively thicker bundles of BNNSs were formed under

a DC field, providing a higher degree of interconnection between the BNNSs, leading to a κ of 0.73 W m^{-1} K^{-1} in the through-plane direction. 30% higher than that prepared under an AC field, at 15 vol% BNNSs of an aspect ratio of 141. The aspect ratio of BNNSs was an important factor determining the degree of interconnection through the formation of bundles, with a higher aspect ratio of 228 giving rise to an even higher κ of 1.56 W m^{-1} K^{-1}. The functionalization of BNNSs was found to increase the responsivity to electric fields. For instance, TiO_2 NPs applied on the BNNS surface allowed facile orientation of BNNSs with weak electrical dipoles even under a low voltage of 600 V.[205] In addition to alignment in the molten matrix, the fillers can also be pre-aligned in the form of arrays prior to the infiltration of polymers. The chopped CFs with a maximum length of 1 mm and excellent κ of 832 W m^{-1} K^{-1} along the length axis were oriented using electric fields to obtain 1D fiber arrays in a large area, as shown in Fig. 8d-f.[206] When the CFs were placed between two plates under an applied potential of 30 kV, they were gradually propelled toward the opposing electrode because of electrostatic attraction, giving rise to a highly oriented CF array. The CF/rubber composite fabricated by infiltrating molten rubber exhibited a remarkable through-plane κ of 23.3 W m^{-1} K^{-1} at a filler loading of 13.2 wt%.

Inducing a magnetic field is also useful for filler orientation. In this case, employing magnetic NPs that are responsive to magnetic fields as fillers is essential owing to the lack of magnetic dipoles of common thermally conductive fillers, except CNTs and graphene that can be aligned using an exceptionally high magnetic field.[207] BNNSs have been widely used as a representative thermally conductive filler, where their surface is functionalized with magnetic NPs, such as Fe, Fe_2O_3, and Fe_3O_4, to facilitate rotational mobility of BNNSs under the magnetic field, as shown in Fig. 8g-i.[208-212] In view of ease of synthesis and excellent magnetic

responsivity of Fe_3O_4, thermally conductive fillers, such as graphene, CNTs, SiC, AlN, Al_2O_3, and diamond particles, have been hybridized with Fe_3O_4 NPs for vertical orientation.[213-218] Meanwhile, Ag-coated Ni particles that are magnetically responsive and thermally conductive were also studied.[219] Under a magnetic field, the Ag-coated Ni particles were not only aligned along the field direction but also were soldered by the soft Ag layers to form interconnected bundles. The Ag-coated Ni/poly(dimethylsiloxane) (PDMS) composite exhibited a high through-plane κ of ~6 W m^{-1} K^{-1} by overcoming the chronic problems of filler-to-filler contact resistance.

In summary, the electric and magnetic field-assisted strategies are more versatile to align both 1D and 2D fillers than the bottom-up growth of 1D fillers by CVD. Nevertheless, relatively high electric and magnetic fields and a long time are needed to achieve good alignment, depending on the responsiveness of the fillers. Therefore, these techniques are most suitable for small-scale alignments such as those in thin TIMs.

3.2.3. Directional freeze casting by ice templating

Ice templating – mostly unidirectional freezing – is a technique that exploits the nucleation and growth of solvents along the temperature gradient with directionality as the liquid medium solidifies at the freezing point.[165,220] During the solidification of water, the dispersed particles are rearranged into the empty space excluding the volume of ice crystals, causing vertical distribution of fillers, as shown in Fig. 9a. By sublimation of the ice crystals, followed by filling of the polymeric materials, the resulting materials are composed of vertically confined nanoparticles within the polymeric matrix. Thus, the ice templating approach is advantageous for forming vertical conduction paths using any kind of fillers regardless of its dimensions by

controlling the sacrificial ice-phase exploding particles. Many researchers have adopted this approach to host vertical percolation using a variety of low-dimensional fillers.[221-224] A highly oriented network structure of BNNSs was realized in the epoxy matrix using the unidirectional freeze casting.[225] The ice crystals growing from the cold fingers expelled the 2D BNNS fillers so that the jammed BNNSs were naturally oriented along the vertical direction bridged by PVA matrix (Fig. 9b). The interconnected 3D BNNS skeleton was obtained after freeze drying, and a composite is produced after infiltration with molten epoxy. The percolated structure of 3D-BNNSs in the epoxy matrix delivered an improved κ of 2.85 W m^{-1} K^{-1} at a relatively low BNNS content of 9.29 vol%. To further control the filler orientation, a bidirectional freezing approach has been also proposed.[226] Unlike the unidirectional freezing, the bidirectional freezing method generates temperature gradients along both the horizontal and vertical directions by introducing a PDMS wedge between the cooling stage and suspension, so that the ice crystals nucleate and grow into a long-range lamellar pattern, as shown in Fig. 9c. During freezing, the fillers are spontaneously assembled into large-sized 2D domains confined between the ice crystals, which are beneficial for improving the in-plane κ by providing long-range microstructures (Fig. 9d).[227] The aligned structures are affected by a number of freeze-casting parameters, including the filler content and freezing temperature. A higher BNNS content resulted in a higher density and better alignment of BNNS aerogel prepared by unidirectional freezing casting, giving rise to a higher κ value of the final composite.[225] Given this approach driving the rearrangement of fillers by external force, various types of fillers, including BNNSs, rGO, CFs, SiCNWs, and SiC microwires (MWs), have been successfully adapted regardless of their dimensional characteristics.[223,228-232] Moreover, different types of organic or inorganic fillers are additionally incorporated into the dispersion to complement the

structural weakness of the as-cast filler architecture or to synergistically increase κ of the finished products.[233-241]

Beyond the unidirectional and bidirectional freezing methods, the long-range order of 2D fillers was controlled via the radial freezing method, where ice crystals were radially grown from the periphery towards the center of a cylindrical container, resulting in radially symmetric ice scaffolds (Fig. 9e).[242] Through radial freezing of BNNS/chitosan aqueous slurry followed by freeze-drying, radially-aligned BNNS aerogels with a long-range lamellar structure were fabricated.[243] After infiltration of epoxy, the composite containing BNNSs aligned in both the *x*-*y* plane and the *z* axis exhibited a high in-plane κ of 3.78 W m^{-1} K^{-1} as well as a through-plane κ of 4.02 W m^{-1} K^{-1} at a filler loading of 15 vol%. Further, the radial freezing method was particularly useful in designing biomimetic scaffolds of low-dimensional fillers. For example, a tree-leap-like structure with multiple side branches was designed by radially freezing rGO followed by vertically growing graphene nanofins onto the rGO (Fig. 9f).[244] The PMMA composite with such bimodal graphene frameworks delivered a through-plane κ of 4.01 W m^{-1} K^{-1} even at an ultralow filler loading of 1.53 vol%. In addition, the GO/BN hybrid scaffold mimicking conifer trees with vertically- and radially-aligned channels allowed a high comprehensive κ of 2.94 W m^{-1} K^{-1} at a filler loading of 11.65 vol% after impregnating PEG into the scaffold.[245]

3.2.4. Transformation of oriented direction.

Among various thermally conductive fillers, anisotropic fillers with excellent κ along the axial direction have been extensively used for designing thermally conductive polymer composites. Because such fillers tend to lie parallel to the in-plane direction by gravity, it has been also

proposed to improve the through-plane κ by transforming the direction of freestanding materials or their polymer composites with strong anisotropy along the in-plane direction.[136] For example, graphite freestanding films with extremely high in-plane κ could be stacked by polyline folding or rolling (Fig. 10a-b).[246,247] After infiltrating the multi-stacks of graphite films with a molten thermoset, such as epoxy and PDMS resins, followed by cutting in the perpendicular direction, a composite with vertically-aligned graphite fillers could be successfully fabricated. The resultant composite exhibited excellent through-plane κ values as higher as 614.85 W m^{-1} K^{-1} due to its high degree of orientation. Similarly, several polymer composite films with highly-oriented rGO or BN filler networks could also be cut in the thickness direction to obtain high through-plane κ values. To further increase the orientation of fillers in the polymer before cutting, a thinning process was introduced for the melt-processed thermoplastic PP/graphite composites, in which the graphite fillers dispersed in the PP matrix were oriented horizontally together with PP.[248] The ensuing composite after stacking and cutting with vertically-oriented graphite fillers exhibited through-plane κ values of 4 W m^{-1} K^{-1} at a filler loading of 20 vol% with a high anisotropy of 8.37.

Apart from changing the stacking direction by 90 degrees, the L-shaped kinked tube was utilized to extrude PVDF composites containing aligned GNPs in the in-plane direction to achieve high through-plane κ (Fig. 10c). During extrusion, the pre-oriented GNPs in the PVDF matrix was preferentially aligned perpendicular to the flow direction by the laminar flow of PVDF melt, resulting in a high through-plane κ of approximately 10 W m^{-1} K^{-1} at a filler loading of 25 vol% (Fig. 10d).[189] While the intuitive transformation process of filler orientation is attractive as an effective approach that can significantly improve the through-plane κ, it is necessary to establish how such a process can be applied in practical applications.

3.2.5. Other methods

Natural templating. In addition to ice templating, a variety of templates with specific structures have been used to guide the anisotropic rearrangement of fillers to induce through-plane thermal conduction. As discussed in Section 3.2.3, the use of a template with oriented pores is also advantageous to organize anisotropic fillers along the vertical direction. For example, natural wood – an anisotropic material – was used to prepare templates, as shown in Fig. 11a-b.[249] When the lignin in wood is removed, the pure, well-aligned cellulose microchannels allow for the infusion of poly(amide imide) (PAI). High-temperature heat treatment of PAI-infiltrated lignin-removed wood yielded a carbonized wood/PAI composite which exhibited anisotropic thermal conduction. Cigarette filters composed of vertically aligned cellulose fibers were also employed to achieve anisotropic orientation of fillers along the fiber axis, as shown in Fig. 11c-d.[250,251] Low dimensional fillers like Cu flakes and graphene nanoplatelets (GNPs) could be coated onto the cellulose fibers as thermally conductive fillers, improving the κ of epoxy-infused composites in the transverse direction.

Vertical double percolation. The double percolation approach is based on the common phase separation of the polymer matrix. When two immiscible polymers are mixed, they automatically guide the micro-phase separation.[252,253] By properly controlling the molar ratio, solubility, and experimental conditions, a vertical double percolation (VDP) structure composed of two phases separately aligned along the perpendicular direction was obtained (Fig. 11e).[254] When thermally conductive fillers with specific chemical characteristics are incorporated in the binary polymer, the fillers migrate into one or the other phase due to the compatibility with the matrix phase determined by the hard/soft acid/base (HASB) principle.[255] Therefore, the fillers concentrated in any one of the two phases can efficiently reduce the

percolation threshold to obtain κ in the vertical direction. Consequently, the double percolation approach leads to the concentrated structure of fillers via selective dispersion with chemical characteristics, which is quite similar to the ice templating approach where the solvent phase also pushes out and makes the fillers concentrated with physical confinement.

Yorifuji *et al*. first reported on polyimide (PI) blend films with silver nanoparticles (AgNPs). A blend of two PIs with sulfur and fluorine moieties, respectively, was realized via simple spin-coating, followed by thermal curing. The pre-mixed silver nitrate was precipitated in the PI phase containing a sulfur moiety by the difference in affinity, leading to the formation of thermal conduction paths by concentrated AgNPs, as shown in Fig. 11f-g.[256] The use of pyramidal ZnO NPs also helped the NPs precipitate into the PI phase with a fluorine moiety. The resulting PI blend films with selectively dispersed ZnO NPs exhibited a κ of 1.54 W m^{-1} K^{-1}, which is 3.1 times that of a PI film with homogeneous 27 vol.% ZnO NPs.[257] Further, the use of needle-shaped ZnO with a high aspect ratio to replace the pyramidal ZnO NPs improved the κ value up to ~2.1 W m^{-1} K^{-1} because the ZnO NPs confined within the PI phase with fluorine moiety formed thermal conduction networks along the vertical direction.[258] Recent studies on the double percolation approach also indicate improved mechanical properties and κ of the composite film. Although only a few studies have reported on the VDP structure, this is a simple yet straightforward approach for achieving a structure that allows high through-plane κ values from a practical viewpoint.

3D printing. 3D printing, known as additive manufacturing, has promised as a versatile approach to manufacture components with complex 3D structures through computer-aided design. With these advantages, the 3D printing method has been employed in thermal management.[259] The technique is particularly useful in modulating the filler orientation in the

intermediate product by controlling the printing direction. Among a variety of 3D printing methods, the ink-based approach utilizing nozzles allows the direction of objects extruded from the nozzle to be controlled. In this sense, one can expect that the filler orientation in the polymer matrix is tunable because the orientation direction of low dimensional fillers is strongly affected by the shear force applied in extrusion. For example, BNNS inks dispersed by a bioreagent (pluronic F-127) aqueous solution were 3D printed in the form of microscale rod arrays in which the BNNSs were vertically-oriented along the geometry of rods (Fig. 11h).[260] After infiltration with PDMS resin, the PDMS composites with vertically-oriented BNNSs presented a through-plane κ of 1.5 W m^{-1} K^{-1} at a filler loading of 22 wt%. With an advantage of easy inking process for drawing complex shapes, epoxy composite inks composed of GNPs and chopped CFs were also directly printed to form heat sinks with a complex 3D shape.[261,262] In addition, by incorporating a CNT buckypaper between the 3D-printed heat sink layers, its heat dissipation performance was further increased, while demonstrating a large reduction of the LED device temperature by 11.4 °C with the heat sink.

Combination of multiple processing methods. In order to vertically orient anisotropic fillers with high κ, it is required to apply a force against gravity as previously discussed. Therefore, efforts have been reported towards designing polymer composites with vertically-oriented low-dimensional fillers by sequentially using two or more different techniques. Multiple processes are combined to prepare a composite having fillers oriented in the plane direction and to restructure their orientation. For example, electrospinning of PVA/BNNS composites led the oriented structure of BNNS fillers along the fiber direction.[136] After rolling up the strip of fiber membranes and impregnation with PDMS, a cylindrical composite was obtained with the BNNSs vertically oriented along the cylinder axis. The composite delivered a through-plane κ

of 1.94 W m^{-1} K^{-1} at a filler loading of 28.7 wt%. Otherwise, the 3D printing method is well-established in preparing composites with fillers oriented primarily in the in-plane direction. By mainly, A variety of thermoplastics, such as TPU, PA6, and LLDPE, have been successfully employed as the matrix for large scale fabrication using the fused deposition modeling (FDM)-based 3D printing technique.[263-266] Such melt-processable thermoplastics facilitated the orientation of low-dimensional fillers, such as hBN, graphite, and GNPs, owing to the strong shear force induced by the viscous polymer melt during extrusion through a nozzle. When the filament bundles of the polymer composites drawn by FDM-based 3D printing were cut vertically and rearranged to fuse in the horizontal direction, the through-plane κ values of the resultant composites were efficiently increased even at a relatively low filler loading thanks to the long-range network structure of the oriented fillers (Fig. 11i).[266] However, the voids generated by fusion of bundles of cylindrical filaments need to be removed. Interestingly, with the advantage of 3D printing that allow directly manufacturing end-products, study has also been reported to induce simultaneously magnetic fields for leading vertical orientation of thermally conductive fillers.[267] Unique thermal transport patterns were created for effective heat dissipation in the hBN/epoxy composite using the stereolithographic (SLA)-based 3D printing, in which the hBN platelets modified by superparamagnetic iron oxide NPs were vertically oriented. The resulting composite exhibited an excellent through-plane κ of 7.28 W m^{-1} K^{-1} at a filler loading of 60 vol%, facilitating steady-state passive cooling of high-density electronics.

The through-plane κ values of composites made from different fillers using the foregoing approaches are compared in Fig. 12. The vertical growth is most suitable for producing high-quality 1D fillers such as CFs, CNTs and metal NWs (red symbols) with excellent alignment,

resulting in higher κ values than those containing 1D fillers (hollow symbols) made by other techniques. Both external electric/magnetic fields and ice templating facilitate the vertical orientation of 2D fillers (solid symbols), while ice templating (purple symbols) and transformation of oriented direction (blue symbols) are more effective in constructing interconnected filler networks than electric/magnetic fields (green symbols), giving rise to generally higher κ of composites at similar filler loadings. Nonetheless, it is still a challenge to achieve a through-plane κ of over 10 W m^{-1} K^{-1} because of the difficulty in vertically aligning the fillers at a high density.

3.3. Isotropic, thermally conductive composites

Many studies have attempted to establish thermal conduction pathways in polymer composites in the parallel or perpendicular direction by controlling not only spatial distribution but also the geometrical orientation of fillers. In particular, the structures capable of vertical thermal conduction are aimed to form interconnected networks at a percolation threshold lower than that achieved by usual filler dispersion. The κ values of conventional particulate-filled polymer composites depend on the directionality of fillers in the matrix, which also suffer from the requirement of high filler content to reach a percolation threshold. Thus, rational design of filler distribution is important for overcoming the limitation of conventional polymer composites by not only reducing the percolation threshold but also maintaining the isotropic κ regardless of the filler directionality.[268] In this section, research efforts devoted to revealing three-dimensional (3D) isotropic thermal conduction by controlling the macrostructure of filler distribution in the polymer matrix are reviewed. They include deformable fillers, foam structure, hydrogel networks, and particulate segregation, whose details are discussed in the following. Table 4 summarizes the thermal conductivities of the polymer composites with these

special filler architectures.

3.3.1. Deformable fillers

Common thermally conductive fillers are composed of rigid inorganic or metallic crystals. Although these fillers are in contact with each other upon the formation of percolation, the electrons or phonons are scattered at the interface between them, causing significant reductions in thermal conduction.[269] The interfacial resistance means that the use of conventional fillers in the polymer matrix limits the ideal κ of the composite. Therefore, designing an architecture that forms continuous thermal conduction pathways is required to minimize the interfacial resistance. The melting temperature of crystalline materials depends on their size, especially for NPs and NWs with a large surface area, and the value for nanofillers is significantly lower than that of bulk materials.[270,271] One can expect that the use of thermally conductive fillers with such nanoscale features would be beneficial in forming continuous networks in the polymer matrix when the nanofillers have a similar temperature for deformation to the polymer materials. Highly interconnected Ag networks are formed in an epoxy composite, as shown in Fig. 13a-c.[272] The Ag NPs were uniformly dispersed in the mixture of uncured epoxy resin and a curing agent. Upon heating the mixture for curing, the AgNPs partly fused with each other owing to their lower melting temperature when they are at nanoscale, forming self-assembled Ag networks in the matrix. The epoxy composite containing AgNPs of 20 nm in diameter showed an extremely high κ of 26.94 W m^{-1} K^{-1}, while the epoxy composites with the same loading of Ag MPs having a diameter of 4.2 μm had a κ of only 0.58 W m^{-1} K^{-1}. This surprising particle-diameter-dependent observation indicates that metallic nanoparticles could allow the formation of thermally conductive interconnected networks thanks to their advantageous deformable characteristics at nanoscale, which otherwise was not possible in their bulk form.

By optimizing the processing condition by (i) aggregation of poly(vinylpyrrolidone) (PVP)-coated AgNPs, (ii) removing the PVP stabilizer, and (iii) sintering of AgNPs, the κ was further improved reaching an exceptionally high value of ~38.5 W m^{-1} K^{-1} at a filler loading of 45 vol%.[273] The networks of AuNWs with a high aspect ratio of ~100 and a diameter of ~5 nm were formed in the PDMS matrix by cold-welding among neighboring wires.[274] Further, microwave heating of PDMS nanocomposites with AgNW reinforcements having a diameter of ~10 nm allowed the formation of a AgNW network structure by partial fusion without deteriorating the PDMS properties. The resulting composite exhibited an excellent κ of ~6 W m^{-1} K^{-1} at a low filler content of ~4 vol%, as shown in Fig. 13d-f.[275,276] The branched morphology of AgNWs was found to favor a higher κ than the composites with unbranched and single wires.

3.3.2. Foam templating

Foam-like structures can produce highly percolative networks by growing or depositing conductive fillers directly on the foam surface. A thermal network structure was achieved by fabricating quasi-continuous AlN foam, followed by polymerization of polystyrene to form pores.[277] At above approximately 55 vol% of AlN, the percolation was obtained by forming a continuous thermal conduction path of AlN, resulting in a drastically increased κ value of approximately 200 W m^{-1} K^{-1} at a filler content of 70 vol%. Metal foams that are widely used in energy absorption and lightweight construction have been investigated as not only thermally conductive skeletons but also ideal templates for depositing or growing conductive nanofillers with 3D interconnection.[278-280] The composites consisting of Cu foam impregnated with paraffin wax exhibited a high κ of ~4.95 W m^{-1} K^{-1}.[281] The surface coating of Ni foam with GO improved the interfacial compatibility with an epoxy matrix, giving rise to an interface-

stabilized metallic foam composites with a high κ.[282] In addition to depositing nanofillers, high-quality nanofillers can be grown on Ni or Cu foam surface by CVD to form freestanding nanofiller foams. A 3D graphene foam/PDMS composite was designed via chemical treatment of CVD-grown graphene foam using PDA for improved interfacial compatibility, resulting in a κ of 28.77 W m^{-1} K^{-1} at 11.6 wt% graphene foam loading.[283] The foam structure composed of hybrid carbonaceous materials was also advantageous for improving κ owing to the synergistic reduction in interfacial resistance between the nanocarbon fillers. A CNT sponge coated with polyimides (PIs) followed by graphitization of PIs enabled the formation of a graphene network structure between the CNT sponge and PI, as shown in Fig. 14a-b.[284] Further, a coating of PAA and subsequent imidization led to the realization of PI/CNT sponge composites with an excellent κ of ~10.89 W m^{-1} K^{-1} and a low σ of 0.29 S m^{-1}. Given the low density of graphene or CNT foams, the total filler content to be obtained in the composites after infiltrating a polymer is rather limited. To further increase the filler loading, other fillers have also been incorporated into the polymer matrix before impregnating the foam networks.[285-289] For example, the graphene foam/PDMS composite infiltrated with graphene flakes showed significant improvement in κ, where both the graphene foam skeleton and graphene flakes played the role of multiple thermal conduction pathways. In addition to carbon foams, freestanding hBN foams synthesized using atmospheric-pressure chemical vapor deposition (APCVD) showed potential for structural thermal conduction through thermally conductive yet electrically insulative pathways for wide-ranging applications.[290]

Recent efforts have focused on the use of polymeric foams rather than metallic ones. The polymeric foams can provide a template for forming continuous thermally conductive pathways along their interconnected structures. Representative sponge materials capable of

forming the foam structure, such as melamine and poly(urethane) (PU), are commonly used. As thermally conductive fillers, 2D materials – mainly graphene allotropes and BN – are widely employed to construct such a continuous structure with a large surface area that facilitates areal contacts with the non-planar foam with a curvature. Once the assembly is impregnated with a polymeric matrix, such as epoxy or PDMS, the polymer composite possesses thermally conductive pathways formed along the surface of continuous soft foams, as shown in Fig. 14c-f.[291,292] Furthermore, the graphene nanomaterials assembled onto the soft foam could be tuned to a highly crystalline nanomaterial via pyrolysis or a continuous morphology via high-frequency heating and removing the sacrificial foam skeleton so as to obtain high κ values.[293,294] Polymerization and foaming of PU precursors with BN dispersion also produced a composite foam composed of BN nanosheets embedded in the continuous PU.[295]

Both metal and polymer foams serve as versatile templates for rational assembly of thermally conductive fillers to form interconnected 3D networks. High-quality fillers can be grown on metal foams by CVD to achieve highly conductive foam structures, leading to higher κ of composites than those made on polymer foams. Nevertheless, the overall process using polymer templates is simpler than that involving metal templates because the metal foams need to be removed by acids.

3.3.3. Hydrogel networks

Another option for obtaining 3D filler networks such as foam structures is to form hydrogels. A hydrogel is a network of hydrophilic polymers that hold a large amount of water as the dispersion medium, in which the 3D solid structure of the colloidal gel is preserved.[296] The hydrogel scaffolds are constructed after careful freeze drying of water, which is quite similar

to directional freeze casting based on ice templating as discussed in Section **3.2.3**. However, there is a significant difference between these two approaches in that the hydrogel scaffolds have no specific directionality enabling the formation of isotropic thermal conduction pathways. Several types of well-known thermally conductive fillers with favorable dispersibility in aqueous media favor applications in the form of hydrogel structures. For instance, 2D materials, such as GO and hydroxylated BN, are dispersible in water.[297-299] When these materials are dispersed in aqueous dispersion of PVA, a 3D framework of thermally conductive fillers coated with PVA could be obtained by freeze drying of water. By filling the porous structure with a polymer matrix, such as epoxy and poly(imide amide) (PAA), the resulting polymer composites exhibited increased isotropic κ arising from the 3D filler network structure.[300,301]

The quality of 3D thermally conductive networks in hydrogels is controlled by the gelation characteristics and effective interconnection between fillers. The gelation characteristics of hydrophilic GO are useful for achieving a GO-only hydrogel framework without hydrophilic polymers.[302,303] During the reduction, a gel-like structure is formed by swelling of self-assembled GO with the aid of water. To improve the interconnection between the fillers, hybrid filler networks containing nanofillers of different dimensionalities are normally constructed in the hydrogels. For example, thermally conductive 1D Cu NWs in 2D GO and L-ascorbic acid synergistically increased the κ of the composite.[304] A skeleton of 1D cellulose nanofibers assembled with 2D BNNSs was also used to strengthen the contact of each BNNS as well as the 3D structures, as shown in Fig. 15a-b.[305] The epoxy-infiltrated 3D BNNS/cellulose nanofiber composite (Fig. 15c) exhibited a high κ of 3.13 W m^{-1} K^{-1} at 9.6 vol% of BNNSs, which is 11 times that of the epoxy composite with randomly dispersed BNNSs. In addition to nanofillers of different dimensionalities, those 2D fillers of different lateral sizes could also

synergistically improve the κ of composites. In the presence of BNNSs with a lateral size ranging 200–400 nm, the GO sheets with a larger size of 1 to 2 μm were assembled to form a hybrid 3D network structure, in which PA6 was covalently grafted onto the GO sheets for infiltration of the PA6 matrix.[306] The defects presented in the large-size GO sheets were patched by small-size BNNSs which in turn ameliorated the phonon scattering, leading to 87.6 % higher κ than that containing GO sheets alone.

3.3.4. Particulate segregation

Traditionally, the segregation of fillers in the polymer matrix has been used to enhance the electrical properties, such as σ and EMI shielding performance, arising from the significantly reduced percolation threshold.[307-309] The segregation of fillers also affects the κ of polymer composites by introducing quasi-continuous thermal conduction pathways. A segregated structure of Cu continuous layers was fabricated by electroless plating onto polystyrene (PS) beads followed by hot pressing of Cu-plated PS beads, as shown in Fig. 15d-f.[310] The segregation of Cu layers between each PS domain led to a κ of ~26 W m^{-1} K^{-1} at 23.0 vol% Cu, which is 58 times that of the conventional PS/Cu composite (Fig. 15g). Encouraged by the possibility of high κ values of segregated structures, many researchers have attempted to design segregated polymer composites using common thermally conductive fillers. In particular, powders were simply mixed to achieve a segregated structure by considering the size difference between the polymer and the filler particles, in which the fillers are naturally located between the jammed polymer particles.[311] Hot pressing above the glass transition temperature of polymer particles led to different types of segregated polymer composites by incorporating a variety of fillers, including AlN, BN, Cu NPs, CNTs, graphene, and Al_2O_3, while the polymers, such as polypropylene (PP), ultra-high molecular weight PE (UHMWPE), poly(methyl

methacrylate) (PMMA), poly(vinylidene) (PVDF), and poly(butyl terephthalate) (PBT), served as structural agents for segregation of the fillers.[312-320] Meanwhile, the self-assembly of the fillers onto the polymer particles provides other advantages by forming definite continuous yet segregated structures as thermal conduction pathways. Anisotropic fillers, such as graphite, BN, multi-walled CNTs, GNP, rGO, and Ag-rGO, were explored owing to their facile functionalization and interaction with the surface of polymer particles, while PP, poly(phenylene sulfide) (PPS), UHMWPE, TPU, melamine urea formaldehyde (MUF), PS, PA6, polyimide, and PMMA were used as structural agents for the segregation of fillers.[311,321-333] In addition, hybrid fillers were simultaneously introduced to form double-segregated structure in a polymer matrix, in which each filler increased the 3D network density with a bridging effect, resulting in a synergistically increased κ or imparting additional properties, such as high insulation or electromagnetic wave interference shielding.[317,324,334]

Interestingly, the segregation of fillers can be also achieved by actively evolving polymer phases. For instance, natural rubber or latex was used as a structural agent for the segregation of rGO fillers during the spontaneous coagulation of latex particles, which did not restrict the fabrication process of the bulk composite.[335] Several different approaches, such as the crystallization of liquid crystalline epoxy, reaction-induced phase separation (RIPS) of multiphase polymers, and thermally expandable hollow polymers, were also used to induce jamming of fillers between the expanding polymer particles, where the fillers, such as GNPs and BN, were simultaneously segregated, leading to solid physical contacts for high κ regardless of the direction.[336-340]

The isotropic κ of composites containing different fillers prepared by aforementioned techniques are compared in Fig. 16. Deformable fillers (red symbols) are suitable for metal

NWs and NPs by taking advantage of their lower melting points to form strong bonds between fillers, delivering high κ values of over 20 W m^{-1} K^{-1} at high filler loadings. For other types of fillers, foam templates (purple symbols), especially growing 2D graphene and BNNS on metal foam templates, are more effective than hydrogel networks (green symbols) and particulate segregation (yellow symbols) to construct high-quality filler networks, giving rise to higher κ values at similar filler loadings. However, it is still challenging to achieve a high κ of over 10 W m^{-1} K^{-1} at low filler loadings of less than 10 vol%.

4. Conclusions and perspectives

Given many functional and structural requirements for high κ materials, it is obvious that classical polymer composites with homogeneous dispersion of fillers in the polymer matrix have limitations. The methodological approaches we introduced herein indicate that the modulation of filler distribution is an efficient approach for improving the κ of polymer composites along the intended direction. Compared to conventional particulate-filled polymer composites, the κ values of the rationally-designed composites significantly ameliorated, by several times to a couple of orders of magnitude, owing to the facile transport of electrons and phonons along the conduction networks, while the homogeneous dispersion of fillers makes it difficult to reach the identical percolation threshold at the same filler loading. Furthermore, realizing the thermal conduction of polymer composites with an extremely low percolation threshold for long-range connectivity would be an efficient strategy for fabricating these materials for specific end applications.

With regard to the efforts devoted to developing such macroscopic structures, the approaches

we investigated are classified into polymer composites with in-plane, through-plane, and isotropic thermal conduction pathways. The detailed methodologies employed to achieve the intended filler distributions and the corresponding κ values of the polymer composites in these three different categories are summarized in Tables 2-4. Polymer composites with high in-plane κ are designed by modulating the distribution of anisotropic fillers horizontally with respect to the normal plane. The prepreg approach is highly attractive for obtaining high κ values in the fiber direction due to the perfectly continuous geometry of ultralong 1D CF bundles. While electrospinning makes it possible to orient the low-dimensional fillers in the spun fiber direction, the κ values of the composites are limited by the low content of fillers that can be incorporated in the precursor polymer because of the constraint associated with the spinning operation, such as viscosity and surface tension. The vacuum-assisted assembly and hot pressing approaches can be employed mainly for generating orientation of 2D fillers that form layered structures with long range orders for high κ of the composites. Composites with in-plane orientation of fillers can be best utilized as heat spreader or flat heat pipe. Heat spreaders are aimed to resolve the cooling difficulties in mobile devices, such as smartphones and smart pads, requiring a thin thickness, and especially is effective for heat dissipation in the region with a large heat capacity per unit area. They serve to quickly dissipate the heat to other objects rather than directly cooling the electronic circuits without using forced air.

Polymer composites with high through-plane κ values can be designed by placing anisotropic fillers against gravity, or by arranging the spatial distribution of fillers in a vertical direction. Arrays of vertically-grown fillers offer an ideal morphology with continuous structures conducting or dissipating heat in the vertical direction, leading to high through-plane κ of polymer composites. Applying external fields is useful for guiding orientation of the fillers that

are responsive to an electric or magnetic field while dispersed in the polymeric matrix. The field-induced alignment results in improved κ of the polymer composites either in-plane or through-plane direction depending on how the external fields are applied with respect to the composite plane. The through-plane κ can also be improved by introducing a directional porous structure through ice template-based freezing. Thus, the assembly of oriented fillers provides efficient thermal conduction pathways along the freezing direction, giving rise to high κ values even at low filler contents. Additionally, other approaches that use natural templates or phase separation of polymer matrix have also been suggested for filler orientation in the vertical direction, but the absolute κ values of these polymer composites still need to be improved. Composites with through-plane orientation of fillers are best suited for TIMs with various applications. TIMs play an important role in transferring heat generated from the active component in heat-producing devices to a heat sink by placing in-between. These heat-producing and heat-dissipating devices often have rough and contaminated surfaces, inevitably creating physical voids or air gaps and thus giving rise to a high thermal interfacial resistance. The TIMs have several different types, such as paste, adhesive and pad, and should be flexible enough to minimize such a detrimental effect of inadequate surfaces to be bonded with TIMs. Moreover, certain TIMs employed in electronic devices need to be highly thermally conductive yet electrically insulating. TIMs prepared with polymer nanocomposites containing orientated BNNSs or other non-electrically conducting fillers would be the best choice for this purpose.

To prepare polymer composites that allow isotropic thermal conduction, it is important to realize a 3D network structure of fillers in the polymer matrix. The use of nanostructured metal fillers that are deformable upon heating or microwave irradiation is advantageous for preparing 3D thermal conduction pathways. The facile deformation allows locally fused junctions

between the metal fillers, leading to obviously high κ. Filler network structures can also be achieved using common metallic foams or hydrogel networks which serve as thermally conductive medium or substrate for conductive filler coating. Nevertheless, the κ values of the composites made using these porous structures remain lower than expected due to the limitation of low filler loading. In addition, powder processing that is universal for fabricating bulk solids is another powerful route to develop interconnected structures of fillers. In this approach, the fillers segregated between polymer particles are concentrated at the interfaces, forming thermal conduction pathways. This process has advantages of utilizing a variety of fillers and controlling the filler content for composite fabrication. Besides, efforts have been made towards realizing 3D network structures by chemical or physical confinements to bring about filler segregation, but further improvement is needed to modulate precisely the interconnection of fillers. Unlike the aforementioned methods that require thermal conduction in a specific direction, composites with an isotropic thermal conduction pathway can be mainly used as packaging materials or heat sinks in wide industrial applications, including lights, electronics, and automotive. Because the shapes of the end products to which the packaging materials are used are different along with different applications, polymer composites that allow isotropic thermal conduction are expected to be useful for facile heat dissipation regardless of their complex geometries.

Compared to conventional polymer composites that possess poor κ values, the rational design of filler distribution can contribute to improved κ of polymer composites even with small filler contents. Nevertheless, many challenges still remain to realize thermally conductive polymer composites with well-defined thermal conduction pathways along the intended direction(s). With the backdrop of the above overview of the various strategies, in the following are among

the remaining important challenges that need to be addressed in future studies:

(1) Most of previous studies are performed by utilizing BN or graphite as thermally conductive fillers for modulation of filler distribution. Although the bulk BN or graphite powder can be easily used in dry processes, the wet process requires the exfoliation and functionalization of these fillers to utilize their intrinsically high κ values while facilitating good dispersion during processing. Despite of recent significant advances on exfoliation techniques of high-quality 2D materials, such as ultrasonication, high-shear mixing, ball milling, and hydrothermal reaction, it is challenging to achieve their high aspect ratios or large lateral sizes even after exfoliation which contribute to high κ of resulting composites. In addition, because functionalization – mainly covalent functionalization – usually involves severe reaction conditions to create reactive groups, many defects are created in the fillers inevitably reducing their intrinsic κ. This means that high-quality BNNSs or GNPs/graphene sheets exfoliated from bulk BN or graphite are in high demand. Novel approaches need to be developed to enable milder exfoliation and functionalization environments so as to minimize the process-induced damages to the 2D fillers.

(2) Local contacts between the thermally conductive fillers through modulation of their distribution result in increased κ of polymer composites. However, such physical contacts also cause thermal contact resistance, and thus the composites exhibit lower κ than expected. The use of nano-sized fillers with large surface areas is also expected to generate high ITR with matrix as well as other fillers. The issue of ITR is among the major reasons for significantly lower κ values of most nanofiller/polymer composites for TIM applications than the ROM predictions. Appropriate strategies need to be developed to reduce the ITR at the multiple interfaces to an acceptable level.

(3) Various approaches, such as field-induced orientation, directional casting, natural templating, can significantly increase the through-plane κ values of polymer composites by geometrically controlling the orientation of anisotropic fillers. Nevertheless, it is still challenging to achieve perfect orientation of the fillers in the perpendicular direction, and the fillers are most often slightly tilted, resulting in loss of κ values of polymer composites. New approaches therefore need to be established which enable controlling the filler orientation closer to 90° for much enhanced through-plane κ of composites compared to the current level.

(4) Beyond the direct contact between fillers, it is proven that the formation of perfectly continuous and durable thermal pathways, such as fused junctions, can significantly increase the κ of polymer composites by overcoming the contact resistances. This means that exploring new types of fillers that can be fusible under external stimuli would be an effective strategy to form ideal network structures. Low-melting-temperature metals and metal-coated polymers in the form of NPs or NWs can be ideal candidates for fusible conductive fillers.

(5) Several approaches demonstrate that the modulation of filler distribution can also be achieved by modulating the matrix phase, *e.g.*, phase separation of multi-phase polymers. Such future-oriented methodologies could be the basis for developing thermally conductive polymer composites with high κ without reliance on processing instruments.

(6) While the review preferentially focuses on the improvement of κ via modulation of thermally conductive filler distribution based on the methodological approaches, there are still key challenges ahead in developing large-scale production with uniform quality. In addition, several approaches introduced to realize specific structures are far from preexisting processes used commonly in industries, *e.g.*, compounding, high-shear mixing and molding. Therefore,

much more efforts are needed to establish the relationship between the realization of such structures and the processes capable of not only achieving excellent κ, but also meeting the practical needs for mass production of such composites. Moreover, apart from the attempts for obtaining high κ along the intended direction(s), important features of the newly developed approaches like the processing conditions, material parameters and potentials for large-scale production as well as the mechanical and fracture properties of the polymer composites with oriented fillers should be carefully taken into account in the selection and application of these techniques.

Author contributions

Seunggun Yu and Xi Shen contributed equally to this work. Seunggun Yu: conceptualization, writing – original draft, supervision. Xi Shen: writing – review & editing. Jang-Kyo Kim: review & editing, supervision.

Conflicts of interests

There are no conflicts to declare.

Acknowledgements

The authors appreciate the financial supports from the Korea Electrotechnology Research Institute (KERI) Primary Research Program (21A02093), the Research Grants Council (GRF project: 16205517, 16200720) and the Innovation Technology Commission (ITS/012/19) of Hong Kong SAR.

References

1. S.-K. Kang, R. K. J. Murphy, S.-W. Hwang, S. M. Lee, D. V. Harburg, N. A. Krueger, J. Shin, P. Gamble, H. Cheng, S. Yu, Z. Liu, J. G. McCall, M. Stephen, H. Ying, J. Kim, G. Park, R. C. Webb, C. H. Lee, S. Chung, D. S. Wie, A. D. Gujar, B. Vemulapalli, A. H. Kim, K.-M. Lee, J. Cheng, Y. Huang, S. H. Lee, P. V. Braun, W. Z. Ray and J. A. Rogers, *Nature*, 2016, **530**, 71-76.
2. R. Chau, B. Doyle, S. Datta, J. Kavalieros and K. Zhang, *Nat. Mater.*, 2007, **6**, 810-812.
3. S. J. Kang, C. Kocabas, T. Ozel, M. Shim, N. Pimparkar, M. A. Alam, S. V. Rotkin and J. A. Rogers, *Nat. Nanotechnol.*, 2007, **2**, 230-236.
4. G. Huang, F. Li, X. Zhao, Y. Ma, Y. Li, M. Lin, G. Jin, T. J. Lu, G. M. Genin and F. Xu, *Chem. Rev.*, 2017, **117**, 12764-12850.
5. Y. Zhang, F. Zhang, Z. Yan, Q. Ma, X. Li, Y. Huang and J. A. Rogers, *Nat. Rev. Mater.*, 2017, **2**, 17019.
6. M. J. Cima, *Nat. Biotechnol.*, 2014, **32**, 642-643.
7. W. Zeng, L. Shu, Q. Li, S. Chen, F. Wang and X.-M. Tao, *Adv. Mater.*, 2014, **26**, 5310-5336.
8. X. Chen, J. A. Rogers, S. P. Lacour, W. Hu and D.-H. Kim, *Chem. Soc. Rev.*, 2019, **48**, 1431-1433.
9. C. Choi, Y. Lee, K. W. Cho, J. H. Koo and D.-H. Kim, *Acc. Chem. Res.*, 2019, **52**, 73-81.
10. S. Hong and S. Myung, *Nat. Nanotechnol.*, 2007, **2**, 207-208.
11. R. W. Keyes, *IBM J. Res. Dev.*, 1988, **32**, 84-88.
12. M. Mills, *IEEE Ann. Hist. Comput.*, 2011, **33**, 24-45.

13. J. Kim, R. Ghaffari and D.-H. Kim, *Nat. Biomed. Eng.*, 2017, **1**, 0049.

14. N. A. Kyerematen, T. Brousse and D. Pech, *Nat. Nanotechnol.*, 2017, **12**, 7-15.

15. P. S. Peercy, *Nature*, 2000, **406**, 1023-1026.

16. J. Kim, A. Banks, Z. Xie, S. Y. Heo, P. Gutruf, J. W. Lee, S. Xu, K.-I. Jang, F. Liu, G. Brown, J. Choi, J. H. Kim, X. Feng, Y. Huang, U. Paik and J. A. Rogers, *Adv. Funct. Mater.*, 2015, **25**, 4761-4767.

17. G. E. Moore, *IEEE Solid-State Circuits Soc. Newsl.*, 2006, **11**, 33-35.

18. C. Lipeng, J. P. Krusius, M. A. Korhonen and T. S. Fisher, *IEEE Trans. Compon., Packag., Manuf. Technol.*, 1998, **21**, 113-123.

19. A. Koyuncuoğlu, R. Jafari, T. Okutucu-Özyurt and H. Külah, *Int. J. Therm. Sci.*, 2012, **56**, 77-85.

20. C. Woodcock, C. Ng'oma, M. Sweet, Y. Wang, Y. Peles and J. Plawsky, *Int. J. Heat Mass Transfer*, 2019, **128**, 504-515.

21. J. Mei, R. Haug, O. Lanier, T. Grözinger and A. Zimmermann, *Microelectron. Reliab.*, 2018, **88-90**, 684-690.

22. N. M. Vichare and M. G. Pecht, *IEEE Trans. Compon., Packag. Technol.*, 2006, **29**, 222-229.

23. M. Andresen, K. Ma, G. Buticchi, J. Falck, F. Blaabjerg and M. Liserre, *IEEE Trans. Power. Electron.*, 2018, **33**, 765-776.

24. H. C. Chen, G. F. Chen, P. H. Chen, S. P. Huang, J. J. Chen, K. J. Zhou, C. W. Kuo, Y. C. Tsao, A. K. Chu, H. C. Huang, W. C. Lai and T. C. Chang, *IEEE Electron Device Lett.*, 2019, **40**, 1447-1450.

25. P. Saxena and N. E. Gorji, *IEEE J. Photovolt.*, 2019, **9**, 1693-1698.

26. J. Schleeh, J. Mateos, I. Íñiguez-de-la-Torre, N. Wadefalk, P. A. Nilsson, J. Grahn and A. J. Minnich, *Nat. Mater.*, 2015, **14**, 187-192.

27. X. Xu, J. Chen, J. Zhou and B. Li, *Adv. Mater.*, 2018, **30**, 1705544.

28. K. G. Baiju, B. Murali, R. Subba Rao, K. Jayanarayanan and D. Kumaresan, *Chem. Eng. Process.*, 2020, **149**, 107817.

29. J. Park, H. Ham and C. Park, *Org. Electron.*, 2011, **12**, 227-233.

30. N. Han, T. Viet Cuong, M. Han, B. Deul Ryu, S. Chandramohan, J. Bae Park, J. Hye Kang, Y.-J. Park, K. Bok Ko, H. Yun Kim, H. Kyu Kim, J. Hyoung Ryu, Y. S. Katharria, C.-J. Choi and C.-H. Hong, *Nat. Commun.*, 2013, **4**, 1452.

31. L. Yin, Y. Wang, W. Duan, X. Wu and J. Zhang, *IEEE Access*, 2019, **7**, 60104-60110.

32. R. E. B. Makinson, *Math. Proc. Cambridge Philos. Soc.*, 1938, **34**, 474-497.

33. D. Lacroix, K. Joulain and D. Lemonnier, *Phys. Rev. B*, 2005, **72**, 064305.

34. G. A. Slack, *J. Appl. Phys.*, 1964, **35**, 3460-3466.

35. A. A. Balandin, *Nat. Mater.*, 2011, **10**, 569-581.

36. C. L. Choy, *Polymer*, 1977, **18**, 984-1004.

37. D. R. Anderson, *Chem. Rev.*, 1966, **66**, 677-690.

38. N. Burger, A. Laachachi, M. Ferriol, M. Lutz, V. Toniazzo and D. Ruch, *Prog. Polym. Sci.*, 2016, **61**, 1-28.

39. W. Knappe and O. Yamamoto, *Kolloid Z. Z. Polym.*, 1970, **240**, 775-783.

40. S.-h. Song, H. Katagi and Y. Takezawa, *Polymer*, 2012, **53**, 4489-4492.

41. G.-H. Kim, D. Lee, A. Shanker, L. Shao, M. S. Kwon, D. Gidley, J. Kim and K. P. Pipe, *Nat. Mater.*, 2015, **14**, 295-300.

42. C. Huang, X. Qian and R. Yang, *Mater. Sci. Eng., R*, 2018, **132**, 1-22.

43. H. Ma, B. Gao, M. Wang, Z. Yuan, J. Shen, J. Zhao and Y. Feng, *J. Mater. Sci.*, 2021, **56**, 1064-1086.

44. A. G. Evans, J. W. Hutchinson and M. F. Ashby, *Prog. Mater. Sci.*, 1998, **43**, 171-221.

45. X.-h. Qu, L. Zhang, M. Wu and S.-B. Ren, *Prog. Nat. Sci.: Mater. Int.*, 2011, **21**, 189-197.

46. T. Iikawa, T. Sakai, S. Okamoto, K. Natori and T. Nagai, *IEEE Trans. Compon., Hybrids, Manuf. Technol.*, 1986, **9**, 513-517.

47. Y. K. Gautam, N. Somani, M. Kumar and S. K. Sharma, *AIP Conf. Proc.*, 2018, **2018**, 020017.

48. G. Schider, J. R. Krenn, A. Hohenau, H. Ditlbacher, A. Leitner, F. R. Aussenegg, W. L. Schaich, I. Puscasu, B. Monacelli and G. Boreman, *Phys. Rev. B*, 2003, **68**, 155427.

49. P. Christopher and S. Linic, *J. Am. Chem. Soc.*, 2008, **130**, 11264-11265.

50. N. Stojanovic, J. M. Berg, D. H. S. Maithripala and M. Holtz, *Appl. Phys. Lett.*, 2009, **95**, 091905.

51. N. Stojanovic, D. H. S. Maithripala, J. M. Berg and M. Holtz, *Phys. Rev. B*, 2010, **82**, 075418.

52. Y. Zhao, M. L. Fitzgerald, Y. Tao, Z. Pan, G. Sauti, D. Xu, Y.-Q. Xu and D. Li, *Nano Lett.*, 2020, **20**, 7389-7396.

53. M. Lagrange, D. P. Langley, G. Giusti, C. Jiménez, Y. Bréchet and D. Bellet, *Nanoscale*, 2015, **7**, 17410-17423.

54. D. Jariwala, V. K. Sangwan, L. J. Lauhon, T. J. Marks and M. C. Hersam, *Chem. Soc. Rev.*, 2013, **42**, 2824-2860.

55. L. Dai, D. W. Chang, J.-B. Baek and W. Lu, *Small*, 2012, **8**, 1130-1166.

56. W. Ruland, *Adv. Mater.*, 1990, **2**, 528-536.

57. J. G. Lavin, D. R. Boyington, J. Lahijani, B. Nystem and J. P. Issi, *Carbon*, 1993, **31**, 1001-1002.

58. A. A. Balandin, S. Ghosh, W. Bao, I. Calizo, D. Teweldebrhan, F. Miao and C. N. Lau, *Nano Lett.*, 2008, **8**, 902-907.

59. Y. Zhu, S. Murali, W. Cai, X. Li, J. W. Suk, J. R. Potts and R. S. Ruoff, *Adv. Mater.*, 2010, **22**, 3906-3924.

60. Y. Bai, R. Zhang, X. Ye, Z. Zhu, H. Xie, B. Shen, D. Cai, B. Liu, C. Zhang, Z. Jia, S. Zhang, X. Li and F. Wei, *Nat. Nanotechnol.*, 2018, **13**, 589-595.

61. S. Berber, Y.-K. Kwon and D. Tománek, *Phys. Rev. Lett.*, 2000, **84**, 4613-4616.

62. X. Huang, P. Jiang and T. Tanaka, *IEEE Electr. Insul. Mag.*, 2011, **27**, 8-16.

63. M. Xiao and B. X. Du, *High Voltage*, 2016, **1**, 34-42.

64. J. García Ten, M. J. Orts, A. Saburit and G. Silva, *Ceram. Int.*, 2010, **36**, 1951-1959.

65. J. E. Graebner, S. Jin, G. W. Kammlott, J. A. Herb and C. F. Gardinier, *Appl. Phys. Lett.*, 1992, **60**, 1576-1578.

66. Q. Cai, D. Scullion, W. Gan, A. Falin, S. Zhang, K. Watanabe, T. Taniguchi, Y. Chen, E. J. G. Santos and L. H. Li, *Sci. Adv.*, 2019, **5**, eaav0129.

67. I. Jo, M. T. Pettes, J. Kim, K. Watanabe, T. Taniguchi, Z. Yao and L. Shi, *Nano Lett.*, 2013, **13**, 550-554.

68. N. G. Chopra, R. J. Luyken, K. Cherrey, V. H. Crespi, M. L. Cohen, S. G. Louie and A. Zettl, *Science*, 1995, **269**, 966-967.

69. C. Zhang, R. Huang, Y. Wang, Z. Wu, S. Guo, H. Zhang, J. Li, C. Huang, W. Wang and L. Li, *J. Mater. Chem. A*, 2018, **6**, 20663-20668.

70. C. Fu, Q. Li, J. Lu, S. Mateti, Q. Cai, X. Zeng, G. Du, R. Sun, Y. Chen, J. Xu and C.-P. Wong, *Compos. Sci. Technol.*, 2018, **165**, 322-330.

71. L. Lindsay, D. A. Broido and T. L. Reinecke, *Phys. Rev. Lett.*, 2013, **111**, 025901.

72. J. S. Kang, M. Li, H. Wu, H. Nguyen and Y. Hu, *Science*, 2018, **361**, 575-578.

73. S. Li, Q. Zheng, Y. Lv, X. Liu, X. Wang, P. Y. Huang, D. G. Cahill and B. Lv, *Science*, 2018, **361**, 579-581.

74. X. Ji, Y. Xu, W. Zhang, L. Cui and J. Liu, *Composites, Part A*, 2016, **87**, 29-45.

75. P. Noorunnisa Khanam, M. A. AlMaadeed, M. Ouederni, E. Harkin-Jones, B. Mayoral, A. Hamilton and D. Sun, *Vacuum*, 2016, **130**, 63-71.

76. R. Ramasubramaniam, J. Chen and H. Liu, *Appl. Phys. Lett.*, 2003, **83**, 2928-2930.

77. S. Depaifve, C. E. Federico, D. Ruch, S. Hermans and A. Laachachi, *Carbon*, 2020, **167**, 646-657.

78. Y. Wang, C. Yang, Q.-X. Pei and Y. Zhang, *ACS Appl. Mater. Interfaces*, 2016, **8**, 8272-8279.

79. S. Shenogin, A. Bodapati, L. Xue, R. Ozisik and P. Keblinski, *Appl. Phys. Lett.*, 2004, **85**, 2229-2231.

80. S.-Y. Yang, C.-C. M. Ma, C.-C. Teng, Y.-W. Huang, S.-H. Liao, Y.-L. Huang, H.-W. Tien, T.-M. Lee and K.-C. Chiou, *Carbon*, 2010, **48**, 592-603.

81. R. Gulotty, M. Castellino, P. Jagdale, A. Tagliaferro and A. A. Balandin, *ACS Nano*, 2013, **7**, 5114-5121.

82. K. Ruan, X. Shi, Y. Guo and J. Gu, *Compos. Commun.*, 2020, **22**, 100518.

83. B. Deng, A. Chernatynskiy, M. Khafizov, D. H. Hurley and S. R. Phillpot, *J. Appl. Phys.*, 2014, **115**, 084910.

84. G. L. Pollack, *Rev. Mod. Phys.*, 1969, **41**, 48-81.

85. P.-C. Ma and J.-K. Kim, *Carbon nanotubes for polymer reinforcement*, Taylor & Francis Boca Raton, 2011.

86. P.-C. Ma, N. A. Siddiqui, G. Marom and J.-K. Kim, *Composites, Part A*, 2010, **41**, 1345-1367.

87. X. Liu, I. Marangon, G. Melinte, C. Wilhelm, C. Ménard-Moyon, B. P. Pichon, O. Ersen, K. Aubertin, W. Baaziz, C. Pham-Huu, S. Bégin-Colin, A. Bianco, F. Gazeau and D. Bégin, *ACS Nano*, 2014, **8**, 11290-11304.

88. J. M. González-Domínguez, A. M. Díez-Pascual, A. Ansón-Casaos, M. A. Gómez-Fatou and M. T. Martínez, *J. Mater. Chem.*, 2011, **21**, 14948-14958.

89. T. Sainsbury, A. Satti, P. May, Z. Wang, I. McGovern, Y. K. Gun'ko and J. Coleman, *J. Am. Chem. Soc.*, 2012, **134**, 18758-18771.

90. H. Shin, J. Guan, M. Z. Zgierski, K. S. Kim, C. T. Kingston and B. Simard, *ACS Nano*, 2015, **9**, 12573-12582.

91. J.-K. Kim and Y.-W. Mai, *Engineered interfaces in fiber reinforced composites*, Elsevier, 1998.

92. P. C. Ma, J.-K. Kim and B. Z. Tang, *Carbon*, 2006, **44**, 3232-3238.

93. Z. Zhou, S. Wang, L. Lu, Y. Zhang and Y. Zhang, *Compos. Sci. Technol.*, 2008, **68**, 1727-1733.

94. X. Huang, C. Zhi, P. Jiang, D. Golberg, Y. Bando and T. Tanaka, *Adv. Funct. Mater.*, 2013, **23**, 1824-1831.

95. Z. Tang, H. Kang, Z. Shen, B. Guo, L. Zhang and D. Jia, *Macromolecules*, 2012, **45**, 3444-3451.

96. Y. Wang, H. F. Zhan, Y. Xiang, C. Yang, C. M. Wang and Y. Y. Zhang, *J. Phys. Chem. C*, 2015, **119**, 12731-12738.

97. X. Shen, Z. Wang, Y. Wu, X. Liu and J.-K. Kim, *Carbon*, 2016, **108**, 412-422.

98. C.-C. Teng, C.-C. M. Ma, C.-H. Lu, S.-Y. Yang, S.-H. Lee, M.-C. Hsiao, M.-Y. Yen, K.-C. Chiou and T.-M. Lee, *Carbon*, 2011, **49**, 5107-5116.

99. A. A. Vasileiou, A. Docoslis, M. Kontopoulou, P. Xiang and Z. Ye, *Polymer*, 2013, **54**, 5230-5240.

100. D. Ponnamma, S. H. Sung, J. S. Hong, K. H. Ahn, K. T. Varughese and S. Thomas, *Eur. Polym. J.*, 2014, **53**, 147-159.

101. S. Das, F. Irin, H. S. Tanvir Ahmed, A. B. Cortinas, A. S. Wajid, D. Parviz, A. F. Jankowski, M. Kato and M. J. Green, *Polymer*, 2012, **53**, 2485-2494.

102. S. H. Song, K. H. Park, B. H. Kim, Y. W. Choi, G. H. Jun, D. J. Lee, B.-S. Kong, K.-W. Paik and S. Jeon, *Adv. Mater.*, 2013, **25**, 732-737.

103. T. Terao, Y. Bando, M. Mitome, C. Zhi, C. Tang and D. Golberg, *J. Phys. Chem. C*, 2009, **113**, 13605-13609.

104. M. Sugavaneswaran and G. Arumaikkannu, *Mater. Des.*, 2015, **66**, 29-36.

105. B. K. Sarkar, M. K. Mukherjee and A. Natarajan, *Materialwiss. Werkstofftech.*, 1982, **13**, 269-273.

106. N. F. Uvarov, *Solid State Ionics*, 2000, **136-137**, 1267-1272.

107. J. F. Ely and H. J. M. Hanley, *Ind. Eng. Chem. Fundam.*, 1981, **20**, 323-332.

108. R. F. Hill and P. H. Supancic, *J. Am. Ceram. Soc.*, 2002, **85**, 851-857.

109. I. H. Tavman, *J. Appl. Polym. Sci.*, 1996, **62**, 2161-2167.

110. H. Zhao and L. Guo, *Adv. Mater.*, 2017, **29**, 1702903.

111. J. Wang, Q. Cheng and Z. Tang, *Chem. Soc. Rev.*, 2012, **41**, 1111-1129.

112. J. Dalal, S. Lather, A. Gupta, S. Dahiya, A. S. Maan, K. Singh, S. K. Dhawan and A. Ohlan, *Compos. Sci. Technol.*, 2018, **165**, 222-230.

113. J.-K. Kim, C. Hu, R. S. C. Woo and M.-L. Sham, *Compos. Sci. Technol.*, 2005, **65**, 805-813.

114. F. Kim, L. J. Cote and J. Huang, *Adv. Mater.*, 2010, **22**, 1954-1958.

115. Q. Zheng, W. H. Ip, X. Lin, N. Yousefi, K. K. Yeung, Z. Li and J.-K. Kim, *ACS Nano*, 2011, **5**, 6039-6051.

116. L. Peng, Z. Xu, Z. Liu, Y. Guo, P. Li and C. Gao, *Adv. Mater.*, 2017, **29**, 1700589.

117. M. Zhang, Y. Wang, L. Huang, Z. Xu, C. Li and G. Shi, *Adv. Mater.*, 2015, **27**, 6708-6713.

118. J. D. Renteria, S. Ramirez, H. Malekpour, B. Alonso, A. Centeno, A. Zurutuza, A. I. Cocemasov, D. L. Nika and A. A. Balandin, *Adv. Funct. Mater.*, 2015, **25**, 4664-4672.

119. B. Shen, W. Zhai and W. Zheng, *Adv. Funct. Mater.*, 2014, **24**, 4542-4548.

120. G. Xin, H. Sun, T. Hu, H. R. Fard, X. Sun, N. Koratkar, T. Borca-Tasciuc and J. Lian, *Adv. Mater.*, 2014, **26**, 4521-4526.

121. R. Zhang, X. Chen, X. Shen, X.-Q. Zhang, X.-R. Chen, X.-B. Cheng, C. Yan, C.-Z. Zhao and Q. Zhang, *Joule*, 2018, **2**, 764-777.

122. P. Taynton, H. Ni, C. Zhu, K. Yu, S. Loob, Y. Jin, H. J. Qi and W. Zhang, *Adv. Mater.*, 2016, **28**, 2904-2909.

123. T. Qin, S. Peng, J. Hao, Y. Wen, Z. Wang, X. Wang, D. He, J. Zhang, J. Hou and G. Cao, *Adv. Energy Mater.*, 2017, **7**, 1700409.

124. D. Yu, S. Zhai, W. Jiang, K. Goh, L. Wei, X. Chen, R. Jiang and Y. Chen, *Adv. Mater.*,

2015, **27**, 4895-4901.

125. J.-l. Wang, M. Gu, W.-g. Ma, X. Zhang and Y. Song, *New Carbon Mater.*, 2008, **23**, 259-263.

126. G. Yuan, X. Li, Z. Dong, X. Xiong, B. Rand, Z. Cui, Y. Cong, J. Zhang, Y. Li, Z. Zhang and J. Wang, *Carbon*, 2014, **68**, 413-425.

127. Y.-M. Chen and J.-M. Ting, *Carbon*, 2002, **40**, 359-362.

128. Y. A. Kim, S. Kamio, T. Tajiri, T. Hayashi, S. M. Song, M. Endo, M. Terrones and M. S. Dresselhaus, *Appl. Phys. Lett.*, 2007, **90**, 093125.

129. S. Yu, K. Park, J.-W. Lee, S. M. Hong, C. Park, T. H. Han and C. M. Koo, *Macromol. Res.*, 2017, **25**, 559-564.

130. S. Yu, B.-I. Park, C. Park, S. M. Hong, T. H. Han and C. M. Koo, *ACS Appl. Mater. Interfaces*, 2014, **6**, 7498-7503.

131. D. Li and Y. Xia, *Adv. Mater.*, 2004, **16**, 1151-1170.

132. B. Zhang, F. Kang, J.-M. Tarascon and J.-K. Kim, *Prog. Mater. Sci.*, 2016, **76**, 319-380.

133. G. Kim and W. Kim, *Appl. Phys. Lett.*, 2006, **88**, 233101.

134. X. Yu, Y. Li, X. Wang, Y. Si, J. Yu and B. Ding, *ACS Appl. Mater. Interfaces*, 2020, **12**, 32078-32089.

135. J. Chen, X. Huang, B. Sun and P. Jiang, *ACS Nano*, 2019, **13**, 337-345.

136. J. Chen, X. Huang, B. Sun, Y. Wang, Y. Zhu and P. Jiang, *ACS Appl. Mater. Interfaces*, 2017, **9**, 30909-30917.

137. J. Gu, Z. Lv, Y. Wu, Y. Guo, L. Tian, H. Qiu, W. Li and Q. Zhang, *Composites, Part A*, 2017, **94**, 209-216.

138. T. Terao, C. Zhi, Y. Bando, M. Mitome, C. Tang and D. Golberg, *J. Phys. Chem. C*,

2010, **114**, 4340-4344.

139. Y. Guo, G. Xu, X. Yang, K. Ruan, T. Ma, Q. Zhang, J. Gu, Y. Wu, H. Liu and Z. Guo, *J. Mater. Chem. C*, 2018, **6**, 3004-3015.

140. K. Ruan, Y. Guo, Y. Tang, Y. Zhang, J. Zhang, M. He, J. Kong and J. Gu, *Compos. Commun.*, 2018, **10**, 68-72.

141. D.-L. Zhang, J.-W. Zha, W.-K. Li, C.-Q. Li, S.-J. Wang, Y. Wen and Z.-M. Dang, *Compos. Sci. Technol.*, 2018, **156**, 1-7.

142. X. Yang, Y. Guo, Y. Han, Y. Li, T. Ma, M. Chen, J. Kong, J. Zhu and J. Gu, *Composites, Part B*, 2019, **175**, 107070.

143. Y. Guo, K. Ruan, X. Yang, T. Ma, J. Kong, N. Wu, J. Zhang, J. Gu and Z. Guo, *J. Mater. Chem. C*, 2019, **7**, 7035-7044.

144. J. Wang, Q. Li, D. Liu, C. Chen, Z. Chen, J. Hao, Y. Li, J. Zhang, M. Naebe and W. Lei, *Nanoscale*, 2018, **10**, 16868-16872.

145. D. Miao, X. Wang, J. Yu and B. Ding, *Adv. Funct. Mater.*, 2021, **31**, 2008705.

146. K. S. Kim, M. B. Jakubinek, Y. Martinez-Rubi, B. Ashrafi, J. Guan, K. O'Neill, M. Plunkett, A. Hrdina, S. Lin, S. Dénommée, C. Kingston and B. Simard, *RSC Adv.*, 2015, **5**, 41186-41192.

147. V. Gupta and S. Kumar, *J. Energy Storage*, 2019, **26**, 100960.

148. X. Lin, X. Liu, J. Jia, X. Shen and J.-K. Kim, *Compos. Sci. Technol.*, 2014, **100**, 166-173.

149. X. Lin, X. Shen, Q. Zheng, N. Yousefi, L. Ye, Y.-W. Mai and J.-K. Kim, *ACS Nano*, 2012, **6**, 10708-10719.

150. N. Yousefi, X. Sun, X. Lin, X. Shen, J. Jia, B. Zhang, B. Tang, M. Chan and J.-K. Kim,

Adv. Mater., 2014, **26**, 5480-5487.

151. Q. Li, Y. Guo, W. Li, S. Qiu, C. Zhu, X. Wei, M. Chen, C. Liu, S. Liao, Y. Gong, A. K. Mishra and L. Liu, *Chem. Mater.*, 2014, **26**, 4459-4465.

152. C. Yu, J. Zhang, Z. Li, W. Tian, L. Wang, J. Luo, Q. Li, X. Fan and Y. Yao, *Composites, Part A*, 2017, **98**, 25-31.

153. Z.-G. Wang, M.-Z. Chen, Y.-H. Liu, H.-J. Duan, L. Xu, L. Zhou, J.-Z. Xu, J. Lei and Z.-M. Li, *J. Mater. Chem. C*, 2019, **7**, 9018-9024.

154. Y. Wu, Y. Xue, S. Qin, D. Liu, X. Wang, X. Hu, J. Li, X. Wang, Y. Bando, D. Golberg, Y. Chen, Y. Gogotsi and W. Lei, *ACS Appl. Mater. Interfaces*, 2017, **9**, 43163-43170.

155. H. Hou, W. Dai, Q. Yan, L. Lv, F. E. Alam, M. Yang, Y. Yao, X. Zeng, J.-B. Xu, J. Yu, N. Jiang and C.-T. Lin, *J. Mater. Chem. A*, 2018, **6**, 12091-12097.

156. Y. Yao, X. Zeng, R. Sun, J.-B. Xu and C.-P. Wong, *ACS Appl. Mater. Interfaces*, 2016, **8**, 15645-15653.

157. K. Wu, J. Fang, J. Ma, R. Huang, S. Chai, F. Chen and Q. Fu, *ACS Appl. Mater. Interfaces*, 2017, **9**, 30035-30045.

158. H. Zhu, Y. Li, Z. Fang, J. Xu, F. Cao, J. Wan, C. Preston, B. Yang and L. Hu, *ACS Nano*, 2014, **8**, 3606-3613.

159. N. Song, H. Pan, X. Liang, D. Cao, L. Shi and P. Ding, *J. Mater. Chem. C*, 2018, **6**, 7085-7091.

160. W. Qiu, W. Lin, Y. Tuersun, M. Ou and S. Chu, *Adv. Mater. Interfaces*, 2021, **8**, 2002187.

161. G. Song, R. Kang, L. Guo, Z. Ali, X. Chen, Z. Zhang, C. Yan, C.-T. Lin, N. Jiang and J. Yu, *New J. Chem.*, 2020, **44**, 7186-7193.

162. E. Jiao, K. Wu, Y. Liu, M. Lu, H. Zhang, H. Zheng, C.-a. Xu, J. Shi and M. Lu,

Composites, Part A, 2021, **143**, 106290.

163. L. J. Lanticse, Y. Tanabe, K. Matsui, Y. Kaburagi, K. Suda, M. Hoteida, M. Endo and E. Yasuda, *Carbon*, 2006, **44**, 3078-3086.

164. E. Yang, H. E. Karahan, K. Goh, C. Y. Chuah, R. Wang and T.-H. Bae, *Carbon*, 2019, **155**, 129-137.

165. X. Shen, Q. Zheng and J.-K. Kim, *Prog. Mater. Sci.*, 2021, **115**, 100708.

166. T. Hu, Y. Song, J. Di, D. Xie and C. Teng, *Carbon*, 2018, **140**, 596-602.

167. Y. Liu, M. Lu, K. Wu, E. Jiao, L. Liang, J. Shi and M. Lu, *Compos. Sci. Technol.*, 2021, **213**, 108940.

168. L. Chen, C. Xiao, Y. Tang, X. Zhang, K. Zheng and X. Tian, *Ceram. Int.*, 2019, **45**, 12965-12974.

169. B.-H. Xie, X. Huang and G.-J. Zhang, *Compos. Sci. Technol.*, 2013, **85**, 98-103.

170. C. Teng, L. Su, J. Chen and J. Wang, *Composites, Part A*, 2019, **124**, 105498.

171. L. Su, J. Wang, J. Zhou, J. Wang and C. Teng, *Nano Sel.*, **n/a**.

172. K. Zhao, G. Liu, W. Cao, Z. Su, J. Zhao, J. Han, B. Dai, K. Cao and J. Zhu, *Polymer*, 2020, **206**, 122885.

173. F. Yu, H. Wang, Y. Bai and J. Yang, *Bull. Mater. Sci.*, 2010, **33**, 619-624.

174. C. Tang, A. Dang, T. Li, T. Zhao, H. Li and S. Jiao, *Tribol. Int.*, 2019, **136**, 404-411.

175. Y. E. Pivinskii, D. A. Dobrodon, E. V. Rozhkov, L. A. Karpets, V. G. Savkin and A. G. Donich, *Refract. Ind. Ceram.*, 1997, **38**, 180-183.

176. C.-P. Feng, L. Bai, Y. Shao, R.-Y. Bao, Z.-Y. Liu, M.-B. Yang, J. Chen, H.-Y. Ni and W. Yang, *Adv. Mater. Interfaces*, 2018, **5**, 1700946.

177. P. Ding, J. Zhang, N. Song, S. Tang, Y. Liu and L. Shi, *Compos. Sci. Technol.*, 2015,

109, 25-31.

178. C. Yu, W. Gong, W. Tian, Q. Zhang, Y. Xu, Z. Lin, M. Hu, X. Fan and Y. Yao, *Compos. Sci. Technol.*, 2018, **160**, 199-207.

179. J. Hu, Y. Huang, X. Zeng, Q. Li, L. Ren, R. Sun, J.-B. Xu and C.-P. Wong, *Compos. Sci. Technol.*, 2018, **160**, 127-137.

180. C. Yu, W. Gong, J. Zhang, W. Lv, W. Tian, X. Fan and Y. Yao, *RSC Adv.*, 2018, **8**, 25835-25845.

181. G. Pan, Y. Yao, X. Zeng, J. Sun, J. Hu, R. Sun, J.-B. Xu and C.-P. Wong, *ACS Appl. Mater. Interfaces*, 2017, **9**, 33001-33010.

182. X. Wang and P. Wu, *ACS Appl. Mater. Interfaces*, 2017, **9**, 19934-19944.

183. X. Zhang, K. Wu, Y. Liu, B. Yu, Q. Zhang, F. Chen and Q. Fu, *Compos. Sci. Technol.*, 2019, **175**, 135-142.

184. K. Fu, J. Yang, C. Cao, Q. Zhai, W. Qiao, J. Qiao, H. Gao, Z. Zhou, J. Ji, M. Li, C. Liu, B. Wang, W. Bai, H. Duan, Y. Xue and C. Tang, *ACS Appl. Mater. Interfaces*, 2021, **13**, 2853-2867.

185. Z. Liu, J. Li and X. Liu, *ACS Appl. Mater. Interfaces*, 2020, **12**, 6503-6515.

186. Z. Xu, G. Lin and G. Sui, *J. Appl. Polym. Sci.*, 2020, **137**, 49212.

187. J. Li, X. Zhao, W. Wu, Z. Zhang, Y. Xian, Y. Lin, Y. Lu and L. Zhang, *Carbon*, 2020, **162**, 46-55.

188. M. Khandelwal and M. M. Mench, *J. Power Sources*, 2006, **161**, 1106-1115.

189. H. Jung, S. Yu, N.-S. Bae, S. M. Cho, R. H. Kim, S. H. Cho, I. Hwang, B. Jeong, J. S. Ryu, J. Hwang, S. M. Hong, C. M. Koo and C. Park, *ACS Appl. Mater. Interfaces*, 2015, **7**, 15256-15262.

190. C.-T. Hsieh, C.-E. Lee, Y.-F. Chen, J.-K. Chang and H.-s. Teng, *Nanoscale*, 2015, **7**, 18663-18670.

191. Y. Su, J. J. Li and G. J. Weng, *Carbon*, 2018, **137**, 222-233.

192. H. Huang, C. H. Liu, Y. Wu and S. Fan, *Adv. Mater.*, 2005, **17**, 1652-1656.

193. A. M. Marconnet, N. Yamamoto, M. A. Panzer, B. L. Wardle and K. E. Goodson, *ACS Nano*, 2011, **5**, 4818-4825.

194. J. H. Taphouse, O. N. L. Smith, S. R. Marder and B. A. Cola, *Adv. Funct. Mater.*, 2014, **24**, 465-471.

195. J. Xu, A. Munari, E. Dalton, A. Mathewson and K. M. Razeeb, *J. Appl. Phys.*, 2009, **106**, 124310.

196. M. T. Barako, S. Roy-Panzer, T. S. English, T. Kodama, M. Asheghi, T. W. Kenny and K. E. Goodson, *ACS Appl. Mater. Interfaces*, 2015, **7**, 19251-19259.

197. M. T. Barako, S. G. Isaacson, F. Lian, E. Pop, R. H. Dauskardt, K. E. Goodson and J. Tice, *ACS Appl. Mater. Interfaces*, 2017, **9**, 42067-42074.

198. J. Y. Kim and S. O. Kim, *Nat. Mater.*, 2014, **13**, 325-326.

199. S. U. Khan, J. R. Pothnis and J.-K. Kim, *Composites, Part A*, 2013, **49**, 26-34.

200. K. Zhang, Y. Feng, F. Wang, Z. Yang and J. Wang, *J. Mater. Chem. C*, 2017, **5**, 11992-12022.

201. H.-B. Cho, T. Nakayama, Y. Tokoi, S. Endo, S. Tanaka, T. Suzuki, W. Jiang, H. Suematsu and K. Niihara, *Compos. Sci. Technol.*, 2010, **70**, 1681-1686.

202. H.-B. Cho, T. Nakayama, H. Suematsu, T. Suzuki, W. Jiang, K. Niihara, E. Song, N. S. A. Eom, S. Kim and Y.-H. Choa, *Compos. Sci. Technol.*, 2016, **129**, 205-213.

203. H.-B. Cho, N. C. Tu, T. Fujihara, S. Endo, T. Suzuki, S. Tanaka, W. Jiang, H. Suematsu,

K. Niihara and T. Nakayama, *Mater. Lett.*, 2011, **65**, 2426-2428.

204. H.-B. Cho, T. Nakayama, T. Suzuki, S. Tanaka, W. Jiang, H. Suematsu and K. Niihara, *J. Nanomater.*, 2011, **2011**, 693454.

205. K. Kim, H. Ju and J. Kim, *Ceram. Int.*, 2016, **42**, 8657-8663.

206. K. Uetani, S. Ata, S. Tomonoh, T. Yamada, M. Yumura and K. Hata, *Adv. Mater.*, 2014, **26**, 5857-5862.

207. B. Li, S. Dong, X. Wu, C. Wang, X. Wang and J. Fang, *Compos. Sci. Technol.*, 2017, **147**, 52-61.

208. H.-B. Cho, Y. Tokoi, S. Tanaka, H. Suematsu, T. Suzuki, W. Jiang, K. Niihara and T. Nakayama, *Compos. Sci. Technol.*, 2011, **71**, 1046-1052.

209. Z. Lin, Y. Liu, S. Raghavan, K.-S. Moon, S. K. Sitaraman and C.-P. Wong, *ACS Appl. Mater. Interfaces*, 2013, **5**, 7633-7640.

210. H. S. Lim, J. W. Oh, S. Y. Kim, M.-J. Yoo, S.-D. Park and W. S. Lee, *Chem. Mater.*, 2013, **25**, 3315-3319.

211. C. Yuan, B. Duan, L. Li, B. Xie, M. Huang and X. Luo, *ACS Appl. Mater. Interfaces*, 2015, **7**, 13000-13006.

212. S. Xu, H. Liu, Q. Li, Q. Mu and H. Wen, *J. Mater. Chem. C*, 2016, **4**, 872-878.

213. H. Yan, R. Wang, Y. Li and W. Long, *J. Electron. Mater.*, 2015, **44**, 658-666.

214. Z. Su, H. Wang, J. He, Y. Guo, Q. Qu and X. Tian, *ACS Appl. Mater. Interfaces*, 2018, **10**, 36342-36351.

215. K. Kim, M. Kim, J. Kim and J. Kim, *Ceram. Int.*, 2015, **41**, 12280-12287.

216. K. Kim and J. Kim, *Composites, Part B*, 2016, **93**, 67-74.

217. J.-Y. Chung, J.-G. Lee, Y.-K. Baek, P.-W. Shin and Y.-K. Kim, *Composites, Part B*,

2018, **136**, 215-221.

218. M. Sun, B. Dai, K. Liu, K. Yao, J. Zhao, Z. Lyu, P. Wang, Y. Ding, L. Yang, J. Han and J. Zhu, *Compos. Sci. Technol.*, 2018, **164**, 129-135.

219. M. Ralphs, W. Kong, R. Y. Wang and K. Rykaczewski, *Adv. Mater. Interfaces*, 2019, **6**, 1801857.

220. M. Klotz, I. Amirouche, C. Guizard, C. Viazzi and S. Deville, *Adv. Eng. Mater.*, 2012, **14**, 1123-1127.

221. Y. Wang, D. Kong, W. Shi, B. Liu, G. J. Sim, Q. Ge and H. Y. Yang, *Adv. Energy Mater.*, 2016, **6**, 1601057.

222. S. N. Schiffres, S. Harish, S. Maruyama, J. Shiomi and J. A. Malen, *ACS Nano*, 2013, **7**, 11183-11189.

223. H. Shen, C. Cai, J. Guo, Z. Qian, N. Zhao and J. Xu, *RSC Adv.*, 2016, **6**, 16489-16494.

224. X. Shen and J.-K. Kim, *Funct. Compos. Struct.*, 2020, **2**, 022001.

225. X. Zeng, Y. Yao, Z. Gong, F. Wang, R. Sun, J. Xu and C.-P. Wong, *Small*, 2015, **11**, 6205-6213.

226. Y. Wu, Z. Wang, X. Shen, X. Liu, N. M. Han, Q. Zheng, Y.-W. Mai and J.-K. Kim, *ACS Appl. Mater. Interfaces*, 2018, **10**, 26641-26652.

227. J. Han, G. Du, W. Gao and H. Bai, *Adv. Funct. Mater.*, 2019, **29**, 1900412.

228. G. Lian, C.-C. Tuan, L. Li, S. Jiao, Q. Wang, K.-S. Moon, D. Cui and C.-P. Wong, *Chem. Mater.*, 2016, **28**, 6096-6104.

229. J. Hu, Y. Huang, Y. Yao, G. Pan, J. Sun, X. Zeng, R. Sun, J.-B. Xu, B. Song and C.-P. Wong, *ACS Appl. Mater. Interfaces*, 2017, **9**, 13544-13553.

230. Y. Yao, X. Zhu, X. Zeng, R. Sun, J.-B. Xu and C.-P. Wong, *ACS Appl. Mater. Interfaces*,

2018, **10**, 9669-9678.

231. X.-H. Li, P. Liu, X. Li, F. An, P. Min, K.-N. Liao and Z.-Z. Yu, *Carbon*, 2018, **140**, 624-633.

232. Z. Shen and J. Feng, *Compos. Sci. Technol.*, 2019, **170**, 135-140.

233. Y. Yao, J. Sun, X. Zeng, R. Sun, J.-B. Xu and C.-P. Wong, *Small*, 2018, **14**, 1704044.

234. D. An, S. Cheng, Z. Zhang, C. Jiang, H. Fang, J. Li, Y. Liu and C.-P. Wong, *Carbon*, 2019, **155**, 258-267.

235. X. Hou, Y. Chen, W. Dai, Z. Wang, H. Li, C.-T. Lin, K. Nishimura, N. Jiang and J. Yu, *Chem. Eng. J.*, 2019, **375**, 121921.

236. S. Kang, T.-H. Kang, B. S. Kim, J. Oh, S. Park, I. S. Choi, J. Lee and J. G. Son, *Composites, Part B*, 2019, **162**, 580-588.

237. C. Fu, C. Yan, L. Ren, X. Zeng, G. Du, R. Sun, J. Xu and C.-P. Wong, *Compos. Sci. Technol.*, 2019, **177**, 118-126.

238. Y. Yao, Z. Ye, F. Huang, X. Zeng, T. Zhang, T. Shang, M. Han, W. Zhang, L. Ren, R. Sun, J.-B. Xu and C.-P. Wong, *ACS Appl. Mater. Interfaces*, 2020, **12**, 2892-2902.

239. X. Hou, Y. Chen, L. Lv, W. Dai, S. Zhao, Z. Wang, L. Fu, C.-T. Lin, N. Jiang and J. Yu, *ACS Appl. Nano Mater.*, 2019, **2**, 360-368.

240. F. Guo, X. Shen, J. Zhou, D. Liu, Q. Zheng, J. Yang, B. Jia, A. K. T. Lau and J.-K. Kim, *Adv. Funct. Mater.*, 2020, **30**, 1910826.

241. L. Guo, Z. Zhang, M. Li, R. Kang, Y. Chen, G. Song, S.-T. Han, C.-T. Lin, N. Jiang and J. Yu, *Compos. Commun.*, 2020, **19**, 134-141.

242. C. Wang, X. Chen, B. Wang, M. Huang, B. Wang, Y. Jiang and R. S. Ruoff, *ACS Nano*, 2018, **12**, 5816-5825.

243. T. Huang, Y. Li, M. Chen and L. Wu, *Compos. Sci. Technol.*, 2020, **198**, 108322.

244. Z. Bo, H. Zhu, C. Ying, H. Yang, S. Wu, J. Kong, S. Yang, X. Wei, J. Yan and K. Cen, *Nanoscale*, 2019, **11**, 21249-21258.

245. D. Liu, C. Lei, K. Wu and Q. Fu, *ACS Nano*, 2020, **14**, 15738-15747.

246. C. Li, L.-Y. Tan, X.-L. Zeng, D.-L. Zhu, R. Sun, J.-B. Xu and C.-P. Wong, *Compos. Sci. Technol.*, 2020, **188**, 107970.

247. Y.-F. Zhang, D. Han, Y.-H. Zhao and S.-L. Bai, *Carbon*, 2016, **109**, 552-557.

248. K. Wu, D. Liu, C. Lei, S. Xue and Q. Fu, *Chem. Eng. J.*, 2020, **394**, 124929.

249. L. Chen, N. Song, L. Shi and P. Ding, *Composites, Part A*, 2018, **112**, 18-24.

250. Z. Liu, Y. Chen, W. Dai, Y. Wu, M. Wang, X. Hou, H. Li, N. Jiang, C.-T. Lin and J. Yu, *RSC Adv.*, 2018, **8**, 1065-1070.

251. V. C. Doan, M. C. Vu, N. A. T. Thieu, M. A. Islam, P. J. Park and S.-R. Kim, *Composites, Part B*, 2019, **165**, 772-778.

252. R. M. Briber and B. J. Bauer, *Macromolecules*, 1988, **21**, 3296-3303.

253. D. Cho, W. Hu, J. T. Koberstein, J. P. Lingelser and Y. Gallot, *Macromolecules*, 2000, **33**, 5245-5251.

254. M. Sumita, K. Sakata, Y. Hayakawa, S. Asai, K. Miyasaka and M. Tanemura, *Colloid Polym. Sci.*, 1992, **270**, 134-139.

255. P. W. Ayers, *J. Chem. Phys.*, 2005, **122**, 141102.

256. D. Yorifuji and S. Ando, *Macromol. Chem. Phys.*, 2010, **211**, 2118-2124.

257. D. Yorifuji and S. Ando, *J. Mater. Chem.*, 2011, **21**, 4402-4407.

258. S. Uchida, T. Murakami, T. Iwamura, R. Ishige and S. Ando, *RSC Adv.*, 2017, **7**, 15492-15499.

259. L. M. Guiney, N. D. Mansukhani, A. E. Jakus, S. G. Wallace, R. N. Shah and M. C. Hersam, *Nano Lett.*, 2018, **18**, 3488-3493.

260. Z. Liang, Y. Pei, C. Chen, B. Jiang, Y. Yao, H. Xie, M. Jiao, G. Chen, T. Li, B. Yang and L. Hu, *ACS Nano*, 2019, **13**, 12653-12661.

261. N. Nguyen, S. Zhang, A. Oluwalowo, J. G. Park, K. Yao and R. Liang, *ACS Appl. Mater. Interfaces*, 2018, **10**, 27171-27177.

262. N. Nguyen, E. Melamed, J. G. Park, S. Zhang, A. Hao and R. Liang, *Macromol. Mater. Eng.*, 2017, **302**, 1700135.

263. J. Liu, W. Li, Y. Guo, H. Zhang and Z. Zhang, *Composites, Part A*, 2019, **120**, 140-146.

264. Y. Geng, H. He, Y. Jia, X. Peng and Y. Li, *Polym. Compos.*, 2019, **40**, 3375-3382.

265. Y. Jia, H. He, Y. Geng, B. Huang and X. Peng, *Compos. Sci. Technol.*, 2017, **145**, 55-61.

266. J. Jing, Y. Chen, S. Shi, L. Yang and P. Lambin, *Chem. Eng. J.*, 2020, **402**, 126218.

267. A. Gurijala, R. B. Zando, J. L. Faust, J. R. Barber, L. Zhang and R. M. Erb, *Matter*, 2020, **2**, 1015-1024.

268. F. Zhang, Y. Feng and W. Feng, *Mater. Sci. Eng., R*, 2020, **142**, 100580.

269. J. R. Choi, S. Yu, H. Jung, S. K. Hwang, R. H. Kim, G. Song, S. H. Cho, I. Bae, S. M. Hong, C. M. Koo and C. Park, *Nanoscale*, 2015, **7**, 1888-1895.

270. W. H. Qi and M. P. Wang, *Mater. Chem. Phys.*, 2004, **88**, 280-284.

271. J. Wang, X. Chen, G. Wang, B. Wang, W. Lu and J. Zhao, *Phys. Rev. B*, 2002, **66**, 085408.

272. K. Pashayi, H. R. Fard, F. Lai, S. Iruvanti, J. Plawsky and T. Borca-Tasciuc, *J. Appl. Phys.*, 2012, **111**, 104310.

273. K. Pashayi, H. R. Fard, F. Lai, S. Iruvanti, J. Plawsky and T. Borca-Tasciuc, *Nanoscale*, 2014, **6**, 4292-4296.

274. N. Balachander, I. Seshadri, R. J. Mehta, L. S. Schadler, T. Borca-Tasciuc, P. Keblinski and G. Ramanath, *Appl. Phys. Lett.*, 2013, **102**, 093117.

275. I. Seshadri, G. L. Esquenazi, T. Borca-Tasciuc, P. Keblinski and G. Ramanath, *Adv. Mater. Interfaces*, 2015, **2**, 1500186.

276. I. Seshadri, G. L. Esquenazi, T. Cardinal, T. Borca-Tasciuc and G. Ramanath, *Nanotechnology*, 2016, **27**, 175601.

277. G. Pezzotti, I. Kamada and S. Miki, *J. Eur. Ceram. Soc.*, 2000, **20**, 1197-1203.

278. S.-f. Fan, T. Zhang, K. Yu, H.-j. Fang, H.-q. Xiong, Y.-l. Dai, J.-j. Ma, D.-y. Jiang and H.-l. Zhu, *Trans. Nonferrous Met. Soc. China*, 2017, **27**, 117-124.

279. B. V. S. Dinesh and A. Bhattacharya, *J. Energy Storage*, 2020, **28**, 101190.

280. Y. Conde, A. Pollien and A. Mortensen, *Scr. Mater.*, 2006, **54**, 539-543.

281. X. Xiao, P. Zhang and M. Li, *Appl. Energy*, 2013, **112**, 1357-1366.

282. L. Huang, P. Zhu, G. Li and R. Sun, *Appl. Phys. A*, 2016, **122**, 515.

283. H. Fang, Y. Zhao, Y. Zhang, Y. Ren and S.-L. Bai, *ACS Appl. Mater. Interfaces*, 2017, **9**, 26447-26459.

284. F. Zhang, Y. Feng, M. Qin, L. Gao, Z. Li, F. Zhao, Z. Zhang, F. Lv and W. Feng, *Adv. Funct. Mater.*, 2019, **29**, 1901383.

285. Y.-H. Zhao, Y.-F. Zhang and S.-L. Bai, *Composites, Part A*, 2016, **85**, 148-155.

286. H. Ji, D. P. Sellan, M. T. Pettes, X. Kong, J. Ji, L. Shi and R. S. Ruoff, *Energy Environ. Sci.*, 2014, **7**, 1185-1192.

287. Z. Wu, C. Xu, C. Ma, Z. Liu, H.-M. Cheng and W. Ren, *Adv. Mater.*, 2019, **31**, 1900199.

288. X. Shen, Z. Wang, Y. Wu, X. Liu, Y.-B. He, Q. Zheng, Q.-H. Yang, F. Kang and J.-K. Kim, *Mater. Horiz.*, 2018, **5**, 275-284.

289. Y. Xue, X. Zhou, T. Zhan, B. Jiang, Q. Guo, X. Fu, K. Shimamura, Y. Xu, T. Mori, P. Dai, Y. Bando, C. Tang and D. Golberg, *Adv. Funct. Mater.*, 2018, **28**, 1801205.

290. T. S. Ashton and A. L. Moore, *Int. J. Heat Mass Transfer*, 2017, **115**, 273-281.

291. M. Qin, Y. Xu, R. Cao, W. Feng and L. Chen, *Adv. Funct. Mater.*, 2018, **28**, 1805053.

292. X. Wang and P. Wu, *Chem. Eng. J.*, 2018, **348**, 723-731.

293. Z. Liu, D. Shen, J. Yu, W. Dai, C. Li, S. Du, N. Jiang, H. Li and C.-T. Lin, *RSC Adv.*, 2016, **6**, 22364-22369.

294. Z. Liu, Y. Chen, Y. Li, W. Dai, Q. Yan, F. E. Alam, S. Du, Z. Wang, K. Nishimura, N. Jiang, C.-T. Lin and J. Yu, *Nanoscale*, 2019, **11**, 17600-17606.

295. H.-J. Hong, S. M. Kwan, D. S. Lee, S. M. Kim, Y. H. Kim, J. S. Lim, J. Y. Hwang and H. S. Jeong, *Compos. Sci. Technol.*, 2017, **152**, 94-100.

296. Y. S. Zhang and A. Khademhosseini, *Science*, 2017, **356**, eaaf3627.

297. D. Li, M. B. Müller, S. Gilje, R. B. Kaner and G. G. Wallace, *Nat. Nanotechnol.*, 2008, **3**, 101-105.

298. M. Hegde, L. Yang, F. Vita, R. J. Fox, R. van de Watering, B. Norder, U. Lafont, O. Francescangeli, L. A. Madsen, S. J. Picken, E. T. Samulski and T. J. Dingemans, *Nat. Commun.*, 2020, **11**, 830.

299. W. Cai, D. Zhang, B. Wang, Y. Shi, Y. Pan, J. Wang, W. Hu and Y. Hu, *Compos. Sci. Technol.*, 2018, **168**, 74-80.

300. C. Liang, H. Qiu, Y. Han, H. Gu, P. Song, L. Wang, J. Kong, D. Cao and J. Gu, *J. Mater. Chem. C*, 2019, **7**, 2725-2733.

301. F. Jiang, S. Cui, N. Song, L. Shi and P. Ding, *ACS Appl. Mater. Interfaces*, 2018, **10**, 16812-16821.

302. V. H. Luan, J. S. Chung, E. J. Kim and S. H. Hur, *Chem. Eng. J.*, 2014, **246**, 64-70.

303. V. H. Luan, H. N. Tien, L. T. Hoa, N. T. M. Hien, E.-S. Oh, J. Chung, E. J. Kim, W. M. Choi, B.-S. Kong and S. H. Hur, *J. Mater. Chem. A*, 2013, **1**, 208-211.

304. X. Yang, S. Fan, Y. Li, Y. Guo, Y. Li, K. Ruan, S. Zhang, J. Zhang, J. Kong and J. Gu, *Composites, Part A*, 2020, **128**, 105670.

305. J. Chen, X. Huang, Y. Zhu and P. Jiang, *Adv. Funct. Mater.*, 2017, **27**, 1604754.

306. L. Shao, L. Shi, X. Li, N. Song and P. Ding, *Compos. Sci. Technol.*, 2016, **135**, 83-91.

307. H. Pang, L. Xu, D.-X. Yan and Z.-M. Li, *Prog. Polym. Sci.*, 2014, **39**, 1908-1933.

308. D.-X. Yan, H. Pang, B. Li, R. Vajtai, L. Xu, P.-G. Ren, J.-H. Wang and Z.-M. Li, *Adv. Funct. Mater.*, 2015, **25**, 559-566.

309. S.-H. Park, J. Hwang, G.-S. Park, J.-H. Ha, M. Zhang, D. Kim, D.-J. Yun, S. Lee and S. H. Lee, *Nat. Commun.*, 2019, **10**, 2537.

310. S. Yu, J.-W. Lee, T. H. Han, C. Park, Y. Kwon, S. M. Hong and C. M. Koo, *ACS Appl. Mater. Interfaces*, 2013, **5**, 11618-11622.

311. C. Feng, H. Ni, J. Chen and W. Yang, *ACS Appl. Mater. Interfaces*, 2016, **8**, 19732-19738.

312. M. Hu, J. Feng and K. M. Ng, *Compos. Sci. Technol.*, 2015, **110**, 26-34.

313. Y. Wang, X. Qiao, J. Wan, Y. Xiao and X. Fan, *RSC Adv.*, 2016, **6**, 80262-80267.

314. H. Zhou, H. Deng, L. Zhang and Q. Fu, *ACS Appl. Mater. Interfaces*, 2017, **9**, 29071-29081.

315. Z.-G. Wang, F. Gong, W.-C. Yu, Y.-F. Huang, L. Zhu, J. Lei, J.-Z. Xu and Z.-M. Li,

Compos. Sci. Technol., 2018, **162**, 7-13.

316. Y.-H. Bae, M.-J. Yu, M. C. Vu, W. K. Choi and S.-R. Kim, *Compos. Sci. Technol.*, 2018, **155**, 144-150.

317. Z.-G. Wang, Y.-F. Huang, G.-Q. Zhang, H.-Q. Wang, J.-Z. Xu, J. Lei, L. Zhu, F. Gong and Z.-M. Li, *Ind. Eng. Chem. Res.*, 2018, **57**, 10391-10397.

318. G. He, X. Li, Y. Dai, Z. Yang, C. Zeng, C. Lin and S. He, *Composites, Part B*, 2019, **162**, 678-684.

319. Y. Chen, X. Hou, M. Liao, W. Dai, Z. Wang, C. Yan, H. Li, C.-T. Lin, N. Jiang and J. Yu, *Chem. Eng. J.*, 2020, **381**, 122690.

320. B. Liu, Y. Li, T. Fei, S. Han, C. Xia, Z. Shan and J. Jiang, *Chem. Eng. J.*, 2020, **385**, 123829.

321. K. Kim and J. Kim, *Compos. Sci. Technol.*, 2016, **134**, 209-216.

322. K. Kim and J. Kim, *Polymer*, 2016, **101**, 168-175.

323. C. P. Feng, L. Chen, F. Wei, H. Y. Ni, J. Chen and W. Yang, *RSC Adv.*, 2016, **6**, 65709-65713.

324. K. Wu, C. Lei, R. Huang, W. Yang, S. Chai, C. Geng, F. Chen and Q. Fu, *ACS Appl. Mater. Interfaces*, 2017, **9**, 7637-7647.

325. A. Li, C. Zhang and Y.-F. Zhang, *Composites, Part A*, 2017, **101**, 108-114.

326. Y. Jiang, Y. Liu, P. Min and G. Sui, *Compos. Sci. Technol.*, 2017, **144**, 63-69.

327. F. E. Alam, W. Dai, M. Yang, S. Du, X. Li, J. Yu, N. Jiang and C.-T. Lin, *J. Mater. Chem. A*, 2017, **5**, 6164-6169.

328. Z. Qiao and J. Mao, *Mater. Sci. Eng., B*, 2017, **226**, 86-93.

329. F. E. Alam, J. Yu, D. Shen, W. Dai, H. Li, X. Zeng, Y. Yao, S. Du, N. Jiang and C.-T.

Lin, *Polymers*, 2017, **9**, 662.

330. J. Huang, W. Yang, J. Zhu, L. Fu, D. Li and L. Zhou, *Composites, Part A*, 2019, **123**, 79-85.

331. D. Ding, H. Wang, Z. Wu, Y. Chen and Q. Zhang, *Macromol. Rapid Commun.*, 2019, **40**, 1800805.

332. H. Yuan, Y. Wang, T. Li, Y. Wang, P. Ma, H. Zhang, W. Yang, M. Chen and W. Dong, *Nanoscale*, 2019, **11**, 11360-11368.

333. A. Yokoi, W. K. Tan, T. Kuroda, G. Kawamura, A. Matsuda and H. Muto, *Nanomaterials*, 2020, **10**, 134.

334. P. Zhang, X. Ding, Y. Wang, Y. Gong, K. Zheng, L. Chen, X. Tian and X. Zhang, *Composites, Part A*, 2019, **117**, 56-64.

335. J. R. Potts, O. Shankar, L. Du and R. S. Ruoff, *Macromolecules*, 2012, **45**, 6045-6055.

336. M. Harada, N. Hamaura, M. Ochi and Y. Agari, *Composites, Part B*, 2013, **55**, 306-313.

337. H. Ding, Y. Guo and S. N. Leung, *J. Appl. Polym. Sci.*, 2016, **133**.

338. Y. Zhang, Y. Shen, K. Shi, T. Wang and E. Harkin-Jones, *Composites, Part A*, 2018, **110**, 62-69.

339. X. Jin, W. Li, Y. Liu and W. Gan, *Composites, Part A*, 2020, **130**, 105727.

340. Y. Wu, K. Ye, Z. Liu, B. Wang, C. Yan, Z. Wang, C.-T. Lin, N. Jiang and J. Yu, *ACS Appl. Mater. Interfaces*, 2019, **11**, 44700-44707.

Table 1. Physical properties of representative thermally conductive materials used as fillers for polymer composites.

Materials	Thermal conductivity ($W\ m^{-1}\ K^{-1}$)	Electrical resistivity ($\Omega \cdot m$)	Coefficient of thermal expansion ($10^{-6}\ K^{-1}$)	Density ($g\ cm^{-3}$)
Ag	428	1.6×10^{-8}	18.0	10.4
Cu	398	1.7×10^{-8}	17.0	8.9
Au	315	2.4×10^{-8}	14.0	19.3
Al	247	2.7×10^{-8}	23.1	2.7
Mg	151	4.3×10^{-8}	26.9	1.7
Fe	94	1.0×10^{-8}	11.8	7.9
Ni	88	7.1×10^{-8}	13.0	8.9
Graphite	200 ~ 2,000 (∥) 2 ~ 800 (⊥)	5.0×10^{-6} (∥) 3.0×10^{-3} (⊥)	-1.5 (∥) 25 (⊥)	2.1
SWCNT	6,000	1.0×10^{-4}	-0.9	N/A
MWCNT	3,000	5.1×10^{-6}	-1.0	N/A
PAN-based CF	8 ~ 105	7.1×10^{-8}	-0.4 (∥) 5.6 (⊥)	1.8
Pitch-based CF	1,100	1.2×10^{-6}	2.1 (∥) 10.0 (⊥)	2.2

Diamond	600 ~ 2,000	1.0 ~ 10^{12}	0.8	3.5
BeO	250 ~ 300	> 10^{14}	6.5 ~ 6.7	3.0
AlN	170 ~ 220	> 10^{14}	4.3 ~ 4.6	3.3
SiC	150	> 10^{14}	3.7	3.2
BAs (cubic)	1,300	N/A	3.85	5.22
BN (hexagonal)	600 (∥) 30 (⊥)	N/A	-2.7 (∥) 38 (⊥)	2.1

Table 2. Summary of reported κ values of polymer composites with rational design of filler distribution for in-plane orientation.

Method for in-plane distribution	Filler types	Filler content	κ (W m^{-1} K^{-1})		Ref.
			In-plane κ	Through-plane κ	
Impregnation	VGCF bundles	57 vol%	695	36	[127]
	Pitch-based CF bundles mixed with dispersed MWCNTs	-	396	-	[128]
	Cu-plated PAN-based CFs web	32.7 vol%	7.37	0.96	[129]
	Annealed Cu-plated PAN-based CFs	26.2 vol%	47.2	3.9	[130]

Electrospinning	BNNS	18 wt%	7.1	0.12	[134]
	BNNSs	33 wt%	16.3	-	[135]
	BNNTs	4.76 vol%	0.54	0.18	[138]
	BN	30 wt%	0.696	-	[137]
	rGO	15 wt%	0.689	-	[140]
	BN	30 wt%	7.29	-	[141]
	BNNSs	30 wt%	18.63	1.031	[142]
	MWCNTs-*g*-rGO	10 wt%	1.60	-	[143]
	Chemically modified graphene	5 wt%	1.05	-	[139]
	BNNS	20 wt%	9.1	-	[144]
	BNNS	60 wt%	1.137	0.182	[145]
	BNNS	15.6 vol%	1.94	-	[136]
Vacuum filtration	MLG	11.8 wt%	16.75	5.44	[151]
	BNNSs	70 wt%	24.6	-	[153]
	BNNSs	90 wt%	212.8		[154]
	Graphene	6.4 wt%	12.7	2.9	[155]
	AgNPs-decorated BNNSs and AgNPs-decorated SiCNWs	95 wt%	21.67	-	[156]
	BNNS	70 wt%	30.25	-	[157]
	BNNS	50 wt%	145.7	-	[158]
	rGO	8 wt%	6.69		[159]

	BNNS/graphene fluoride	90 wt%	55.65	-	[160]
	$Ti_3C_2T_x$	50 wt%	11.57	-	[161]
	$Ti_3C_2T_x$@Ag	30 wt%	8.84	-	[162]
Doctor blade	Graphene	60 wt%	41.64	-	[166]
	BN microplatelets	10 wt%	3.92	-	[169]
	BN	60 wt%	11.88	-	[170]
	Graphite nanosheet	80 wt%	71.18	-	[171]
	PDDA-nanodiamond/BNNS	30 wt%	15.49	-	[172]
Compression molding	Graphite	49.3 vol%	13.27	-	[176]
	rGO	10 wt%	0.244	-	[177]
	BN	95 wt%	50.3	-	[178]
	BN microplatelets	60 wt%	10.87	-	[179]
	BN	95 wt%	45	-	[180]
	AgNPs-decorated Al_2O_3 platelets	50 wt%	6.71	-	[181]
	BNNS	13.4 vol%	8.0	-	[182]
	GNPs-BN	20.97 vol%	8.96	-	[183]
	BNNS	90 wt%	6.7	-	[184]
	APTES-BNNS	40 wt%	5.86	-	[185]
	hBN/CF	22.3 vol%	3.11	-	[186]
	rGO/BN	50 vol%	16	-	[187]

Table 3. Summary of reported κ values of polymer composites with rational design of filler distribution for through-plane orientation.

Method for in-plane distribution	Filler types	Filler content	κ (W m^{-1} K^{-1})		Ref.
			In-plane κ	Through-plane κ	
Vertical growth	CNTs	0.4 vol%	-	1.21	[192]
	MWCNTs	16.7 vol%	2.41 (14.8 vol%)	4.87	[193]
	AgNWs	9 vol%	-	38.8	[195]
	CuNWs	25 vol%	2.2	70	[196]
Alignment by electric field	BNNSs	15 vol%	-	1.56	[202]
	BNNSs	5 vol%	-	0.14	[204]
	TiO_2-BN	30 vol%	1.85	1.72	[205]
	CFs	13.2 wt%	8.9	23.3	[206]
Alignment by magnetic field	Graphene nanoplates	3 wt%	-	0.488	[207]
	Fe_2O_3-coated BNNSs	30 vol%	-	0.275	[208]
	Iron oxide-coated BN platelets	20 wt%	-	0.85	[209]
	Fe_3O_4-coated BN microplatelets	20 vol%	-	4.70	[210]
	Iron oxide-coated BN platelets	0.14 vol%	-	0.58	[211]

	Fe/BN composite particles	50 wt%	-	3.59	[212]
	Fe_3O_4-coated rGO	0.52 vol%	-	0.361	[213]
	Fe_3O_4-coated BN platelets and CNTs mixing	30 wt%	0.99	0.98	[214]
	Fe_3O_4 nanospheres-coated SiC	20 vol%	-	1.681	[215]
	Fe_3O_4 nanospheres-coated AlN platelets	40 vol%	-	3.15	[216]
	Fe_3O_4 NPs-coated Spherical Al_2O_3	40 vol%	-	1.7	[217]
	Fe_3O_4 NPs-coated microdiamond	5 vol%	-	1.36	[218]
	Ag-coated Ni	50 vol%	-	5.7	[219]
Ice templating	BNNSs	9.29 vol%	-	2.85	[225]
	BNNSs	15 vol%	-	6.07	[227]
	rGO	0.92 vol%	-	2.13	[228]
	BN microplatelet	23.7 wt%	-	1.4	[223]
	BN microplatelet	34.2 vol%	-	4.42	[229]
	SiCNWs	2.17 vol%	-	1.67	[230]
	Graphitized rGO	1.5 wt%	-	6.57	[231]
	SiCMWs	1.32 vol%	-	0.6	[232]

	BN platelet-rGO	13.16 vol%	-	5.05	[233]
	BN-rGO	4.9 vol%	-	1.28	[234]
	Rob-like CFs	12.8 vol%	-	6.04	[235]
	rGO/CNTs	2 wt%	-	1.109	[236]
	AgNPs-coated BNNSs/AgNWs	4.7 vol%	-	0.804	[237]
	BN microplates/SiCNWs	8.35 vol%	-	3.87	[238]
	BNNSs	15.8 vol%	-	7.46	[239]
	BNNSs laminated with rGO	5 vol%	-	1.9	[240]
	$Ti_3C_2T_x$/CFs	30.2 wt%	-	9.68	[241]
Transformation of oriented direction	GNF	25 vol%	-	10	[189]
	Graphite paper	47 wt%	-	24.19	[246]
	Graphite	20 vol%	-	4	[248]
Wood templating	Carbonized cellulose	-	-	0.56	[249]
Cigarette filter-templating	GNP	-	0.298	1.2	[250]
	Cu flake	36.4 wt%	-	1.4	[251]
Double percolation	Nano-pyramidal ZnO	27.1 vol%	-	1.54	[257]

	Needle-shaped ZnO	23 vol%	-	2.0	[258]
3D printing	BNNS	22 wt%	-	1.5	[260]
	GNPs/chopped carbon fiber	16.9 wt%	-	2.0	[262]
Combination of multiple processing methods	BNNS	28.7 wt%	-	1.94	[136]
	hBN platelets	40 wt%	-	2.56	[263]
	BN sheets	30 vol%	-	2.03	[264]
	Graphite	50 wt%	-	5.5	[265]
	GNPs	15 vol%	-	3.43	[266]
	Iron oxide-coated hBN	60 vol%	-	7.28	[267]

Table 4. Summary of reported κ values of polymer composites with rational design of isotropic filler distribution.

Method for in-plane distribution	Filler types	Filler content	κ (W m^{-1} K^{-1})	Ref.
Deformable fillers	Sintering of AgNPs	45 vol%	26.94	[275]
	Sintering of AgNPs	45 vol%	38.5	[276]
	Cold-welding of AuNWs	3.3 vol%	5.0	[277]
	Microwave welding of branched AgNWs	4 vol%	6.0	[278]
Foam templating	Cu foam	-	4.95	[281]
	rGO-coated Ni foam	-	0.71	[282]
	Graphene foam	0.4 wt%	0.62	[283]
	Graphene-crosslinked CNT sponge	-	10.89	[284]
	Graphene foam mixed with multilayer graphene flakes	-	1.08	[285]
	Graphene foam	1.5 vol%	3.61	[286]
	Graphene foam-GNPs	10.27 wt%	11.16	[287]
	Graphene foam	8.3 wt%	8.8	[288]
	BN foam	51 wt%	11.13	[289]
	BN foam	0.07 vol%	0.73	[290]
	rGO foam	4.82 wt%	2.19	[291]

	BNNS foam	1.1 vol%	0.6	[292]
	GNP foam	5 wt%	1.52	[293]
	GNP foam	6.8 wt%	8.04	[294]
Hydrogel networks	GNP/rGO	20.5 wt%	1.56	[300]
	BNNSs	2 vol%	1.17	[301]
	CuNW/rGO	7.2 wt%	0.51	[304]
	BNNS/rGO	6.8 wt%	0.475	[305]
	BNNSs	9.6 vol%	3.13	[306]
Particulate segregation	Electroless-plated Cu shell	23 vol%	26.14	[310]
	AlN	30 vol%	0.81	[312]
	AlN microspheres	60 wt%	1.3	[313]
	Graphite	30 vol%	17.8	[314]
	BN/AlN	50 wt%	7.1	[315]
	CuNPs	30 wt%	1.05	[316]
	BN plate/CNTs	25 vol%	1.80	[317]
	Graphene/CNTs	0.3 wt%	1.3	[318]
	Spherical Al_2O_3/Graphene	54.5 wt%	13.3 (33.4)	[319]
	BN platelets	50 wt%	5.57	[320]
	Graphite flakes	21.2 vol%	5.4	[311]
	BN	18 wt%	1.14	[321]
	Graphite flakes	18.83 vol%	2.276	[323]
	BNNSs	13.4 vol%	8.0	[182]
	GNPs (MWCNT/PS matrix)	5 vol%	1.13	[324]

	rGO	1.04 wt%	0.8	[325]
	BN flakes	40 vol%	4.15	[326]
	GNP	10 wt%	1.84	[327]
	Graphene	10 wt%	1.054	[328]
	AgNPs-decorated rGO	4.78 vol%	0.54	[330]
	hBN (GNP/PA6 matrix)	18.82 vol%	2.69	[183]
	BN platelets	20 vol%	4.47	[331]
	GO	0.96 vol%	4.56 (4.13)	[332]
	BNNSs	26 vol%	1.42	[333]
	CNT/BN@PVDF	25 vol%	1.8	[317]
	GNPs/MWCNT	5 vol%	1.0	[324]
	MWCNT/BN	5 wt%	0.83	[334]
Segregation by coagulation	rGO	5 wt%	0.219	[335]
Segregation by crystallization	BN	35 vol%	2.5	[336]
Segregation by foaming	BN platelets (with expandable bead)	9.21 vol%	1.16	[337]
Segregation by RIPS	GNPs	10 wt%	0.709	[338]
	BNNSs	0.41 vol%	0.33	[339]
Cotton candy-templating	Micron-sized spherical and submicron-sized Al_2O_3	36.2 vol%	3.17	[340]

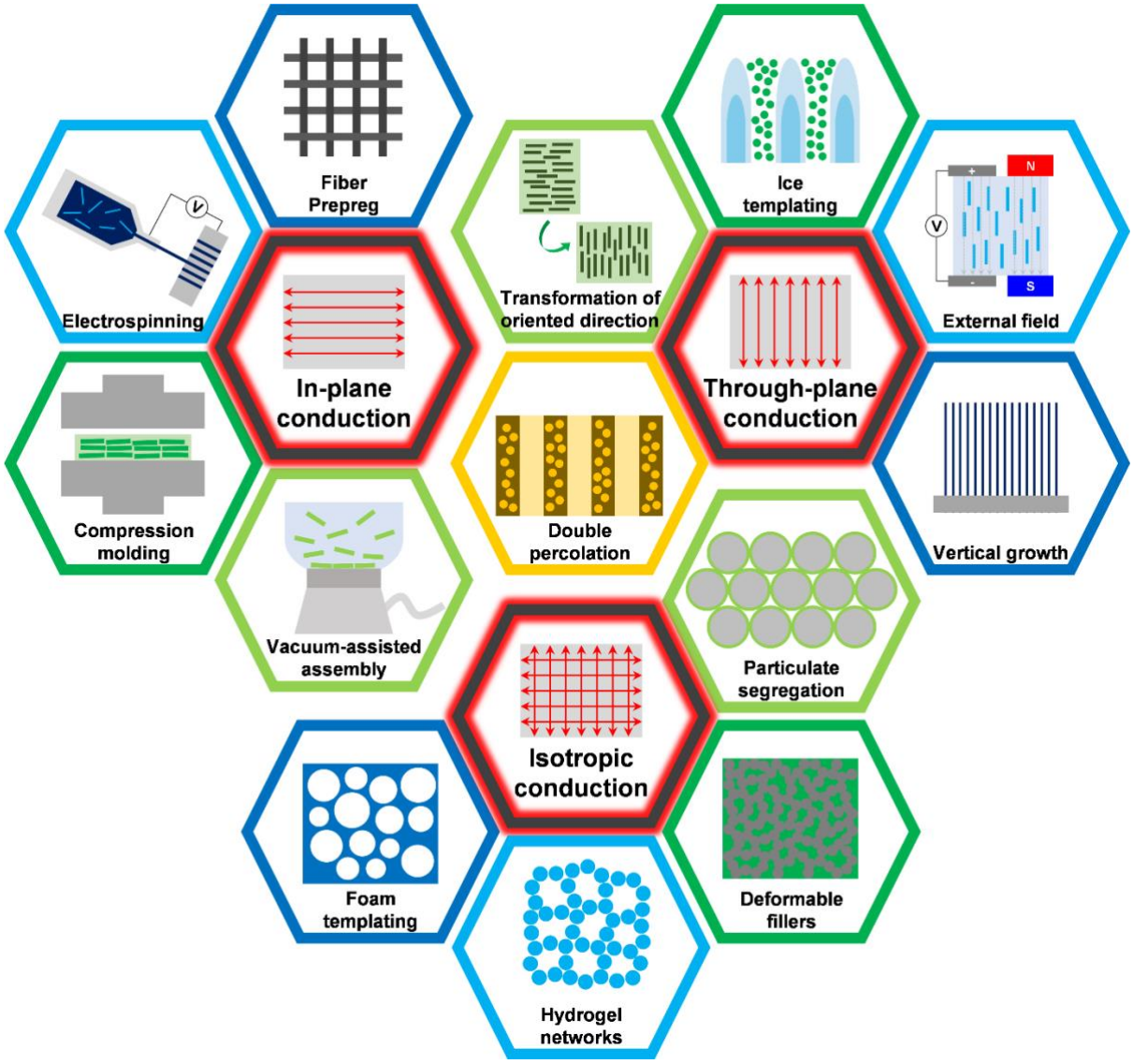

Fig. 1. Schematic illustration of efficient strategies for rationally designing filler distribution in intended direction.

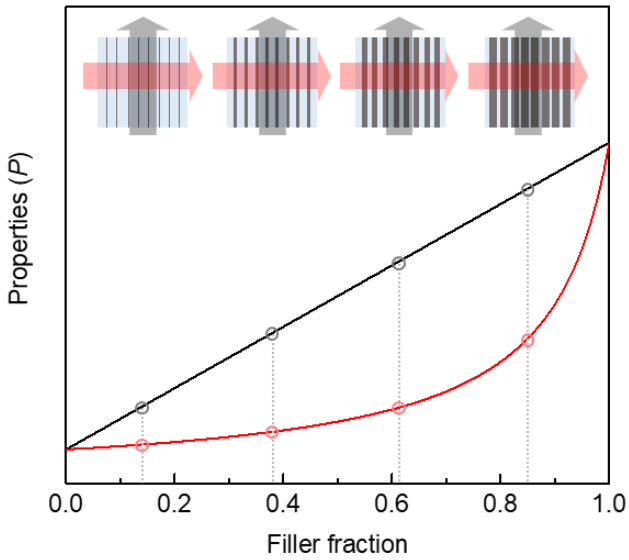

Fig. 2. Properties of composites containing unidirectional, continuous fibers in a continuous matrix calculated using the ROM and inverse ROM equations. Schematic illustrations depict the thermal conduction direction of the composites, in which the gray and red arrows indicate the fiber axial direction and perpendicular to the fiber axis, respectively.

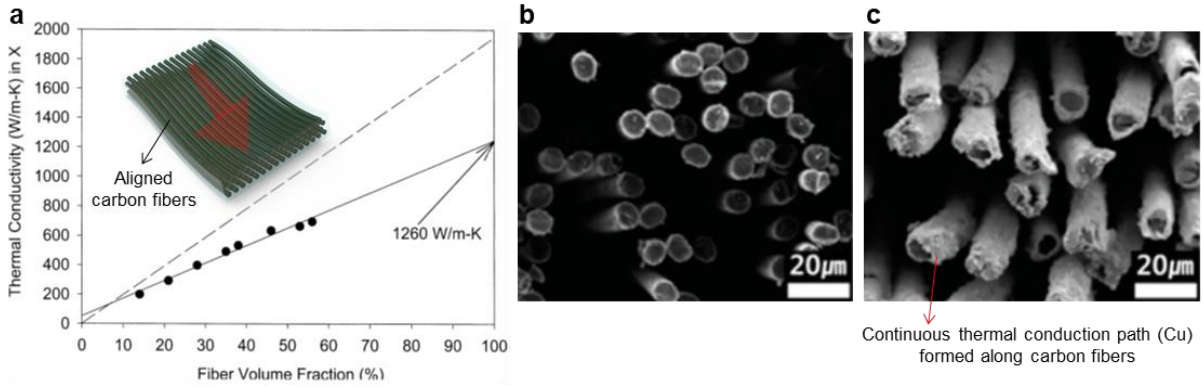

Fig. 3. Polymer composites with aligned CFs. (a) in-plane κ of VGCF/polymer composites. Dashed line represents theoretical values calculated using the ROM equation with 0.1 W m^{-1} K^{-1} and 1,950 W m^{-1} K^{-1} for κ values of the polymer matrix and carbon fiber, respectively. Reproduced with permission.[127] Copyright 2002, Elsevier. Inset shows the schematic illustration of a polymer composite with aligned CFs. Cross-sectional SEM images of (b) pristine CFs and (c) Cu-plated CFs. Reproduced with permission.[130] Copyright 2014, American Chemical Society.

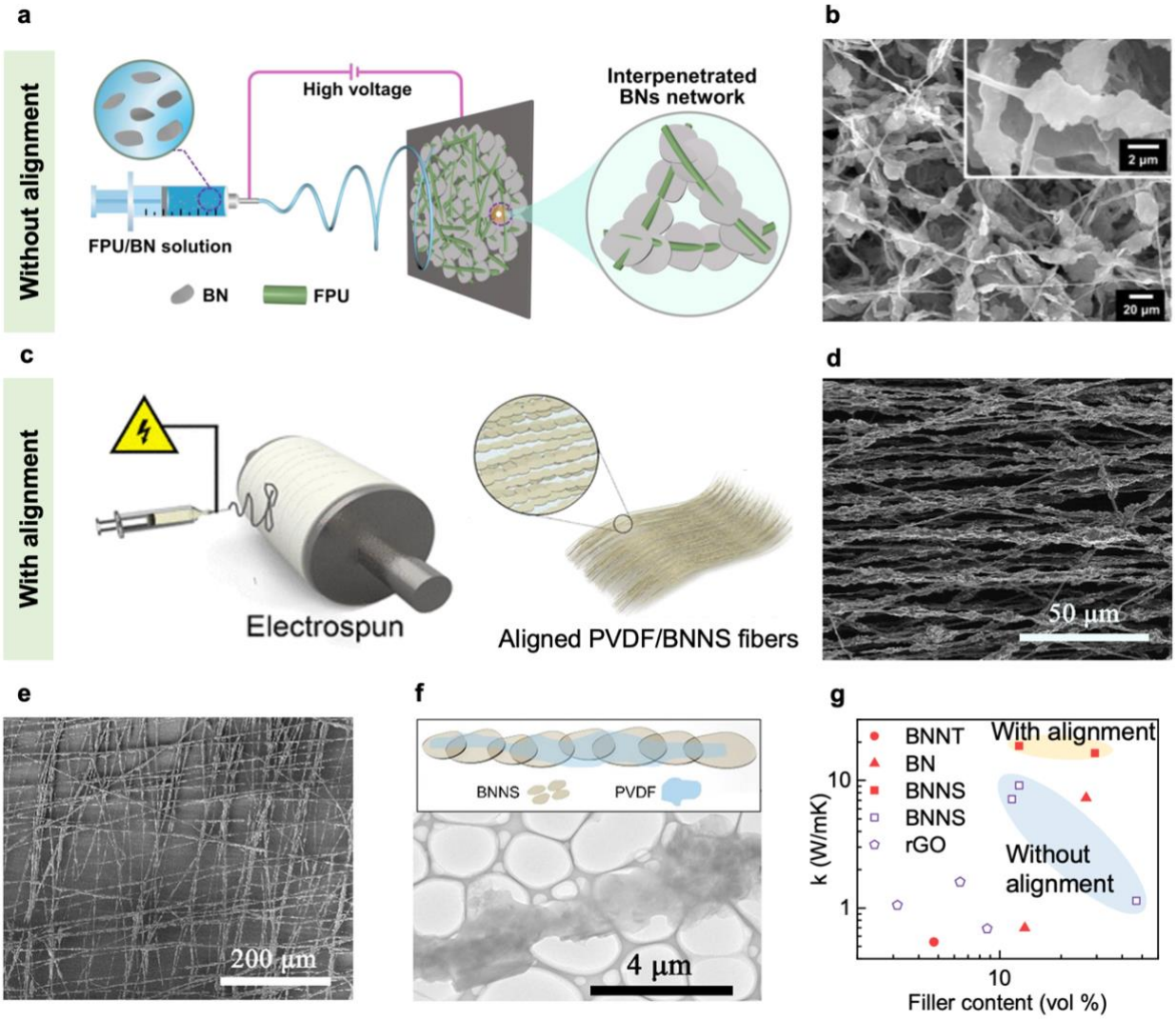

Fig. 4. Electrospinning for orientation of NFs. Schematic illustrations of the fabrication procedures of BNNS/polymer NFs through electrospinning (a) without and (c) with alignments of as-spun fiber. The corresponding SEM images are shown in (b) and (d), respectively. (e) SEM image of cross-stacked BNNS/PVDF fibers. (f) Schematic and TEM image of interconnected BNNSs in the fiber direction. (g) Comparison of in-plane *k* of composites made from different nanofillers including BNNT,[138] BN,[137, 141] BNNS,[134, 135, 142, 144, 145] and rGO[139,

[140, 143] with (solid symbols) and without fiber alignments (hollow symbols). (a-b) Reproduced with permission.[134] Copyright 2020, American Chemical Society. (c-f) Reproduced with permission.[135] Copyright 2019, American Chemical Society.

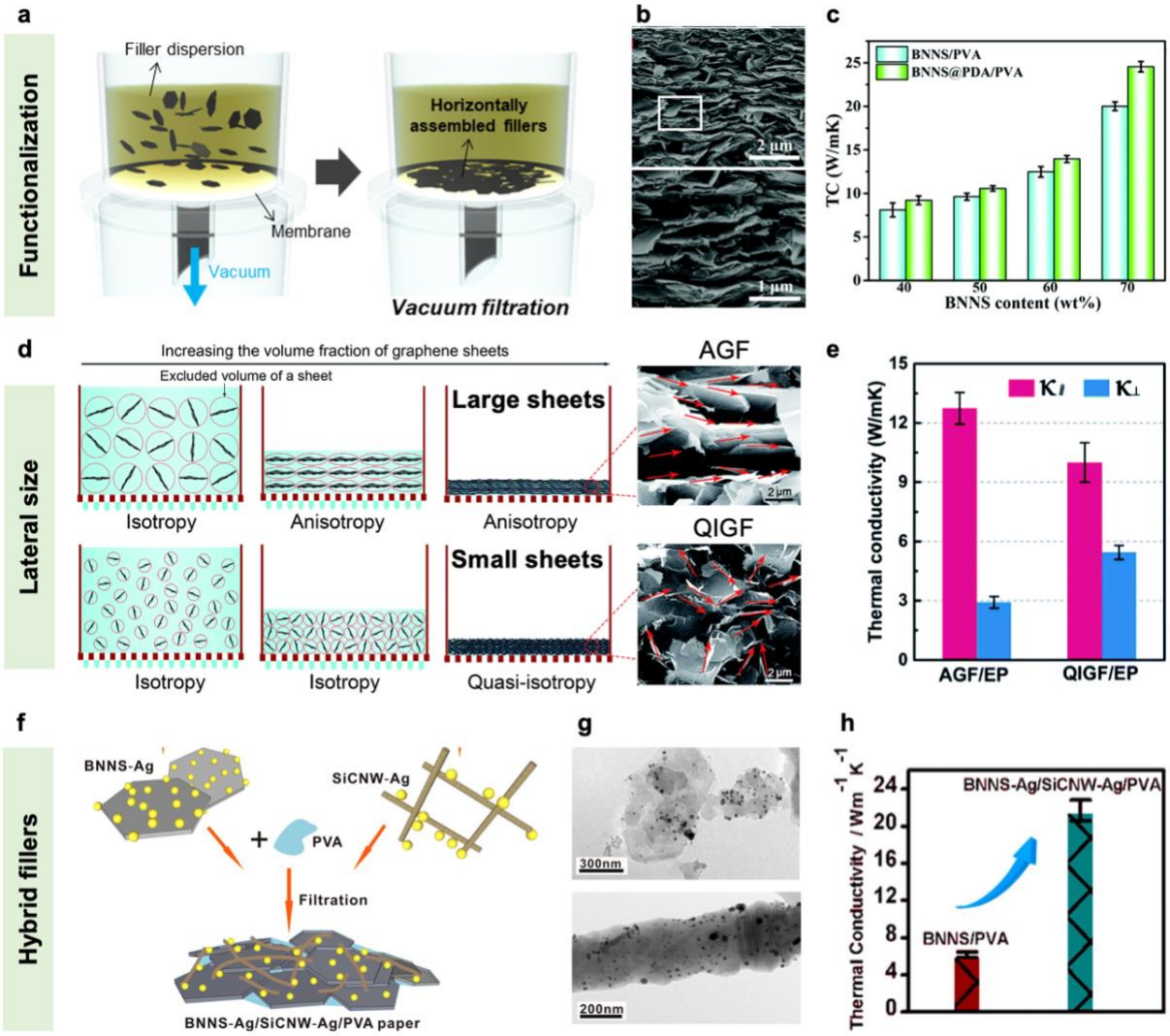

Fig. 5. Vacuum-assisted assembly for orientation of anisotropic fillers. (a) Schematic illustration of the vacuum-assisted assembly of polymer composites with functionalized 2D materials. (b) cross-sectional SEM images of 70 wt% BNNS@PDA/PVA film and enlarged view of the white rectangular area in below. (c) In-plane κ values of BNNS@PDA/PVA and BNNS/PVA films with different filler contents. Reproduced with permission.[153] Copyright 2019, Royal Society of Chemistry. (d) Schematic illustrations of the filtration processes for small and large rGO sheets and the SEM images of the resulting anisotropic graphene film (AGF) and quasi-isotropic graphene film (QIGF) with different degrees of alignments. (e) κ

values of AGF/epoxy and QIGF/epoxy composites. Reproduced with permission.[155] Copyright 2018, Royal Society of Chemistry. (f) Schematic illustration of the fabrication procedure of BNNS-Ag/SiCNW-Ag/PVA composite paper. (g) TEM images of BNNS-Ag and SiCNW-Ag. (h) In-plane κ values of BNNS/PVA and BNNS-Ag/SiCNW-Ag/PVA composite papers. Reproduced with permission.[156] Copyright 2016, American Chemical Society.

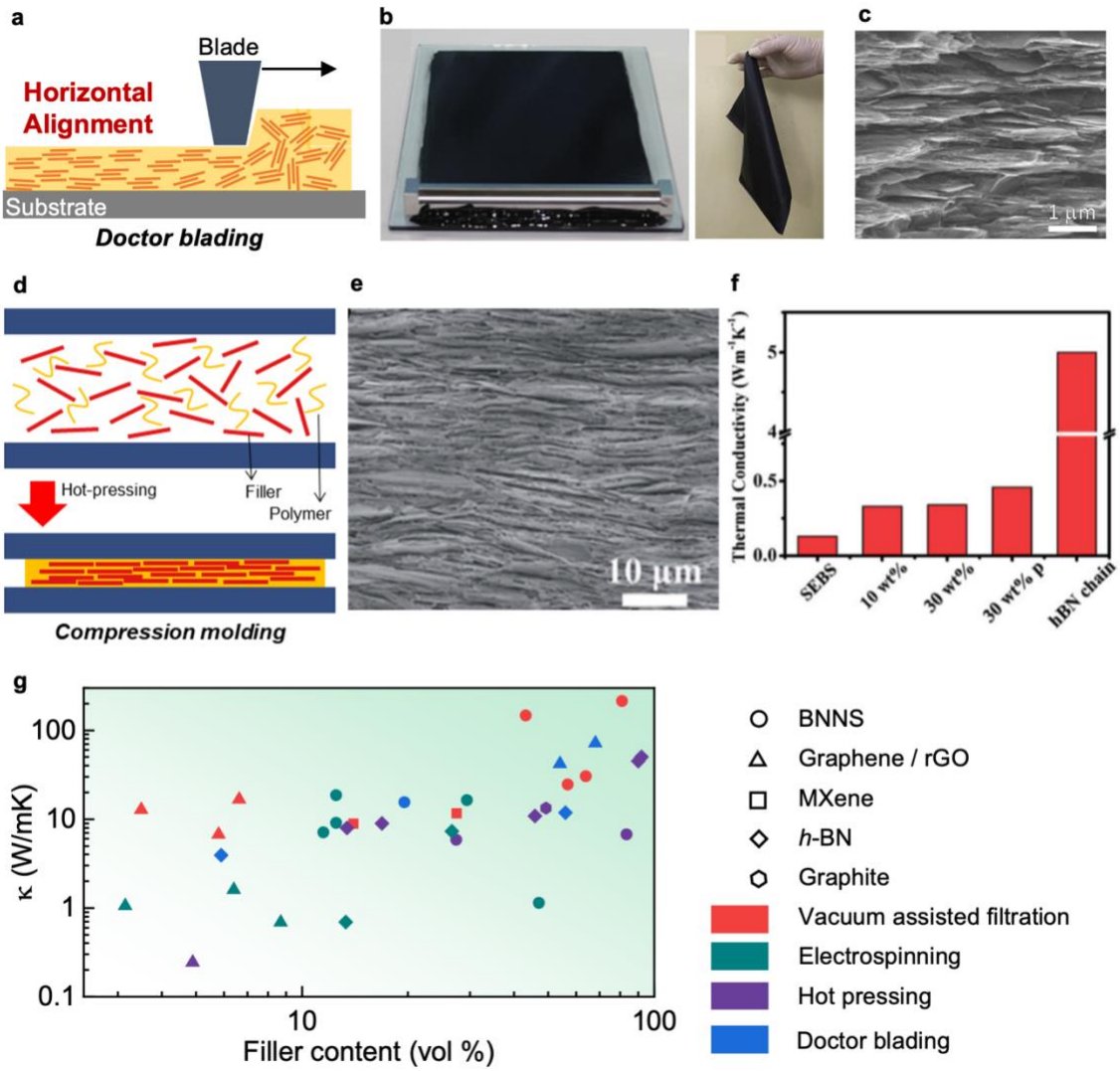

Fig. 6. (a) Schematic illustration of the doctor blading technique for fabricating 2D filler/polymer composites. Reproduced with permission.[165] Copyright 2021, Elsevier. (b) Setup of doctor blading and photograph of a flexible graphene/PVDF thin film made by doctor blading. (c) SEM image of the graphene/PVDF film showing aligned graphene sheets. Reproduced with permission.[166] Copyright 2018, Elsevier. (d) Schematic illustration of compression molding of 2D filler/polymer composites. (e) Cross-sectional morphology of 95

wt% hBN/SEBS composite film. (f) In-plane κ values of composites with different structures estimated by molecular dynamics simulations. The "p" in "30 wt% p" represents the formation of heat-transfer pathways. Reproduced with permission.[180] Copyright 2018, Royal Society of Chemistry. (f) Comparison of in-plane κ values of composites made from different fillers by vacuum assisted filtration, electrospinning, hot pressing, and doctor blading methods introduced in Section 3.1.

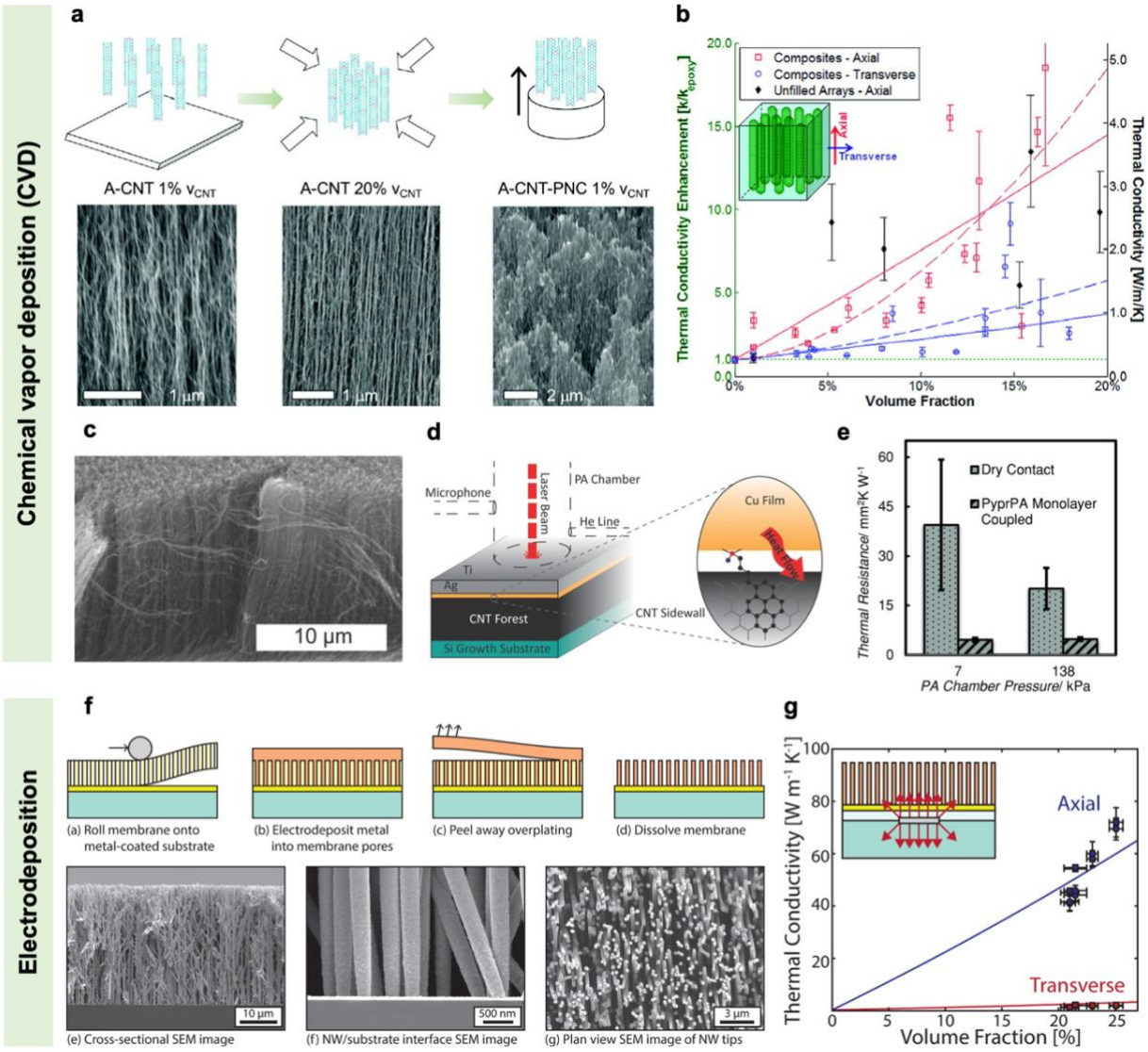

Fig. 7. Vertically-grown fillers by CVD and template-assisted electrodeposition. (a) Schematic illustration and SEM images of densely packed CNT forest and its composites. (b) In-plane (axial) and through-plane (transverse) κ of CNT/epoxy nanocomposites and unfilled CNT forests as a function of volume fraction. Best fits from the effective medium approach (solid lines) and with a power law (dashed line) are shown for the composite data. The dashed green line indicates the thermal conductivity of epoxy. Reproduced with permission.[193] Copyright 2011, American Chemical Society. (c) SEM image of a MWCNT forest used for pyrenylpropyl

phosphonic acid (PPA) interface coupling. Illustrations of (d) photoacoustic measurement configuration (left) used to measure the thermal resistance of MWCNT forests coupled to oxidized Cu surface with the PPA modifier (right). (e) Thermal resistance between MWCNT forests and Cu with and without PPA modifier. Reproduced with permission.[194] Copyright 2014, John Wiley and Sons. (f) Schematic illustration and SEM images of vertically grown Cu NWs by template-assisted electrodeposition. (g) In-plane (axial) and through-plane (transverse) κ of Cu NW arrays at different volume fractions. Reproduced with permission.[196] Copyright 2015, American Chemical Society.

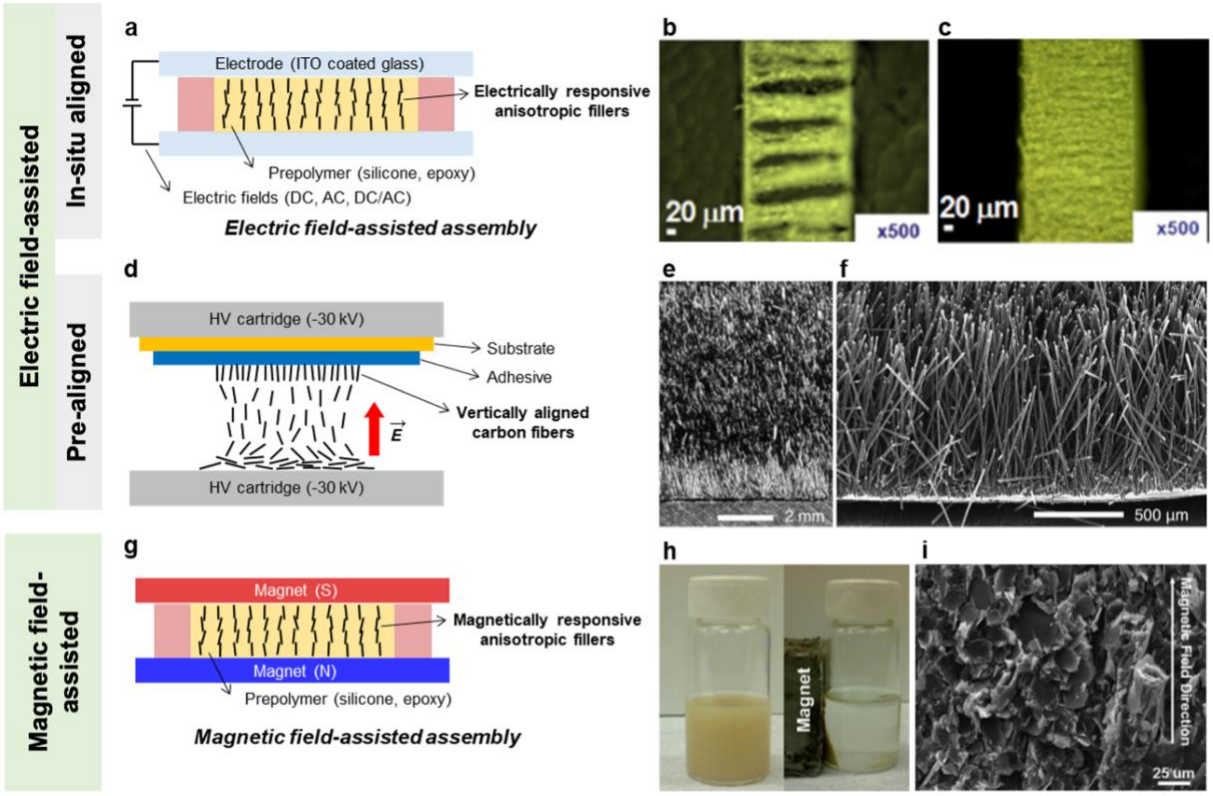

Fig. 8. External field-assisted orientation of anisotropic fillers. (a) Illustration of the electric field-assisted assembly method. Digital micrographs of nanocomposite films with linear densely-packed assemblies of 5 vol% BNNSs fabricated under (b) switching DC and (c) AC electric fields. Reproduced with permission.[202] Copyright 2016, Elsevier. (d) Illustration of the electrostatic flocking method. (e,f) SEM images of vertically-aligned CF scaffolds. Reproduced with permission.[206] Copyright 2014, John Wiley and Sons. (g) Illustration of the magnetic field-assisted assembly method. (h) Photographs of magnetically responsive BN by Fe_2O_3 NP dispersion in acetone and its response to external magnetic field when a magnet is placed near the dispersion. Reproduced with permission.[209] Copyright 2013, American Chemical Society. (i) Cross-sectional SEM image of Fe_3O_4-coated BN/epoxy composite aligned vertically to the film plane. Reproduced with permission.[210] Copyright 2013, American Chemical Society.

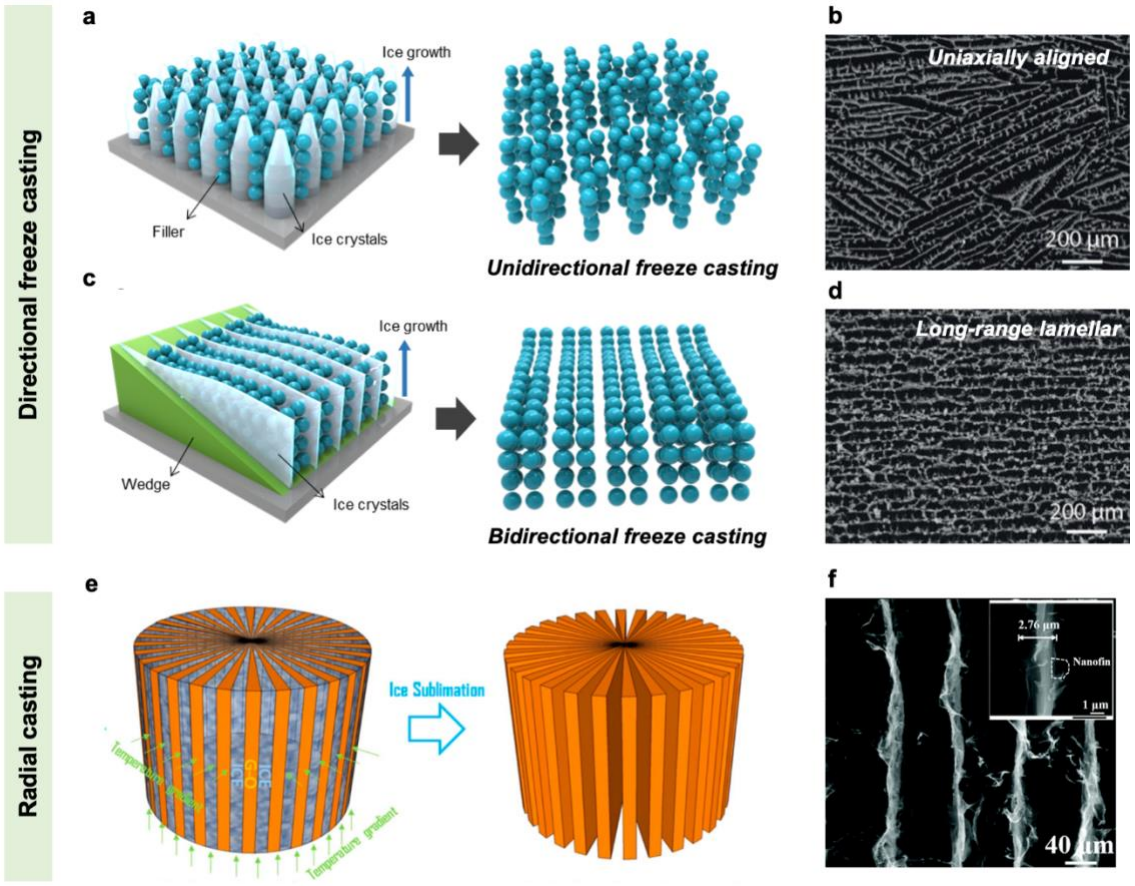

Fig. 9. Ice templating strategy for vertical orientation of fillers. (a) Schematic illustration of the unidirectional freeze casting process. (b) SEM image of 3D-BNNS aerogel in the perpendicular direction to ice growth. (c) Schematic illustration of the bidirectional freeze casting process. (d) SEM image of BNNS aerogel with a lamellar structure. Reproduced with permission.[227] Copyright 2019, John Wiley and Sons. (e) Schematic illustration of the radial freeze casting. Reproduced with permission.[242] Copyright 2018, American Chemical Society. (f) SEM image of graphene nanofin grown on aligned rGO sheets. Reproduced with permission.[244] Copyright 2019, Royal Society of Chemistry.

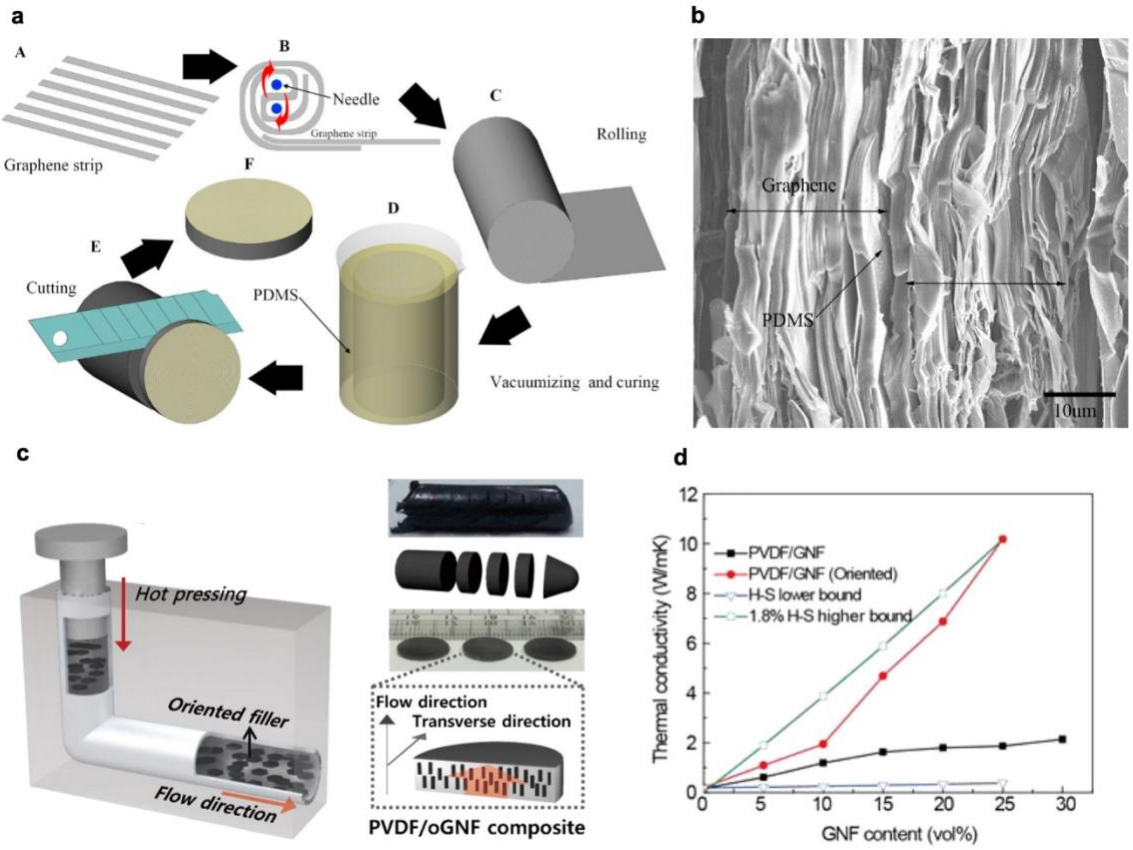

Fig. 10. Transformation of oriented direction. (a) Schematic illustration of transforming the direction of filler orientation by rolling. (b) SEM image showing the vertically aligned graphene after infiltrating PDMS into the rolled graphene strips. Reprinted with permission.[247] Copyright 2016, Elsevier. (c) Schematic illustration of transforming oriented direction by L-shape tube. (d) Through-plane κ of oriented composites. Reprinted with permission.[189] Copyright 2015, American Chemical Society.

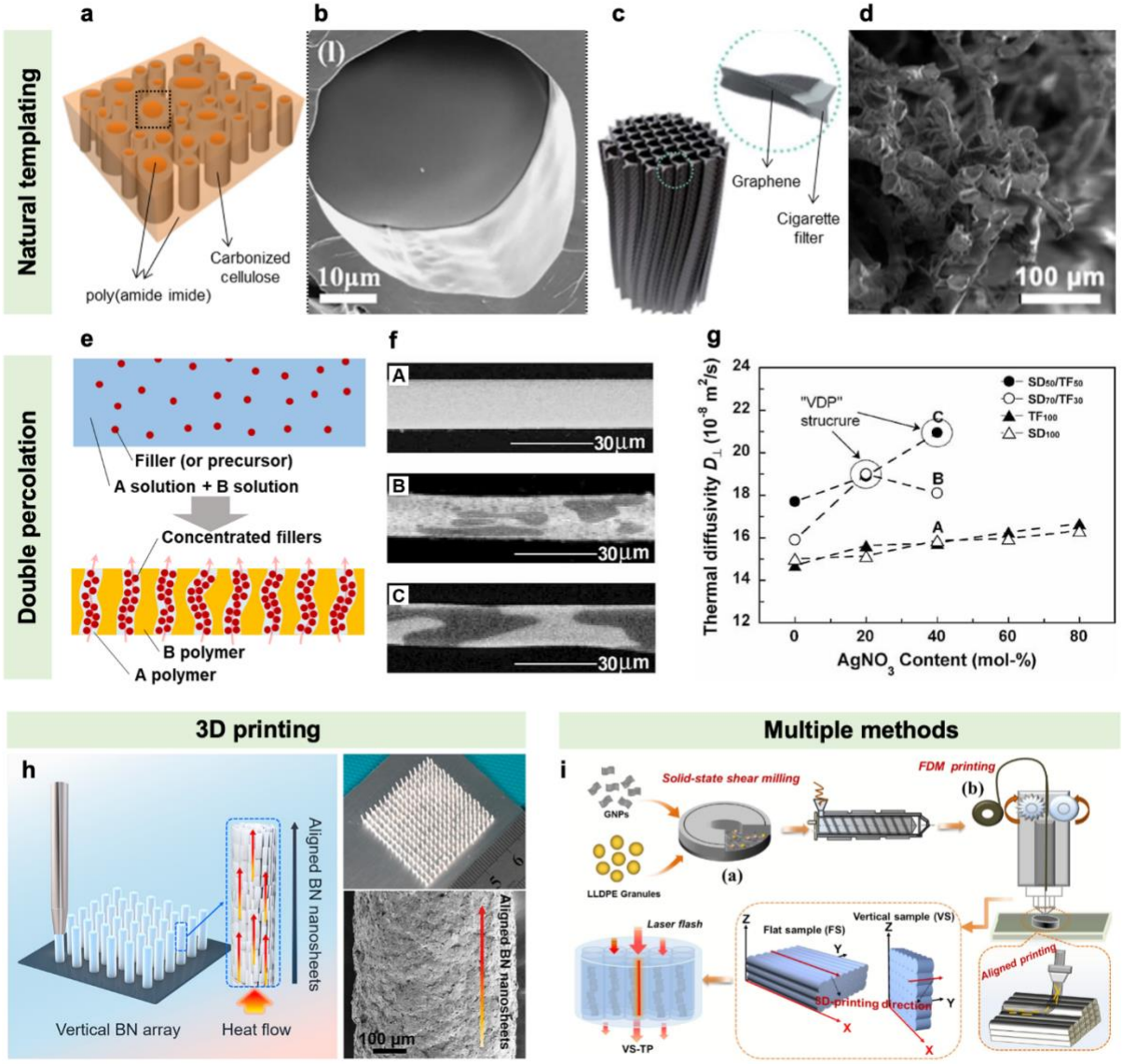

Fig. 11. Other methods to construct vertically aligned fillers by natural templating, vertical double orientation of polymer blends, 3D printing, and combination of multiple processing methods. (a) Illustration of the carbonized wood/PAI composite made of wood template. (b) SEM image of the composite. Reproduced with permission.[249] Copyright 2018, Elsevier. (c) Illustration of the GNP-coated cigarette filter. (d) SEM image of the GNP-coated cigarette filter. Reproduced with permission.[250] Copyright 2018, Royal Society of Chemistry. (e) Schematic

illustration of the fabrication procedure of composites with a VDP structure. (f) Cross-sectional SEM images of PI composites with approximately 1 vol% of Ag NPs at PI blend ratios of (A) SD100, (B) SD70/TF30, and (C) SD50/TF50, where SD and TF denote BPDA-SDA and BPDA-TFDB, respectively. (g) Relationship between the through-plane thermal diffusivity and the morphology of PI films containing Ag NPs in homo-PI and PI blends composed of BPDA-SDA and BPDA-TFDB. The dashed lines are guides for eyes. Reproduced with permission.[256] Copyright 2010, John Wiley and Sons. (h) Schematic illustration, photograph and SEM image of 3D printed, vertically aligned BNNS arrays. Reproduced with permission.[260] Copyright 2019, American Chemical Society. (i) Schematic illustration showing the fabrication of aligned GNP/LLDPE composites by combining shear milling and FDM printing. Reproduced with permission.[266] Copyright 2020, Elsevier.

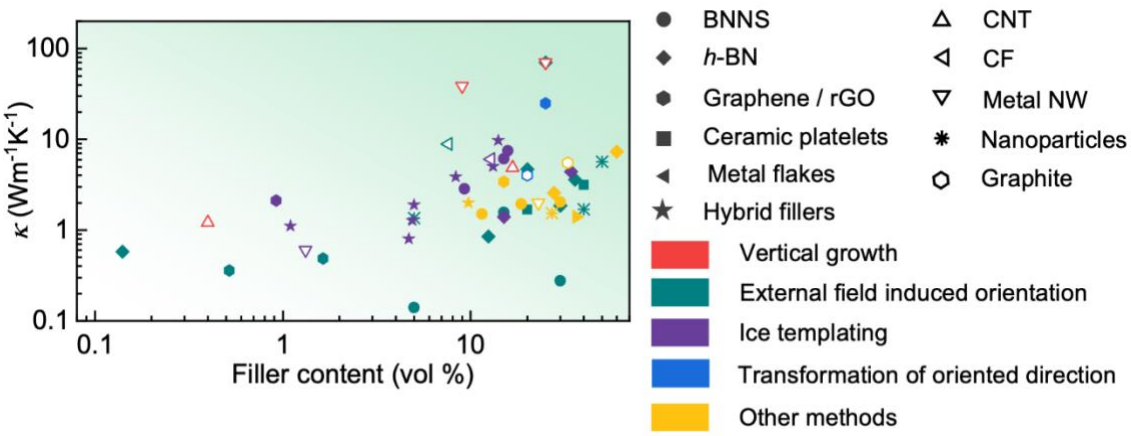

Fig. 12. Comparison of through-plane κ values of composites made from different fillers prepared by vertical growth, external field induced orientation, ice templating, transformation of oriented direction, and other methods introduced in Section 3.2. Solid symbols represent 2D fillers. The data and references are listed in Table 3.

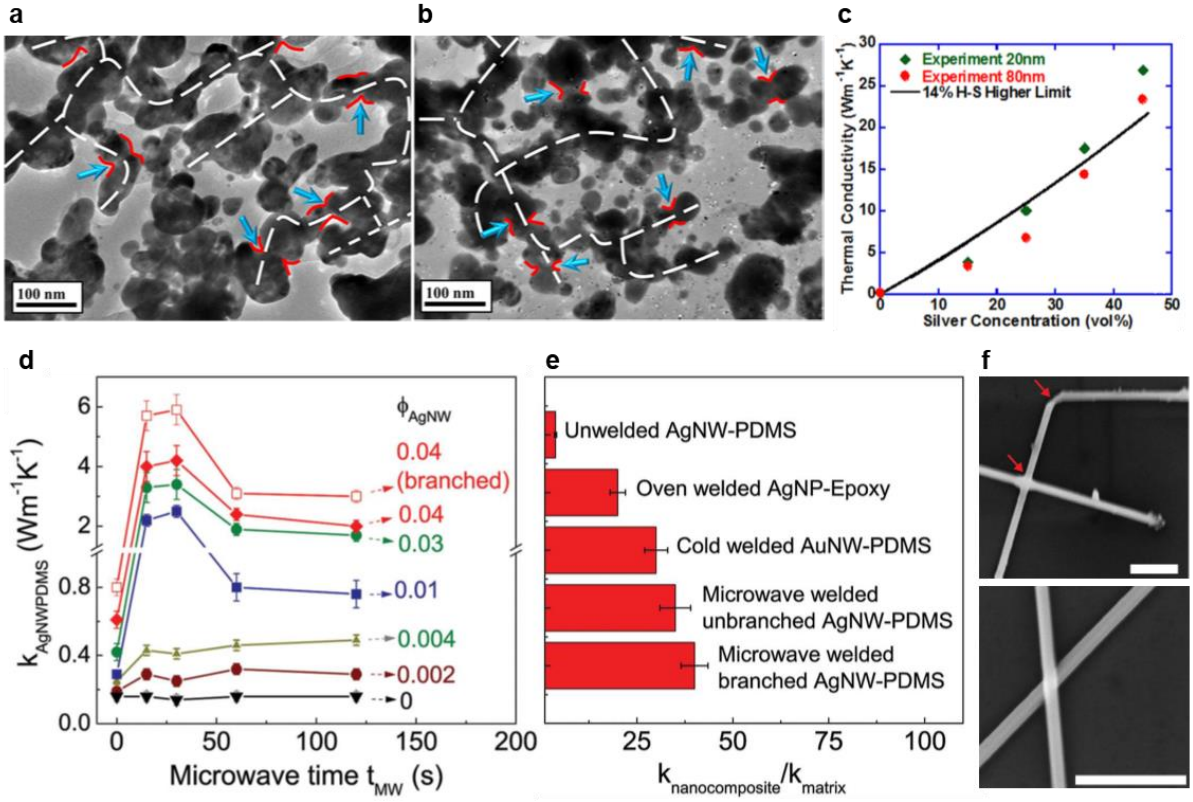

Fig. 13. Formation of percolative structure via deformation of fillers. TEM images of 35 vol% AgNP-epoxy nanocomposites with AgNPs of (a) 20 nm and (b) 80 nm in diameter showing self-assembled, interconnected networks. (c) κ values of AgNP-epoxy nanocomposites as a function of AgNP content. Reproduced with permission.[272] Copyright 2012, AIP Publishing. (d) κ values of AgNW-filled PDMS nanocomposites as a function of precure microwave irradiation time. (e) κ enhancement ratio of microwave welded branched and unbranched AgNW-filled PDMS nanocomposites with filler volume fraction of 0.04 and a microwave irradiation time of 30 s, compared to those filled with similar volume fractions of non-welded AgNWs, cold welded Au NWs (AuNW-PDMS), and fused low aspect ratio AgNPs in an epoxy matrix (AgNP-Epoxy). (f) SEM images of AgNWs in nanocomposites showing welded junctions (top) and overlapping NW junctions prior to microwave exposure (bottom). The scale bars are 0.5 μm. Reproduced with permission.[275] Copyright 2015, John Wiley and Sons.

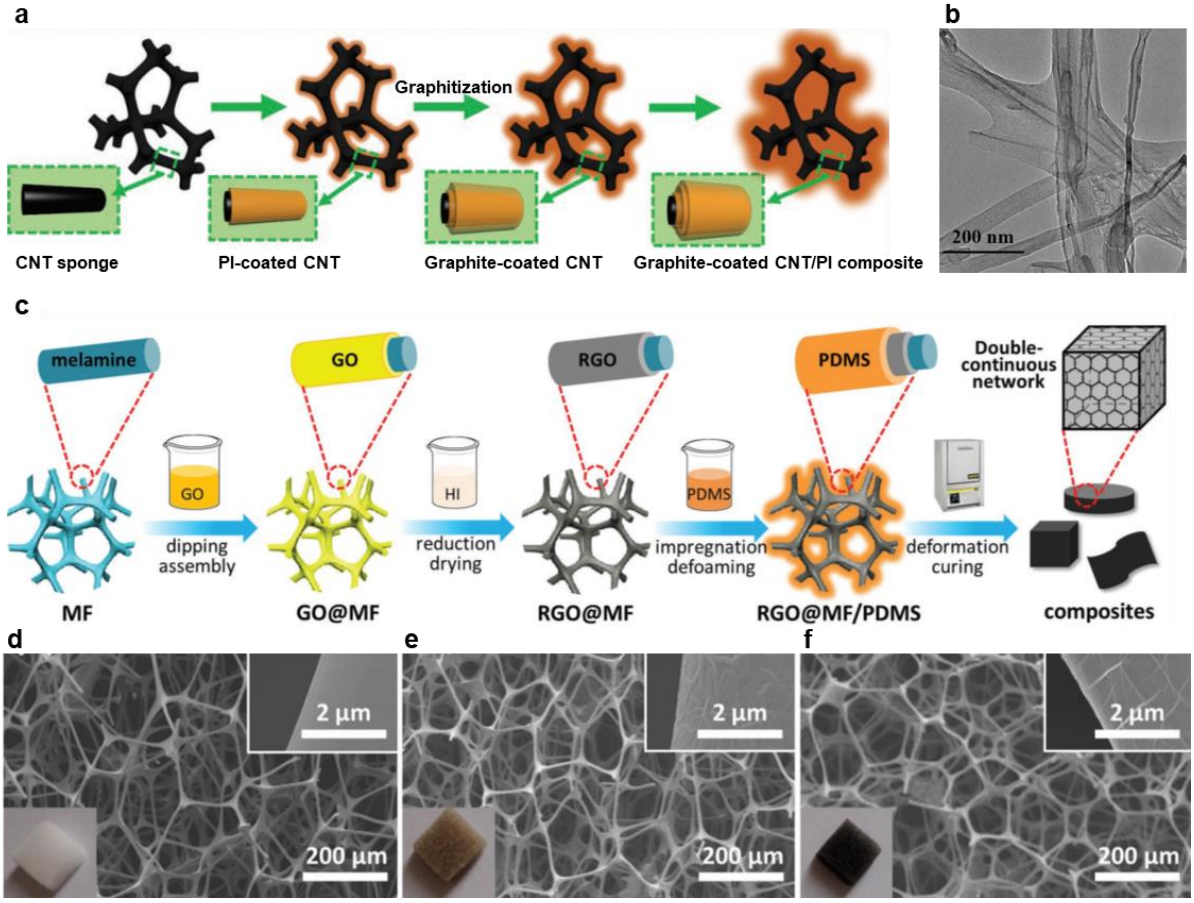

Fig. 14. Use of thermally conductive, continuous foam structure. (a) Schematic illustration of the fabrication of 3D elastic graphene-crosslinked-CNT (G_w-CNT)/PI composites. (b) TEM image of graphite-coated CNTs. Reproduced with permission.[284] Copyright 2019, John Wiley and Sons. (c) Illustration of the overall preparation procedure of flexible double-continuous network of graphene and polymer, and polymer nanocomposite. SEM images and photographs of (d) melamine-formaldehyde foam (MF), (e) GO@MF, and (f) rGO@MF. Reproduced with permission.[289] Copyright 2018, John Wiley and Sons.

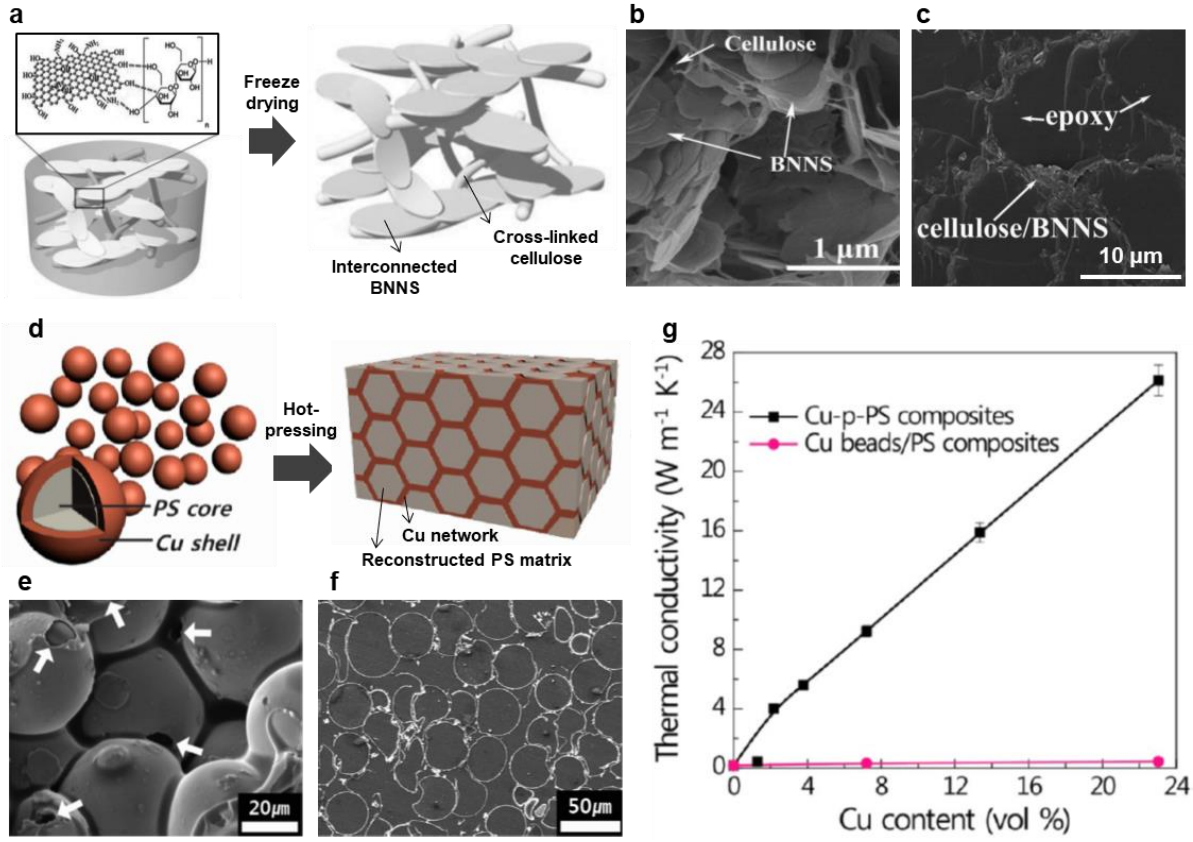

Fig. 15. Strategies for forming 3D thermal conduction pathways of fillers. (a) Schematic illustration of the formation of filler networks based on sacrificial hydrogel networks. SEM images of (b) 3D BNNS aerogel and (c) 3D BNNS/epoxy nanocomposite, respectively. Reproduced with permission.[305] Copyright 2017, John Wiley and Sons. (d) Schematic illustration of the fabrication procedure of Cu-plated PS composite. SEM images of Cu-plated PS composites in (e) fractured side and (f) cross-sectional views. (g) κ values of Cu-plated PS and Cu bead/PS composites as a function of Cu content. Reproduced with permission.[310] Copyright 2013, American Chemical Society.

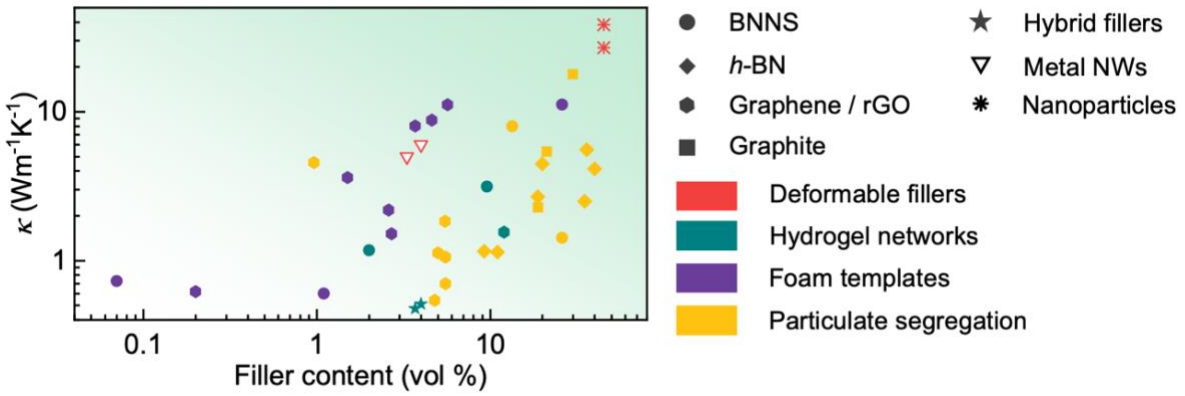

Fig. 16. Comparison of isotropic κ values of composites made from different fillers by use of deformable fillers, hydrogel networks, foam templates, and particulate segregation methods introduced in Section 3.3. Solid symbols represent 2D fillers. The data and references are listed in Table 4.